Copyright Warning & Restrictions

The copyright law of the United States (Title 17, United States Code) governs the making of photocopies or other reproductions of copyrighted material.

Under certain conditions specified in the law, libraries and archives are authorized to furnish a photocopy or other reproduction. One of these specified conditions is that the photocopy or reproduction is not to be "used for any purpose other than private study, scholarship, or research." If a, user makes a request for, or later uses, a photocopy or reproduction for purposes in excess of "fair use" that user may be liable for copyright infringement,

This institution reserves the right to refuse to accept a copying order if, in its judgment, fulfillment of the order would involve violation of copyright law.

Please Note: The author retains the copyright while the New Jersey Institute of Technology reserves the right to distribute this thesis or dissertation

Printing note: If you do not wish to print this page, then select "Pages from: first page # to: last page #" on the print dialog screen

ABSTRACT

Behavior of R/C Columns Under Nonproportional Variations in Axial and Lateral Loads

By
Kaniz Fatema Ahsan

The study on the behavior of reinforced concrete columns subjected to the motion of earthquake suggests that the structure may experiance nonproportional variations in axial and lateral forces. In order to assess the capacity of a reinforced concrete structure under nonproportional loadings, an analytical model is developed using the fiber modeling technique.

The method is based on detailed analytical description of the geometry and material properties used in evaluating the behavior of the critical regions rather than a simplified and predefined set of hysteresis rules. The present study has two principal components of investigation. First, the analyses are done at the section level, to determine the influence of nonproportional axial and lateral loadings on the moment-curvature relationship for various loading level, P-M interaction diagram, degree of confinement of concrete, amount of reinforcing steel etc. Second, analyses on the response of R/C columns in terms of load-displacement hysteresis loops and curvature distribution along the height of the column subjected to nonproportinal variation in axial and lateral loads. Furthermore, the effect of degree of concrete confinement on the response of the R/C columns are also investigated. Finally, the model results are compared with experimental and other analytical models.

BEHAVIOR OF R/C COLUMNS UNDER NONPROPORTIONAL VARIATIONS IN AXIAL AND LATERAL LOADS

by
Kaniz Fatema Ahsan

A Thesis
Submitted to the Faculty of
New Jersey Institute of Technology
in Partial Fulfilment of the Requirements for the Degree of
Master of Science

Department of Civil and Environmental Engineering

January 1993

APPROVAL PAGE

Behavior of R/C Columns Under Nonproportional Variations in Axial and Lateral Loads

Kaniz Fatema Ahsan

Dr. M.A. Saadeghvaziri, Thesis Adviser
Assistant Professor
Department of Civil and Environmental Engineering, NJIT

Dr. C.T. Hsu, Committee Member
Graduate Adviser and Professor
Department of Civil and Environmental Engineering, NJIT

BIOGRAPHICAL SKETCH

Author: Kaniz Fatema Ahsan

Degree: Master of Science in Civil Engineering

Date: January, 1993

Undergraduate and Graduate Education:

- Master of Science in Civil Engineering, New Jersey Institute of Technology, Newark, New Jersey, 1993
- Bachelor of Science in Civil Engineering, Bangladesh University of Engineering and Technology, Dhaka, Bangladesh, 1983

Major: Civil Engineering

This thesis is dedicated to
my parents, husband, Quamrul Ahsan and son, Saquib

ACKNOWLEDGMENT

The author wishes to express her sincere gratitude to her supervisor, Dr. M. A. Saadeghvaziri for his guidence and support throughout this research. Special thanks to Dr. C.T. Thomas Hsu for serving as a member of the comittee. The author is grateful to New Jersy Institute of Technology for funding of the research through SBR program. The author appreciates the timely help given by the system analysts and staff of the computer division.

Finally, my thanks goes to my husband, Quamrul Ahsan, my parents, my son, Saquibul Ahsan, my sister inlaws, Aireen, Shaheen and Jugnu and my brothers for their unwavering love and constant encouragement.

TABLE OF CONTENTS

Chapter **Page**

LIST OF FIGURES

Figure **Page**

Figure **Page**

Figure **Page**

Figure **Page**

Figure **Page**

Figure **Page**

LIST OF SYMBOLS

σ_c	Maximum allowable stress of concrete in compression
ε_c	Allowable strain at σ_c
σ_u	Ultimate strength of concrete in compression
ε_u	Allowable strain at σ_u
σ_i	Concrete stress at strain ε_i
ε_i	Strain in fiber i of the section
E_o	Slope of the envelop curve
ε_p	Plastic strain at unloading
β'	Slope of material (concrete) property curve
σ_t	Tensile strength of concrete
ε_t	Tensile strain of concrete at maximum tensile stress
ε_o	Maximum tensile strain in concrete
E_s	Modulus of Elasticity of steel
f_y	Yield strength of steel
ε_y	Yield strain of steel
E_{sh}	Strain hardening slope of steel
ϕ	Curvature of a R/C section
Δ	Deflection of a member
ρ	Reinforcement ratio

CHAPTER 1

INTRODUCTION

1.0 An Overview

The reinforced concrete columns are a part of lateral force resisting system. In the region of high seismic risk, the response of reinforced concrete columns are very complicated due to complex loading histories that may occur under bi/tri-axial excitations of structure during earthquake motions. During a major earthquake, large uncoupled axial and lateral forces can be developed in the columns of reinforced concrete structures.

Recent analytical and experimental studies indicate that uncoupled variations in the lateral and axial loads plays an important role in the inelastic behavior of R/C structures due to biaxial or triaxial earthquake motions. The complication in response is due to the fact that there are many phenomena which affect the behavior of R/C structures such as cracking and crushing of concrete, yielding of reinforcing steel, strain hardening, slipping and buckling of reinforcement, creep and shrinkage, degree of concrete confinement, etc. Furthermore, under cyclic loading other phenomena such as pinching of hysteresis loops, bond deteriorations and the Bauschinger effect significantly change the behavior of R/C structures. In addition, the axial load also affects the flexural strength, stiffness, ductility, and the energy dissipation capacity of the structures.

Many early studies were performed on columns subjected to axial loads with little or no eccentricity by Fowler (1966), Kent (1969), Sheikh and Uzumeri (1980). They focussed on the effect of transverse reinforcement on the ultimate and post-ultimate strength of reinforced concrete columns. Monotonic loadings are applied until failure and only moment due to eccentricity of the axial load are imposed on the column but no concentric or slightly eccentric loads represents a realistic load

path for a column subjected to strong ground motion. These studies were done under static loads and represents the column behavior under extreme loading conditions. Ramirez and Jirsa (1980) and Rabbat et al (1986) have done some investigations on the behavior of reinforced concrete columns under reversed cyclic constant loading.They have done the analyses for interior columns of frames whereas the exterior columns in frames are not well represented. It is shown that the hysteresis loops for columns under constant axial load are symmetric about the origin of the moment-drift diagram. When a column is under large deformation due to high axial loading, the capacity also decreases becuase of reduction in stiffness, ductility and effective size of section due to spalling of concrete.

Gilbertsen and Moehle (1980) and Epp (1984) conducted the experimental investigations for columns subjected to cyclic axial and lateral loads with constant relative eccentricity. They studied the response of short columns under reversed cyclic lateral loads with both constant and varying axial loads. They emphasized their investigations on the effect of shear behavior of short columns. Epp (1984) used the loading history which had a constant relative eccentricity up to certain axial load at which point axial load was held constant and moment was increased. They wanted to simulate the behavior of an exterior column of a frame structure in the event that hinges were formed on the beams before the hinges developed at the base of the structure. But these studies were done with the axial loads less the balanced capacity of the section.

Emori and Schnobrich (1978) and Keshavarizan and Schnobrich (1984) did the analytical study considering the effect of varying of axial load on the response of R/C frame-wall structures. But in these studies the axial force variation is proportional to moment or lateral load and the level of axial force was small compared to balanced load of the section. The experimental study on nonproportional variations in axial and lateral loads done by Linbeck and Kreger

(1986) has shown that behavior of reinforced concrete section is very much dependent on history of axial force.

The analytical study by Saadeghvaziri and Foutch (1988) showed the effect of non-proportionally varying axial load on post-elastic response of R/C columns. The results of their study indicate that nonproportionally varying axial and lateral loads have significant effect on the post-elastic cyclic response. The hysteresis loops under nonproportional variations in loading does not follow a unique pattern due to phasing of loads. The causes of these behavioral characteristics are explained in the light of axial deformation and axial hysteresis energy.

1.1 Literature Review

So far most of the analytical works discussed on nonproportional loadings are done with current discrete element model which include a one to one correspondence between the elements of the actual frame and the idealized system. However, they are based on set of a predefined phenomenological rules which cannot simulate the interaction between axial and flexural deformation under complex uncoupled variations in axial and lateral loads. Furthermore, the extent and type of damage cannot be evaluated using these models. The experimental and analytical studies done to assess the capacity and performance of the reinforced concrete structures under proportional and nonproportional loadings are reviewed in this section (Kaba and Mahin (1984)).

Gilbertsen (1967) used single component model with two concentrated flexural springs at the ends which modeled the inelastic deformation of a member. Otani and Sozen (1972) used a similar approach to study the response of concrete frame subjected to base acceleration. Takeda et al (1970) then proposed a hysteresis model which better conforms with the results of cyclic loading tests of reinforced concrete connections. The pinching effect associated with shear, bond

deterioration, unequal top and bottom reinforcements in beam and axial load effects in columns were not modeled in the original Takeda model. So a somewhat modified model was introduced by Takayangi and Schnobrich (1976). A thorough study was carried out by Saiidi and Sozen (1979). The shear deformation is neglected, infinitely rigid joints are assumed but the gravity load induced P-Δ are taken into account. Finally a Q-hyst model was developed for Saiidi's study (1979). It differs from Otani's mainly by using softened unloading and load reversal stages. These models did not account for axial load effects, pinching and change in elastic stiffness due to the presence of axial load.

The concentrated spring model is proposed by Chen and Powel (1982) for the dynamic analysis of reinforced concrete frames. The model is capable of representing three dimensional behavior since it takes into account biaxial bending, torsion, and axial load effects. Lai, Will and Otani (1984) developed an analytical model to simulate hysteretic and stiffness degrading behavior of reinforced concrete members subjected to axial load and biaxial bending iteraction. The model seperates the member into two inelastic elements which are composed of individual spring elements simulate the inelastic effects of the member as well as cumulative slip of the anchored bars in the beam-column joint. This model may be used as a practical for three dimensional inelastic analysis and design of R/C structures. Jiang and Saiidi (1990) developed model which uses a hysteretic element consists of four axial springs to analyze the cyclic response of R/C columns subjected to bending and axial loads. The spring sections consist of steel for tensile forces and concrete and steel for compressive forces. The force-deformation relationship is controlled by AQ-Hyst hysteresis model. This model appeared to be successful in simulating the overall response until the axial load is within balanced load limit. Another type of model is the parallel two component formulation proposed by Clough and Benuska (1965 and 1967) known as multi-

component parallel model. The model consists of an elastic element in parallel with an elasto-perfectly plastic element, hence it results in a conventional bilinear hysteresis rule. The elastic portion is assigned a fraction of the members assumed stiffness equal to the proposed post-yield hardening stiffness. The parallel two-component model was used inmany early studies of reinforced concrete structures by Mahin (1974), Powel and Row (1976). The basic bilinear hysteretic formulation would not be expected to result in reliable response prediction for a particular structure and ground motions. Takizawa (1976) modified the two-component bilinear model to better reflect the softening observed on unloading from the yield range and used the modified model to analyze a three-story reinforced concrete frame. In the above two model it is assumed that plastic hinges are developed only at the ends of the members.

Considering the length of plastic hinge region, Hsu (1974) and Takayangi and Schnobrich (1976) proposed a multiple spring model for analyzing wall members. For coupled reinforced concrete shear walls, used the shifting of primary curves technique to account for the interaction of varying axial loads with bending moment in the walls. Emori and Schnobrich (1978) in their study of frame wall structures used single component elements to model beams and columns and multiple spring elements to model the shear walls. Although the multi-spring serial model can represent the behavior of a frame element subjected to a relatively general moment distribution along its length, it still does not directly account for the effect of axial load on member behavior. Meyer et al (1981) proposed a nonlinear reinforced concrete beam element that accounts the spreading of the plastic regions. The model is based on a simplified Takeda moment-curvature relationship.

Next, the analyses for reinforced concrete structures are done using finite element models by Agrawal, Jaeger and Mufti (1976), Schnobrich (1977) using the

plane stress inelastic type of element. Such studies are particularly suited to wall panels. Yuzugullu and Schnobrich (1973) have done the investigation of a shear wall frame under monotonically increasing loading. Suharwardy (1979) used the direct procedure that can take both axial force-biaxial bending moment interactions and stiffness degradation. To study the uniaxial behavior column under nonproportional loading, Saadeghvaziri and Foutch (1988) employed isoparametric plane stress elements for concrete and bar elaments for concrete. Although the correlation with the experimental results were good , but such studies are extremely costly. This is due to the number of elements involved and the nonlinear behavior especially when loads reach significant high levels. To make a dynamic analysis for a large structure, finite element method is very expensive and time-consuming. Though the method is being refined but due to the uncertainties involved in the material and stiffness formulations of the finite elements resulting in approximate results.

1.2 Fiber Model

The fiber model is somewhat more sophisticated than discrete models with a detailed analytical description of the geometry and material properties which are used to evaluate the behavior of critical regions rather than using phenomenological approach with a simplified and predefined set of hysteresis rules. The data necessary to define the fiber are the geometry of the member and section, the stress-strain relationships for concrete and reinforcing steel. Such data is easily available and reliable. The behavior of reinforced concrete structure is quite complicated and quite hard to quantify satisfactorily. The phenomena which effects the response of reinforced concrete structural elements include cracking and crushing of concrete as well as yielding, strain hardening, slipping and buckling of reinforcing steel. Fiber modeling technique is the simplest and

theoretically consistent method of analysis which includes the phenomena stated above and Bauchinger effect and pinching of hysteresis loops. Fiber model is less detailed than finite element model and thus require less storage and computational time.

Mark and Roesset (1976), Ma et al (1976), Emori and Schnobrich (1978) have done an extensive study on fiber model approach to dynamic analyses. The purpose of their study was to investigate the applicability of the fiber model to predict the response of reinforced concrete structure under variations of loadings. Bazant and Bhat (1977) studied the hysteretic response of concrete members using triaxial material properties and deep beam bending theory with transverse shear. Kaba and Mahin (1984) did the dynamic analysis of R/C members with fiber model using multislice fiber element for predicting the inelastic cyclic behavior of R/C columns. The effects of axial loads on strength and stiffness and axial load-bending moment interaction and the pinching of hysteresis loops due to compressive loads acting on the elements are accounted.

It is seen from the studies made by Mark and Roesset (1976), Bazant and Bhat (1977) and Kaba and Mahin (1984) that fiber model is found to be a valuable tool for studying the hysteretic response of reinforced members. These studies included the comparisons of analytical and experimental results which showed that fiber model can provide results that are in good agreement with experiment results and more reliable than phenomenological models.

The procedure is started by dividing member into slices which in turn is divided into concrete and steel fibers. Assuming plane section remains plane, the universal stress-strain history are detemined for each fiber from the given curvature or the strain given at any point of the section along with equilibrium requirement. Linear variation of stiffness between slices is assumed and the forces are calculated using material and sectional properties of the sections. Eventually

moment-curvature relationship are found out considering the effect of axial load. Finally the load-deflection relationship is obtained in element level using the integration method discussed elaborately in chapter 2.

1.3 Objectives

The objective of this study is to develop an analytical model to assess the inelastic response of the reinforced concrete section and/or column due to nonproportional variations in axial and lateral loads which may arise during the bi/tri axial motions due to earthquake loads. Furthermore, the effect of other parameters such as degree of confinement, variations in sectional properties, effect of different levels of nonproportional loading less or greater than balanced capacity of the columns are also investigated.

The structural model is achieved by discretizing the columns into sections which are further discretized into fibers. The inelastic behavior of fibers is monitored by using the material models of concrete and steel. Here the constitutive relationships for concrete and steel are used to generate a model to represent the behavior of a reinforced concrete section which in turn is used to determine the overall response of an entire column. The reinforced concrete section and/or column must be modeled with the following objectives.

a) The model should be capable of handling generalized cross-sections of simple and complex shapes (i,e built up members, composite sections)

b) Complex loading conditions including reversals, sudden changes in loading conditions should be accounted for.

c) It must be able to depict the effect of increase or decrease in stiffness of the columns as a result of the uncoupled variations in axial load and lateral load and its effect on the energy dissipation capacity of R/C member.

d) It should consider the effect of other parameters such as degree of confinement on the response of R/C members subjected to proportional and non proportional variations in the axial and lateral loads.

e) It must be capable of depicting the extent and type of damage to be expected from the uncoupled variations in loadings.

With these objectives in mind, the reinforced concrete section and/or column are modeled using fiber modeling technique. But certain limitations are adopted such as shearing deformations and bond slip will be disregarded at this stage.

1.4 Scope of the Work

The following chapters discuss the theory of the multi-slice fiber model and its use in the analyses of R/C sections and member under proportional and nonproportional axial and lateral loadings. Chapter 2 describes the material properties of concrete and steel and the development of the fiber model to analyze the structural sections to evaluate the general flexural characteristics of cross-section subjected to proportional or non proportional axial forces and/or uniaxial bending moments. Material properties are specified in terms of stress-strain curves using the Hognestad Model for concrete and Bilinear Model and Ramberg and Osgood Model for steel. Cyclic behavior can then be derived from the monotonic envelop using appropriate loading, unloading and load reversal rules.

Chapter 3 discusses the influences of nonproportional axial and lateral loading on reinforced concrete section. Some analyses are done in order to investigate the effects of nonproportional loadings on P-M interaction diagrams. Also the effects on hysteresis loops are studied at different levels of axial loads considering different degrees of concrete confinement and the changes in

unloading/loading paths are also discussed. Some parametric studies are done considering nonproportional loading using sectional and material properties and different levels of axial load for specific curvature distribution of the section. These parametric studies are illustrated by moment curvature relationships and moment-axial load interaction diagrams.

Chapter 4 discusses the analysis on the behavior of reinforced concrete columns due to nonproportional variation in axial loads and lateral loads and the resulting behavoral characteristics due to changes in strength, stiffness and ductility of the structure and comparisons with results of analyses using other available models. Finally conclusions and discussions are presented in chapter 5.

CHAPTER 2

MATERIAL MODELS AND METHOD OF ANALYSIS

2.0 Introduction

Most of the previous study on the behavior of reinforced concrete columns was limited to studies of flexural behavior of reinforced concrete columns under constant axial loads and proportional variations in lateral and axial loads. But recent experimental studies by Kreger and Linbeck (1986) and analytical studies by Saadeghvaziri and Foutch (1988) indicate that uncoupled variations in lateral and axial loads plays an important role in inelastic behavior of R/C columns.

The moment-curvature relationship are generated by assuming the plane section remains plane after deformation. Analytical model developed here is capable of simulating both monotonic and cyclic behavior. Monotonic models considers the member to response to an imposed load or deformation without taking into account changes in the member which may have occurred due to previous loading. Cyclic on the other hand, includes the all behavioral characteristics of the inelastic response of a members. This type of analysis are very complicated and involved many hysteresis rules for determination of the member response based on both previous and current strain-stress relationships.

2.1 Theoretical Development of Model

For a reinforced concrete column, the analysis is done in three levels. Firstly the material level where the behavior of concrete and steel are defined by stress-strain curves which are determined experimentally. Secondly the section behavior is represented by moment-curvature relationship which is derived from the material stress-strain curves. Thirdly, column behavior is defined by load-deformation relationship which are derived from the moment-curvature relationship of the

section. Each of these levels are associated with nonlinearity which causes the changes in stiffness . On the material level, nonlinearity is due to nonlinear properties of steel and concrete. Concrete behaves inelastically from the very low strain level. Steel, although it is assumed to be linear in the post-elastic region, but practically it is nonlinear once the strain exceeds yield strain. On section level, nonlinearity results because section stiffness is very sensitive to axial load. On column level, the nonlinearity arises as the load-deflection relationship is determined from the nonlinear moment-curvature relationship of the sections in columns. The cross-section is divided into a number of fibers. A simple uniaxial state of stress is being assumed and the stress in the concrete and steel fibers are determined from the stress-strain curves. The stress was taken corresponding to the average strain in the fiber. From the stresses and the areas of concrete and steel in each of fiber, after performing the iterations to satisfy equilibrium, the section forces are determined. Furthermore perfect bond between concrete and steel is assumed. The effect of creep and shrinkage of concrete, the effect of temperature and geometric non-linear effects are excluded. The material models implemented in this study are complex enough to reproduce the important non-linear and strength characteristics of concrete and steel are discussed in the following sections.

2.2 Concrete Model

The Model incorporated in the program for evaluating the stress-strain is shown in Figure 2.1 (Saadeghvaziri and Foutch (1988)). It consists of an envelop curve in compression and in tension and a series of rules for cyclic loading. This Model is complex enough to produce the non-linear and strength characteristics of concrete. The Model uses a parabola to define compressive stresses corresponding to strains less than ε_c (the strain at which the stress attains the

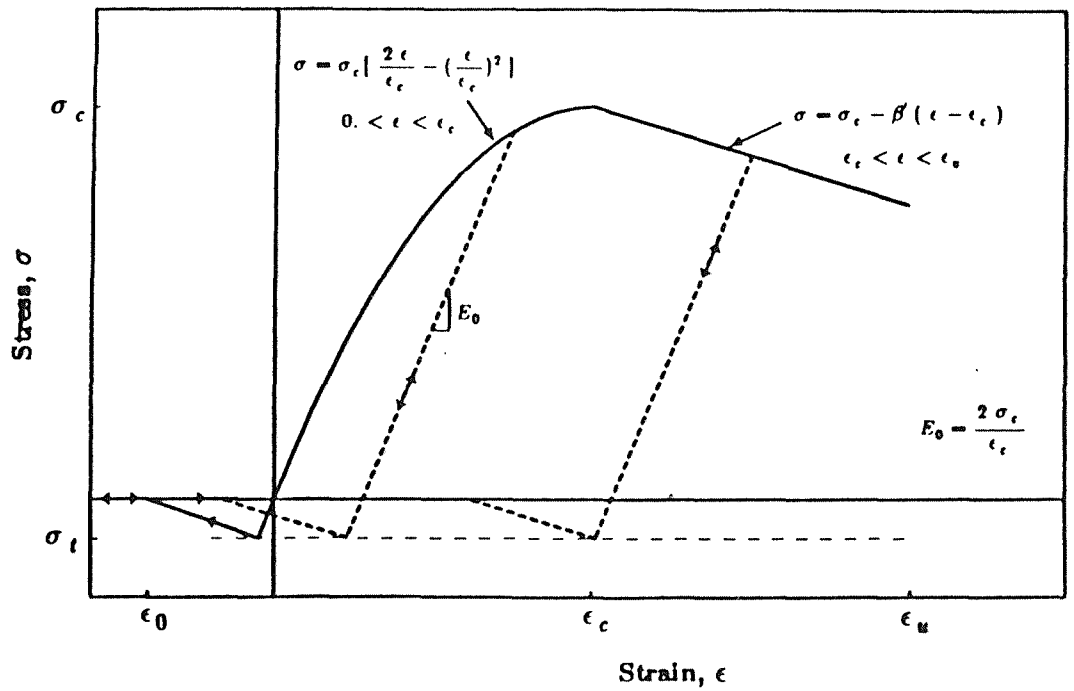

Figure 2.1 Concrete Material Model

maximum compressive stress σ_c) given by Hognestad (1951). This initial parabolic portion is independent of confinement and given by the following expression.

$$\sigma_i = \sigma_c \left[\frac{2\varepsilon_i}{\varepsilon_c} - \left(\frac{\varepsilon_i}{\varepsilon_c}\right)^2 \right] \quad (1)$$

where, σ_i= concrete stress at the strain ε_i, σ_c= maximum allowable strength of concrete in compression, and ε_c= allowable strain at σ_c.

Beyond ε_c the descending portion of the stress-strain relationship is assumed linear with a slope β', β' is a function of ε_c, σ_c and the tie size and spacing. Hence, the rate of decrease of stress with increasing strain, increases with larger tie spacing or smaller tie size.

$$\sigma_i = \sigma_c \left[1 - \beta (\varepsilon_i - \varepsilon_c) \right] \quad (2)$$

Unloading under compressive stress from any point of the envelop curve has slope E_0 until the concrete stress reaches its maximum tensile strength σ_t (Figure 2.2). Then it follows the slope E_1 untill ε_o from plastic strain ε_p. Reloading from this point, the concrete could not take any stress until plastic strain, ε_p, is recovered. Then it follows the slope E_0 until the previous maximum strain is reached. From this point on, the original envelop curve is followed.

Under tensile stress, a bilinear stress-strain relationship is assumed for the concrete as shown in Figure 2.3. From zero to maximum tensile stress of concrete, σ_t, the model assumes the slope of E_0. At this point of stress a crack is initiated and after this point, a descending branch is assigned to the stress-strain curve. Beyond the strain ε_0, the concrete is unable to take any stress and the crack is

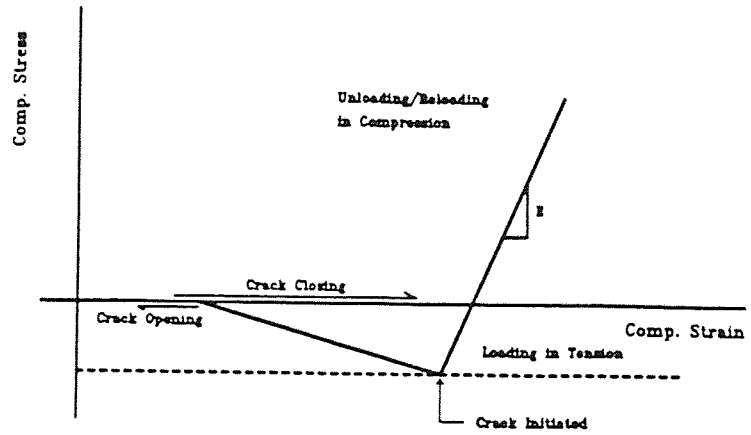

Figure 2.2 Loading and Unloading in Compression

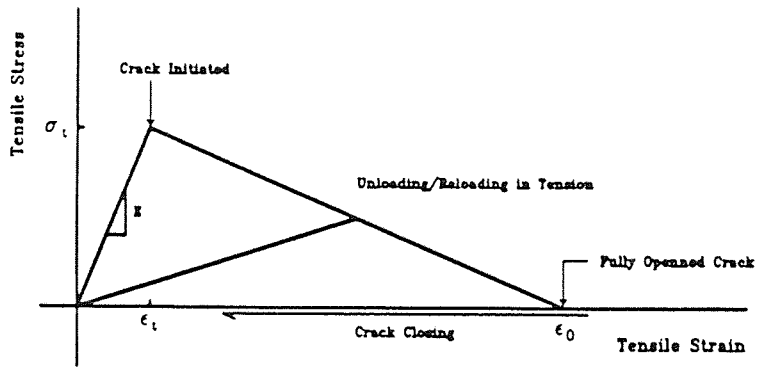

Figure 2.3 Loading and Unloading under Tensile Stress

fully opened. After this strain, the fiber cannot take any stress and the crack is fully opened. Furthermore, it will only resist compression once the crack closes. It is suggested that when the reinforcing steel intersects the cracks at right angle, the value of ε_0 to be taken equal to the yield strain of the reinforcing steel. Modeling of post-cracking in this way accounts for 'tension stiffening' ,i.e., the ability of intact concrete between adjacent cracks to carry tensile stress, but also contributes to the rate of equilibrium convergence. Unloading after initiation of a crack follows a slope equal to the secant modulus of the concrete at maximum tensile strain reached upon loading. Once a crack is closed, it can take compressive stress.

2.3 Steel Model

The steel models incorporated in the program can be referred to as the bilinear elastic-plastic model and the Ramberg and Osgood model . For the bilinear model as shown in Figure 2.4, the only required input are the initial and final slopes and the yield stress. When cyclic behavior is specified, unloading proceeds at a slope E_s until it reaches $2\varepsilon_p$ from where the unloading is started. Then it follows the strain hardening slope E_{sh} until the reloading is started. On reloading it proceeds with a slope E_s until it reaches $2\varepsilon_p$ from the point reloading starts and then it follows E_{sh} again. The model can include both isotropic and kinematic hardening. Kinematic hardening includes the Bauchinger effect which is much more similar to actual behavior of reinforcing steel. The difference between isotropic and kinematic hardening is shown in Figure 2.5 considering a hysteresis loop for the section shown in Figure 3.1 and for P=150 kips.

The input of Ramberg-Osgood model are E_s, f_y, E_{sh}, ε_{max} and σ_{max} (Figure 2.6) and in addition, a polynomial function is used when the stress reverses which was derived by Park,Kent and Sampson (1972).

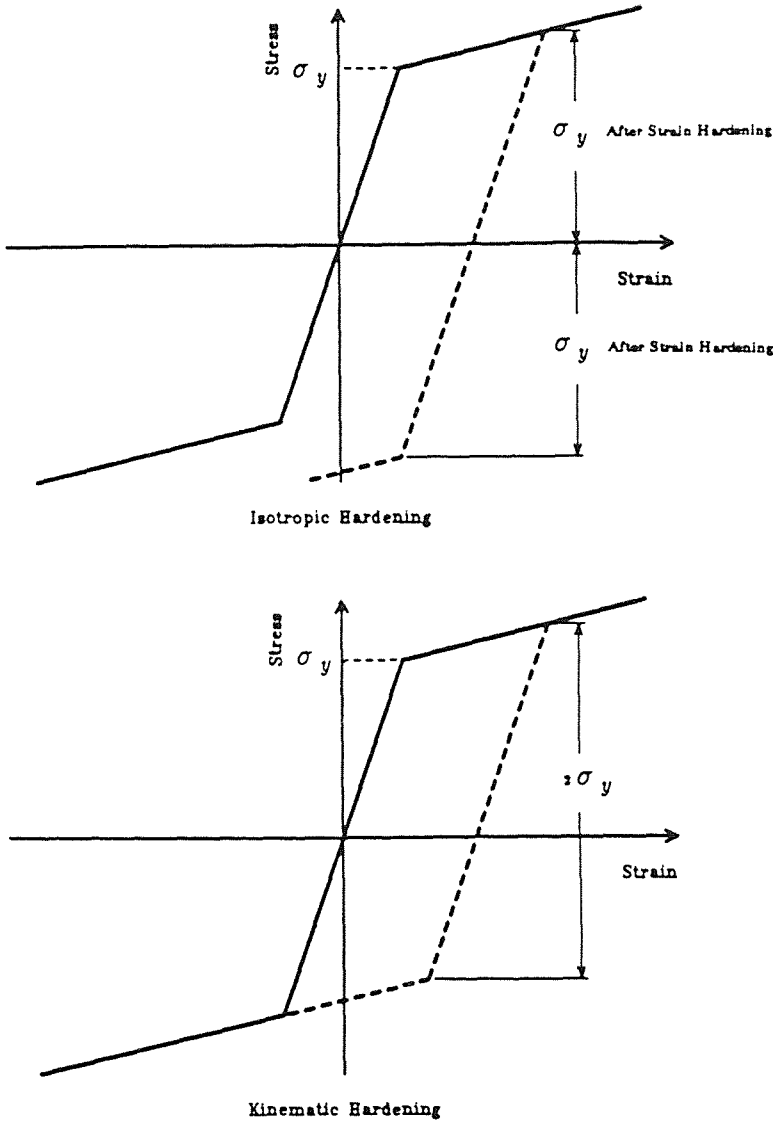

Figure 2.4 Bilinear Material Models for Reinforcing Steel

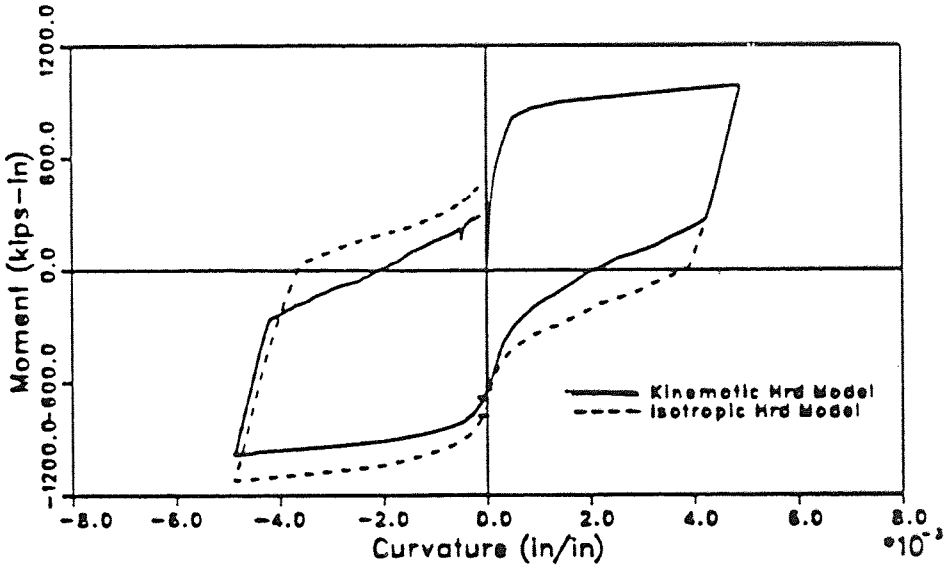

Figure 2.5 Influence of Bilinear Steel Model with Different Types of Strain Hardening on Moment-Curvature Relationships

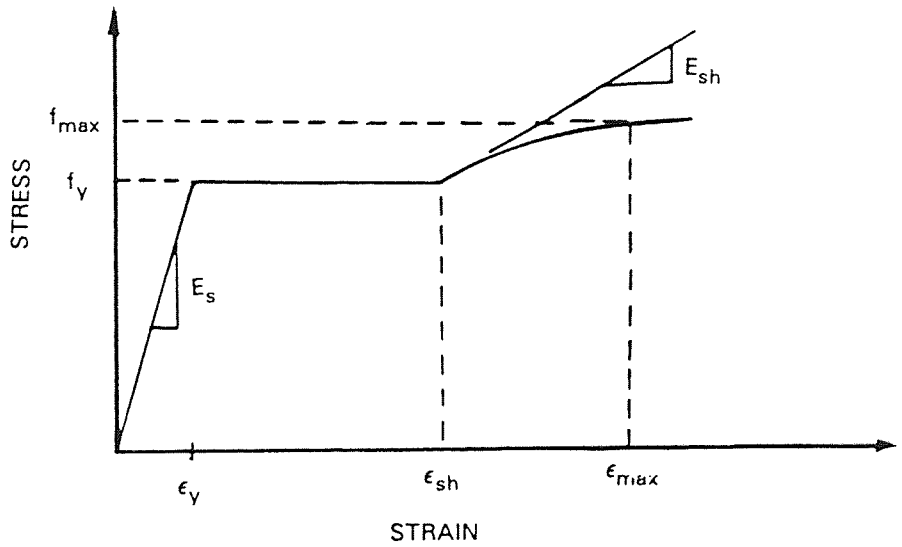

Figure 2.6 Ramberg-Osgood Model for Reinforcing Steel

$$\varepsilon_s = \frac{f_s}{E_s}\left[1 + \left|\frac{f_h}{f_{ch}}\right|^{r-1}\right] \tag{3}$$

$$f_{ch} = f_y\left[\frac{0.744}{\ln(1 + 1000 e_{ip})} - 0.71(1 - e^{1000 e_{ip}} + 0.241)\right] \tag{4}$$

for odd numbered loading runs (n=1,3,5.....)

$$r = \frac{4.49}{\ln(1+n)} - \frac{6.03}{(e_n - 1)} + 0.297 \tag{5}$$

for even numbered loading runs (n=2,4,6,.....)

$$r = \frac{2.20}{\ln(1+n)} - \frac{0.469}{(e_n - 1)} + 3.04 \tag{6}$$

For a Ramberg-Osgood model, an iterative solution is required to evaluate the stress corresponding to a given strain. It is assumed that concrete cover provides sufficient restraint to prevent buckling of longitudinal steel and hence buckling only occur after the adjacent concrete spalls. The difference between bilinear and Ramberg-Osgood model for the reinforcing steel is shown in Figure 2.7 considering the same reinforced concrete section shown in Figure 3.1.

2.4 Model Idealization

To study the response of reinforced concrete columns under proportional and non-proportional variations in axial and lateral loads, an analytical model is

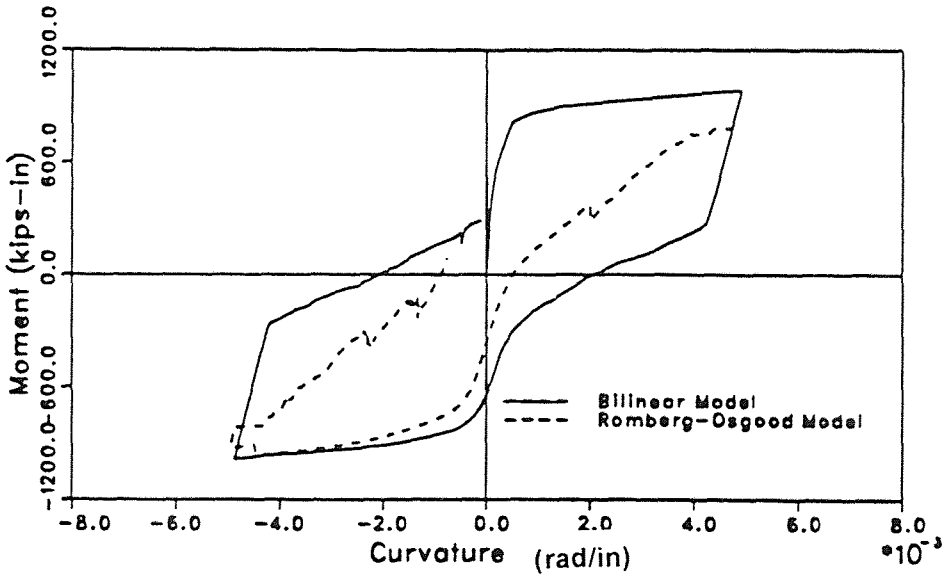

Figure 2.7 Influence of Ramberg-Osgood Steel Models on Moment-Curvature Relationships

required that can account for the effect of changes in the axial rigidity on the flexural behavior of the member. With these objectives, the R/C members are modeled using the fiber model. The fiber model although expensive and time consuming computationally, is capable of simulating the complex behavior of a R/C member under arbitrary loading conditions and histories. The versatility is due to the fact that no predefined phenomenological rules are involved for indicting overall hysteretic behavior of any cross-section. The state of stress is assumed as uniaxial which makes the model computationally more effective and only the stress-strain properties of the constituent materials are required to define the properties of any cross-sections. A computer program is developed to implement fiber model computations which assumes that a column segment consists of uniaxially stressed fibers along its long axis and the section must be symmetric about one axis and the neutral axis must remain perpendicular to the axis of symmetry.

This analytical model is based on two idealizations of the section properties and one assumption about sectional response. First, reinforcing steel is assumed to be concentrated in layers. These layers are assigned an area equal to the actual area od reinforcing steel. The second idealization is the concrete contribution to the section can be represented as a multi-fiber stress zone. The stress zones for these concrete layers has the dimensions of the width of the section and the depth of the neutral axis. Solving for mechanical characteristics of a reinforced concrete section using the fiber model starts by defining the section in terms of layers to which geometric and material data are assigned. Assuming plane sections remain plane, the strains in the various layers of concrete and steel can be calculated from the given strain profile or the curvature of the section (Figure 2.8). Once the strains of the various layers are determined, the stresses can be calculated from the specified stress-strain relationship for concrete and steel. The axial load and the bending moment can be found out by proper

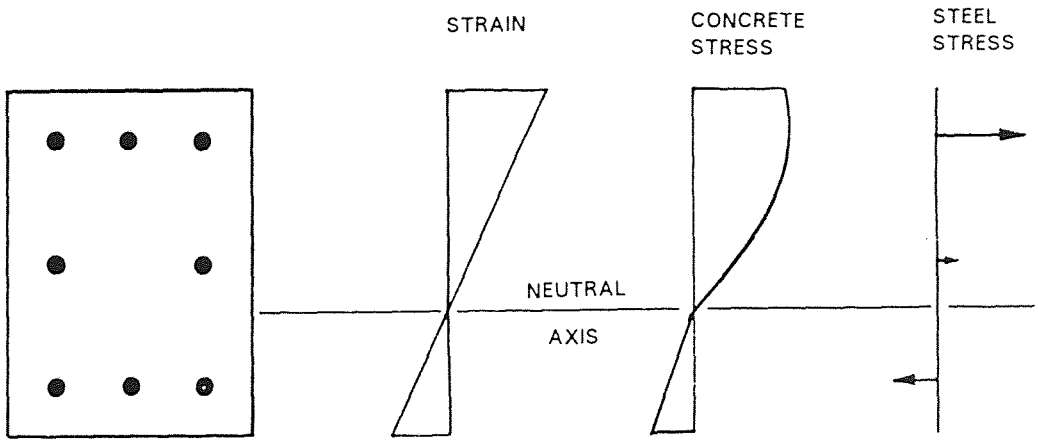

ASSUMPTIONS

1. Linear Strain distribution over cross-section, i.e. plane sections remain plane.

2. Reinforcement concentrated in layers

3. Material behaves as predicted by models discussed in sec 2.2 & 2.3

Figure 2.8 Assumptions for Fiber Model

summation. The most important idealization of the section model is that plane section remain plane for all load combinations. This is a crucial assumption for two reasons. First, it implies that no shear deformation occurs in the column. This is rarely, if ever true. However, shear deformation, in many cases is much smaller than flexural deformation and can be neglected for analysis purposes. Second, the plane-sections remains plane assumption implies a linear strain distribution over the cross-section.

2.5 Section Model

Determination of the axial load-moment-curvature relationship for a reinforced concrete section is accomplished in the following phases. First, limits of responses are calculated based on limits for failure depending on material and sectional properties. These limits keep the search for solutions both confined enough to allow the accurate representation of the response. Once limits have been obtained the next phase begins. In principle to accomplish this phase, sectional and/or column properties such as material properties of concrete and steel, dimensions of the section and/or column and reinforcement ratios are input through the file DATA . Column loads are entered by the data file LOAD and discretized into steps by the subroutine STEP. When the curvature distribution is given, the strain profile is generated by subroutine Profile. Material model are implemented as subroutines. The subroutine CONCRETE defines the stress-strain relationship for concrete whether confined or unconfined. This subroutine is later used by FORCE to determine the stresses in concrete fibers which on summation represents the concrete force in the R/C section. Steel stresses are determined by the subroutine STEEL calculated from the steel strain which in turn used by FORCE to determine the steel force in the section. MOMCAL is the routine which calculates the bending moment for a axial load and the specified curvature or strain profile.

2.5.1 Solution Strategies

Several types of analyses can be performed for determining axial load, moment-curvature relationships on section level by using the following procedures:

(a) A strain profile is specified, the program calculates the axial load and bending moments for a sets of neutral axis position. No iterations are involved in this type of analysis.

(b) The axial load is specified which may be constant or varied and the strain is given at a point. The moment capacity with the distribution curvature is sought. An iterative approach is used on the strain profile for a neutral axis position until the calculated axial load converged to the specified value sought. This permits the evaluation of the cracking moments, the moment at which tension or compression reinforcements yields and also considers the options when the axial load varies nonproportionally during the steps.

(c) The curvature and axial load is specified and the moment-curvature relationship under the axial loading is needed. The program calculates the bending moment when the initial curvature, the number and magnitude of curvature increment and the applied axial load/loads are specified.

(d) The axial load and the lateral load are specified and the load-deflection relationship is sought. The program assumes an initial value of curvature and neutral axis and iterates on both to find the required value for axial load and the bending moment for the lateral load. With the options discussed above, relatively complex load histories can be considered.

2.5.2 Determination of Strain Profile

Since plane section are assumed to remain plane, the strain at any location of the fiber of the reinforced concrete section can be found out using the formulas discussed below adopted from Kaba and Mahin (1983) and Park and Pauley

(1975). It is to be noted that all distances considered are from top of the section.

(a) When the strain at a given location and the curvature of the section is given, the strain at the center of a fiber i is given by

$$\varepsilon_i=\varepsilon_g+ (y_i-y_g)\phi \quad (7)$$

ε_i= the strain sought at distance Y_i for fiber i

ε_g= the given strain at location Y_g

ϕ= curvature of the section

(b) When the neutral axis location is known along with the curvature, the strain at point i of the section is given by

$$\varepsilon_i = (Y_i - Y_{na}) \phi \quad (8)$$

Y_{na}= distance to neutral axis from the top of the section.

2.5.3 Analysis Methods

(a) For noniterative analysis, the input consists of a specified strain profile or the strain given at specified location with neutral axis positions. The section is divided into a number of fibers. With the given strain distribution, the stresses are found out from the strain profile using the material stress-strain relationship of concrete and steel by using the routine CONCRETE and STEEL respectively. Total force is found out by summation of all forces for concrete and steel multiplied by the corresponding areas of concrete layers or reinforcing steels.

Axial load P as a summation of all forces in concrete and steel layers is given as

$$P = \sum_{i=1}^{NC} \sigma_{ci} A_{ci} + \sum_{j=1}^{NS} \sigma_{sj} A_{sj} \quad (9)$$

Then the bending moment M is determined by the routine MOMCAL which is defined as

$$M = \sum_{i=1}^{NC} \sigma_{ci} A_{ci} (y_{ci} - y_p) + \sum_{j=1}^{NS} \sigma_{sj} (y_{sj} - y_p) \qquad (10)$$

NC is total number of concrete fibers, NS is total number of steel fibers, A_{ci} is area of concrete fiber i, A_{sj} is area of steel fiber j, Y_{ci} is distance of concrete fiber i from the top of the section, Y_{sj} is distance of the steel fiber j from the top of the section, Y_p is the distance of the plastic centriod from the top of the section, and σ_{ci} is the stress in concrete fiber due to the strain ε_i at the fiber i, and σ_{sj} is the stress in steel fiber due to the strain $\varepsilon_j(=\varepsilon_i)$ at the fiber j (the flow chart is shown in Figure A-1)

(b) For iterative analysis, two types of analyses are encountered such: 1) the axial load is specified with curvature or strain at any point and moment-curvature relationship is sought, and 2) the axial load and lateral load both are specified for which the load-deflection relationship is sought. For the first case, where the axial load and curvature distribution is given. The analysis starts with a given curvature or strain and a value for the neutral axis position, Y_{na}, is assumed. The stresses in the fibers are computed for this strain profile. Consequently, the forces acting on the elements are calculated using the eq.9 and equilibrium is checked with the given axial load as follows:

$$P_{cal} - P_{given} = \text{tolerance limit}$$

If the equilibrium is not satisfied, the estimated neutral axis position is adjusted using regular falsi method until the equilibrium of forces is achieved. Actually the following strategy is followed. Lower and Upper bounds (Y_{min} and Y_{max}) are set on the possible position of the neutral axis. Corresponding axial loads (P_{min}

and P_{max}) are determined. The bounds are expanded until the required axial load is bracketed by Pmax and Pmin. This is the point where the iteration starts by the following expression (the flow chart is shown in Figure A-2)

$$Y_{target} = Y_{min} + (Y_{max} - Y_{min})\ (P - P_{min})/(P_{max} - P_{min}) \qquad (11)$$

If the axial load corresponding to this neutral axis position does not fall within convergence tolerance, a reduced interval which brackets the solution is adopted and another iteration is performed. Having obtained the equilibrium, the bending moment for the corresponding axial load is determined using eq.10. In any case when the strain at a particular location is specified, the curvature is determined from the following equation

$$\phi = \varepsilon_g / (Y_g - Y_{na}) \qquad (12)$$

ε_g= the specified strain at a location Y_g, Y_{na}= the distance of neutral axis position from the top of the section.

For the second case when the axial and lateral load are given, the analysis starts with a value of assumed curvature and iterated over the neutral axis positions until the axial force is reached the user specified tolerance as stated before. Then the bending moment is determined for the calculated axial load and checked with the specified bending moment due to the lateral load and if not satisfied, the value of curvature is readjusted by the procedure adopted for finding neutral axis position until the computed bending moment reaches the specified bending moment (the flow chart is shown in Figure A-3).

To assess the accuracy of the analytical model, a test is being done with the experimental data from Kent (1969). The cross-section shown in Figure 2.9, has equal areas of tension and compression reinforcement. The longitudinal reinforcement consists of two No 4 bars for top and bottom reinforcements. The transverse reinforcement consists of No 2 bars at 2" on centers. The longitudinal steel has yield strength of 48.4 ksi. Concrete compressive strength of 6.95 ksi and

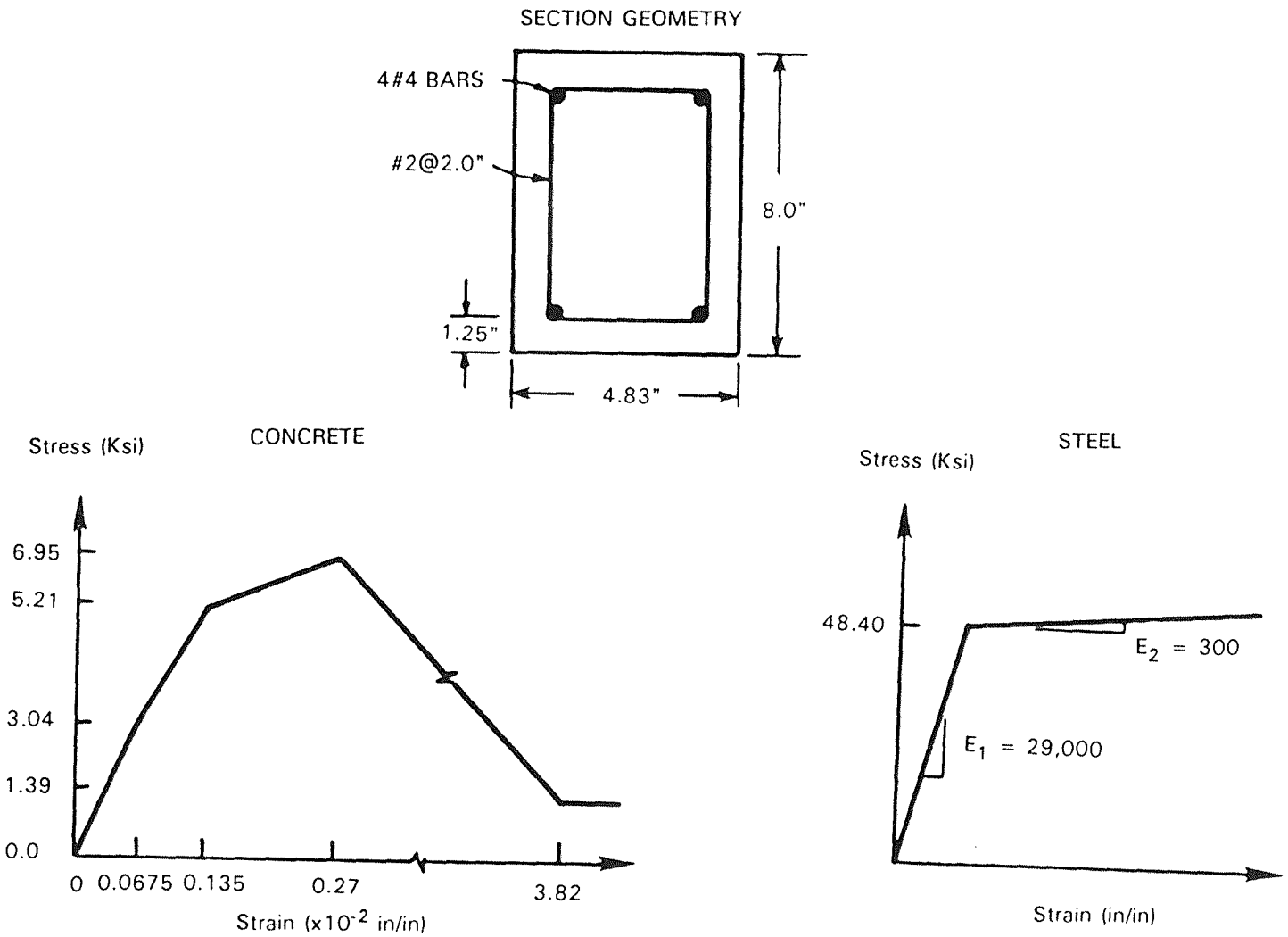

Figure 2.9 Sectional and Material Properties for the Example Section

a concrete tensile strength of 0.95 ksi was experimentally determined.

The material properties are shown in Figure 2.9. Analytically determined moment-curvature curve are compared with the experimental curve in Figure 2.10. Comparison of the experimentally and analytically determined moment-curvature relationship indicates good agreement. As noted by Kent (1969) that under reversal loading after yielding, the section is often cracked over its entire depth in the working strength range and the behavior is completely governed by the steel couple. This accounts in part for the significant reduction in stiffness observed in this range. There is also an increase in stiffness when the section is under increased loading, eventually the crack closes on the compression face and the concrete starts to participate again. Bilinear model is used for reinforcing steel. Both models account for strain reversals in cyclic loadings.

Next three analyses are made with P=0, P=16.75 kips and P=-16.75 kips respectively for the same curvature history. When P=0, the moment-curvature relationship shows that initially on loading and unloading phase, the curve is stiffer due to concrete action. Subsequently, on unloading, when the section starts cracking is incapable of carrying tension. As a result there is a reduction in stiffness and reduces moment capacity compared to the corresponding values in initial loading (Figure 2.11). For the second analysis the axial load is assumed as P=16.75 kips, the initial loading follows the same curve as the previous one with higher moment capacity but pinching effect is more prominent on unloading. As it is symmetrically reinforced concrete section, the crack on the compression side must be closed so that concrete fiber participates again before the steel on the tension side yields. This compression yielding and closing of the crack causes a sudden increase in the section stiffness which causes pinching action on the hysteresis loop as shown in Figure 2.12. In the third analysis axial force is P=-16.75 kips, here concrete affects the section behavior at the initial phases of

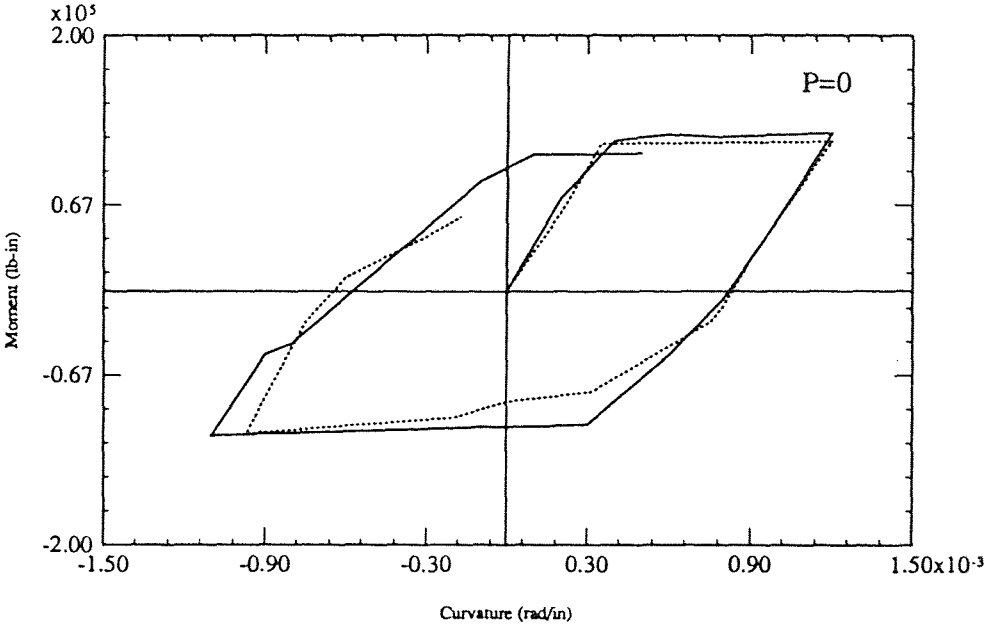

Figure 2.10 Comparison of Analytical and Experimental Moment Curvature Relationships under Constant Axial Loading

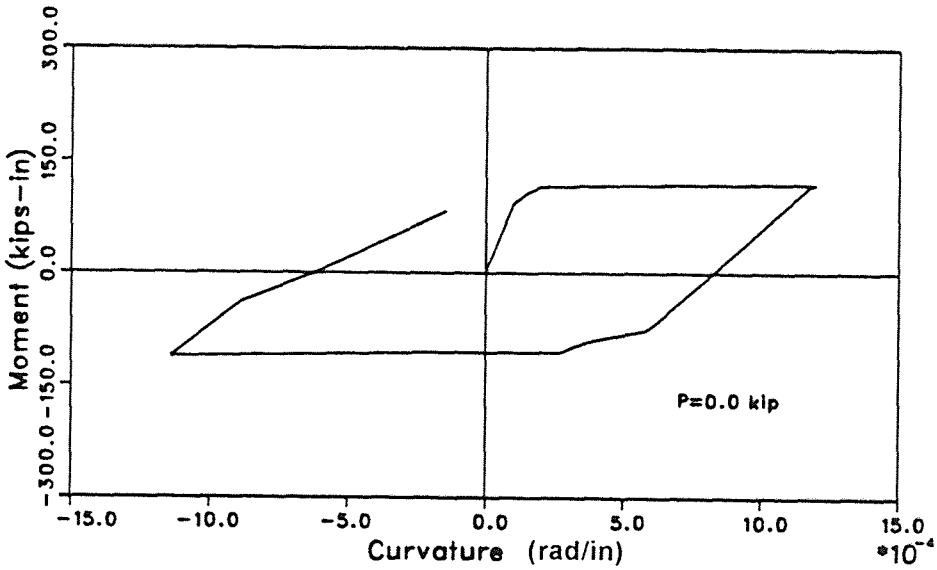

Figure 2.11 Moment-Curvature Relationships for Constant Axial Loading P=0

loading and unloading, beyond that concrete cracks and the section reduces to steel couple. At the initial phase of loadings, the tensile load makes the section to crack and as the moment is applied, the crack closes on the other side increasing the effective stiffness of the section until the yielding of tensile steel as shown in Figure 2.13.

2.6 Column Model

In the present study, the column is divided into several slices/elements where the section in turn is divided into some fibers. To obtain the load deformation relationship for a reinforced concrete column, the material properties of concrete and steel are used to determine the moment-curvature relationship as described in section model. Then column model uses an iterative approach to solve for the lateral load-lateral displacement relationship. The flow chart of this method is shown on Figure A-4. The specified loading program is first divided into number of steps and the column is divided into a number of segments dx which are at a distance x from the free end of the column as shown in Figure 2.14. Each section has width b and depth h. Then, for each load step an estimate of the column end moment is made and equilibrium is satisfied individually for each segment. If the equilibrium is not satisfied, the curvature for the moment is revised and the procedure is repeated. The deflection for the column at the free end is determined by using the formula described below and its flow chart is shown in Figure A-5.

2.6.1 Formulation for Load-Deflection Responses

If the moment curvature relationship for the sections of a member are known, then theoretically, the rotation between any two points A and B is given by Park and Paulay (1975) as shown in Figure 2.14.

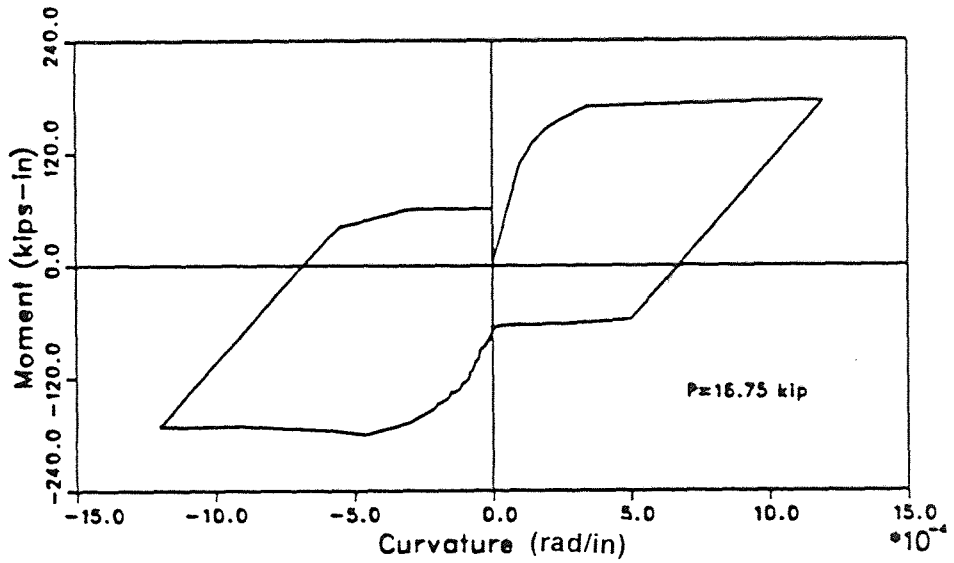

Figure 2.12 Moment-Curvature Relationships for Constant Axial Loading P=16.75 kips

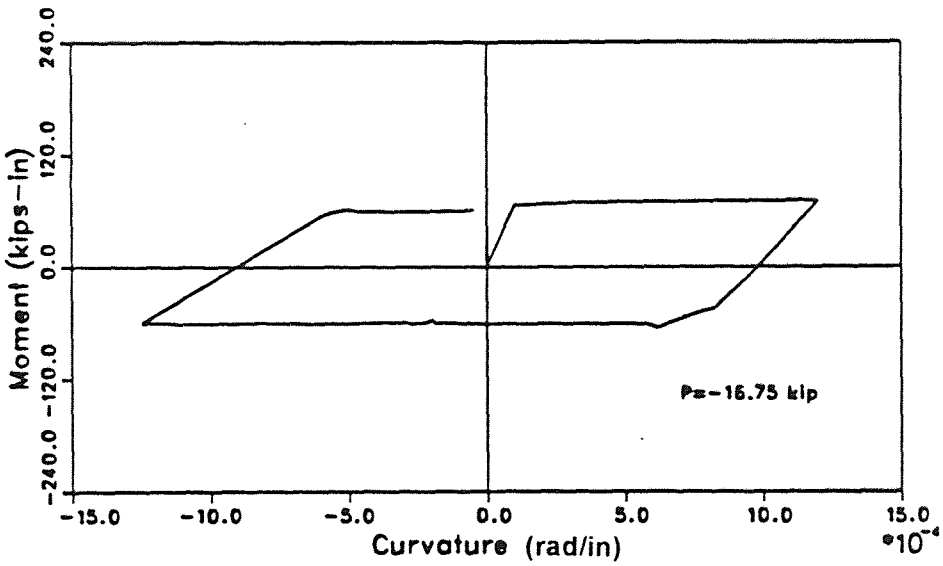

Figure 2.13 Moment-Curvature Relationships for Constant Axial Loading P=-16.75 kips

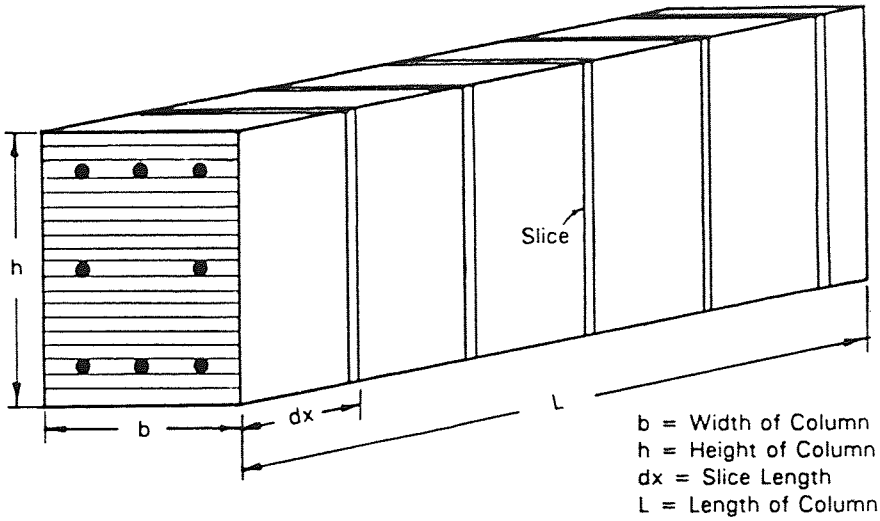

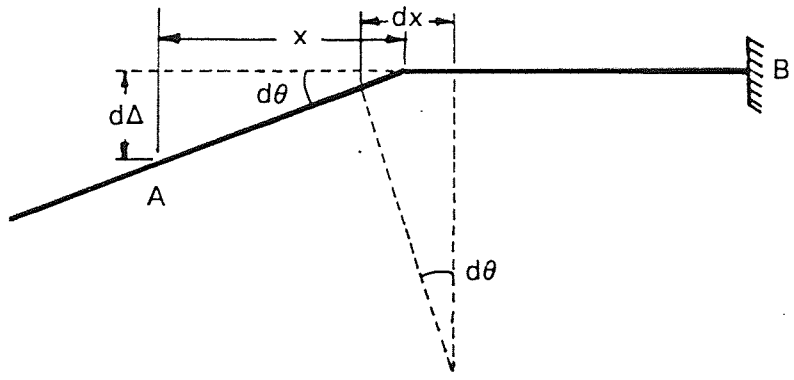

Figure 2.14 Load-Deflection Relationship for the Column Model

$$\theta_{ab} = \int_a^b \theta ds \tag{13}$$

in which ds = an element of length of the member

The transverse deflection of point A from the tangent to the axis of member at point B is given by

$$\Delta_{ab} = \int_a^b x\theta ds \tag{14}$$

Where, x is the distance of element dx from A.These equations ignores the effect of increase of stiffness of member due to tension caused by the diagonal tension cracks due to shear and by bond slip of the reinforcement.

2.7 Convergence Criteria and Tolerance Limit

In the Incremental methods which are used in the fiber model where nonlinear equations are used in the material models, a criteria should be set for the limit of iterations. Such criteria would indicate the signal whether it is the end of solution for that increment within the present tolerance limit or the solution is diverging away from the solution. There are two convergence criteria used in the program. For the analysis of moment-curvature relationship, only axial load convergence is checked if it is within a certain limit which is already set. For analysis of load-deflection relationship, moment convergence for given axial and lateral loads also is checked through the iteration methods. There may arise problem with the criteria which happens when a small change in loads results in large displacement especially for a small increase in axial loads in elastic-plastic zone enters into the plastic zone. Increment size of loads, curvature/strains and neutral axis and tolerance limit are the important factors responsible for the convergence of an

iteration in the nonlinear analysis.

2.7.1 Reasons for Nonconvergent Solutions

The user should set a convergence tolerance for axial load and bending moment and the number of iterations and expansion limit for curvature and neutral axis to get the solutions. If no solution is found within the set number of iterations and expansions, it may be due to the following causes:

(a) There may be no solution possible with specified section properties and the loading histories.

(b) The load steps for axial load and lateral load may be too small or too big for the tolerance limit set for the equilibrium, which may be remedied by changing the loadsteps and convergence limits.

(c) The initial pair of bounds for neutral axis or curvature may be too large. So the user can achieve solution by choosing smaller set of bounds and small bound expansion increments.

(d) The number of bound expansion is insufficient in some cases, the solution may be obtained by increasing the number of bound expansions.

(e) Sometimes the solution cannot be obtained after the neutral axis is bounded, it could be remedied by increasing the convergence tolerance or the number of iterations.

(f) Solution cannot be obtained due to numerical problems, abrupt changes in material properties, specifying large curvature increment, which could be solved by decreasing the load step of axial or lateral load, changing iteration method, varying the bound expansions for neutral axis and curvature etc.

2.8 Conclusion

This technique has the disadvantage of being relatively slow in analyses, but it has the advantage of coping with the unusual stress and curvature distributions which result from cyclic proportional and non-proportional loadings and it is simple to alter the element forces for area reduction due to spalling and to record which elements have cracked.

CHAPTER 3

EFFECT OF NONPROPORTIONAL AXIAL LOADS ON R/C SECTIONS

3.0 Introduction

The axial load has a significant effect on the inelastic behavior of the reinforced concrete columns. The presence of axial load affects the flexural strength, energy dissipation capacity, stiffness and ductility of reinforced concrete members. Most of the previous research on the behavior of reinforced concrete columns are limited to the study of flexural behavior under constant or proportionally varying axial loads. However recently a limited analytical and experimental studies have considered the variation of axial load are by Saadeghvaziri and Foutch (1988), Abrams (1987) and Kreger and Linbeck (1986). Their study showed the importance of uncoupled variations of axial and lateral load on the response of a concrete column. When a structure is subjected to biaxial or triaxial earthquake motions in the horizontal plane, large uncoupled variations in axial and lateral loads may arise (for example in the corner column of a highrise building). Furthermore, Saadeghvaziri and Fouch (1988) have shown that vertical component of an earthquake motion can excite highway bridges which produces nonproportional variations in forces in piers and abutments. Thus, nonproportional axial and lateral forces can be developed in the columns of a structural system due to horizontal as well as vertical component of earthquake forces.

The purpose of this chapter is to investigate the effect of nonproportionally varying axial and lateral loads on a reinforced concrete section. The effects of confinement, different levels of axial loads which are less or greater than balanced load Pb, capacity of a section represented by P-M interaction diagrams, the nature of hysteresis loop under nonproportional loadings are also investigated. The example section and properties are shown in Figure 3.1. This example section was

used in analytical tests by Saadeghvaziri (1990) under nonproportional axial and lateral loadings.

3.1 Influence of Nonproportional Axial Load History

Nonproportional axial load along with the lateral load has a significant effect on inelastic behavior of a reinforced concrete section. In this part of analysis, the objective is to investigate the effect of nonproportionally varying axial loads at different levels (less or greater than balanced load) on the moment capacity of the section. The effect of loading history is considered and the analysis is carried out for fully confined (ε_u=0.1, σ_u= 5500 psi), partially confined as 1% (ε_u=0.025, σ_u=0.0) and unconfined (ε_u=0.004, σ_u=0.0) concrete.

The analysis is carried out in three phases, for proportional loadings, first the analysis is carried out for constant axial load P=0 and P=P_x , the value of axial load for which the analysis is conducted throughout the curvature distribution. For nonproportional loading, value of curvature is assumed and the bending moment corresponding to axial load P=0 is determined. Holding the curvature constant the axial load is increased to the value P_x assumed for proportional analysis. Taking account of strain-stress history for P=0 as the initial condition, the bending moment is found out for P_x . Thus for each curvature increment throughout the curvature distribution, the moment capacity for both proportional and nonproportional loadings are compared to see the effects of nonproportional loading.

First, the analysis is done for proportional and nonproportional axial load with P=100 kips which is lower than balanced load for the section. For confined concrete, it is seen that the moment capacity for nonproportional case is significantly lower than the capacity anticipated for proportional axial loading at P=100 kips. After the curvature, ϕ= 0.0085 rad/in, the moment capacity for

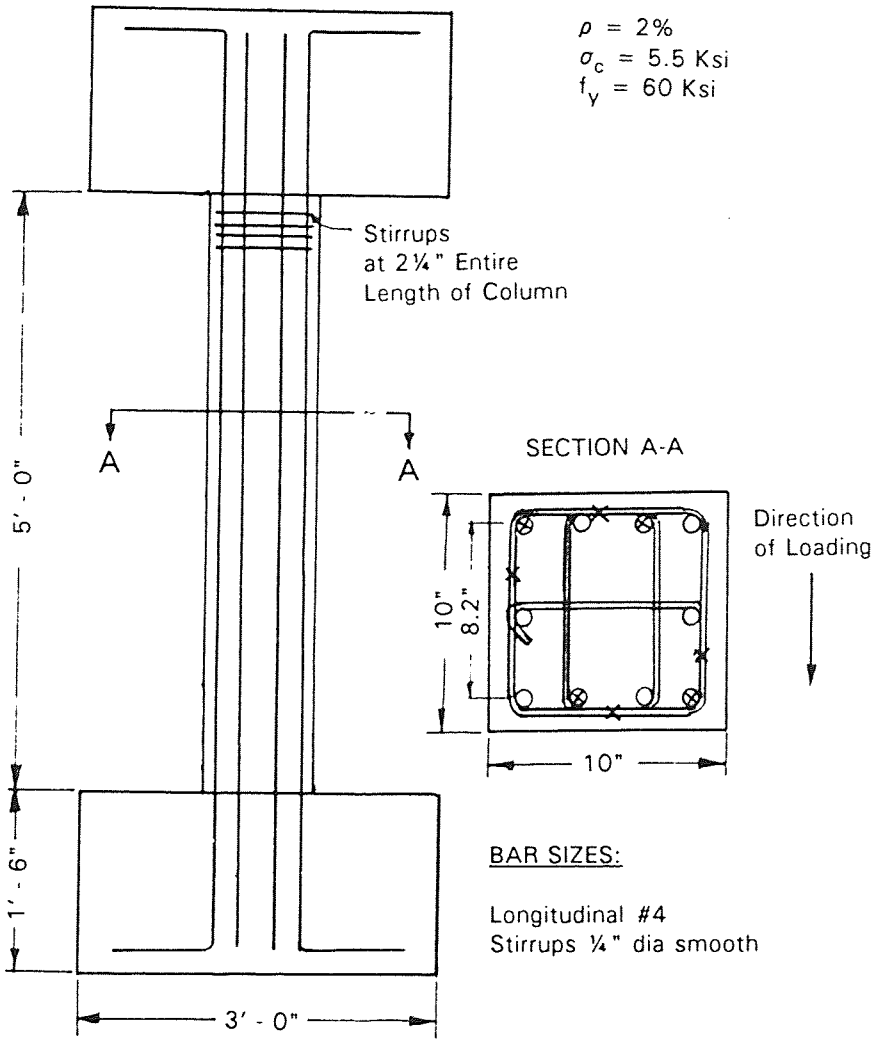

Figure 3.1 Details of the Experimental specimen

nonproportional P=100 kips is less than that for P=0 (Figure 3.2), For unconfined concrete, the moment capacity for nonproportional loading is greater than that for P=100 kips as proportional loading till ϕ= 0.0045 rad/in. Then it decreases after ϕ=0.006 rad/in below the capacity at P=100 kips (proportional) as shown in Figure 3.3. For 1% confined concrete, the moment capacity for nonproportional loading is greater than that at proportional loading P=0 kips and less than that for P=100 kips (proportional) up to ϕ=0.0065 rad/in. After that the moment capacity for nonproportional loadings stays almost constant and having the same capacity as for P=100 kips (proportional) after ϕ=0.01 rad/in as shown in Figure 3.4. In Figure 3.5, all the three curves for nonproportional loading are plotted. The moment capacity peaks higher for the greater confinement as anticipated.

Second, the analysis is done for P=200 kips which is around the balanced load. For confined concrete, the capacity for proportional and nonproportional loadings are same untill yield moment. Then the moment capacity due to nonproportional loading significantly reduces to almost the capacity at P=0 with increase of curvature after ϕ= 0.006 rad/in (Figure 3.6), For unconfined concrete, moment capacity for proportional and nonproportional loading decreases sharply after the yield moment with the increase of curvature as shown in Figure 3.7. The moment capacity for nonproportional loading reduces to zero at ϕ=0.0012 rad/in. For 1% confined concrete, the moment capacity is below the moment capacity for proportional axial load with P=200 kips, upto ϕ=0.00425 rad/in. Then it increases beyond the capacity for proportional loading P= 200 kips but far below that of moment capacity at P=0 as shown in Figure (3.8).The three curves of non-proportional loading are plotted together, it is seen that upto ϕ=0.0045 rad/in, the moment capacity for 1% confined concrete is lagged by a small amount but beyond this curvature, the moment capacity decreases significantly than the capacity for the confined concrete (Figure 3.9). For unconfined concrete, the

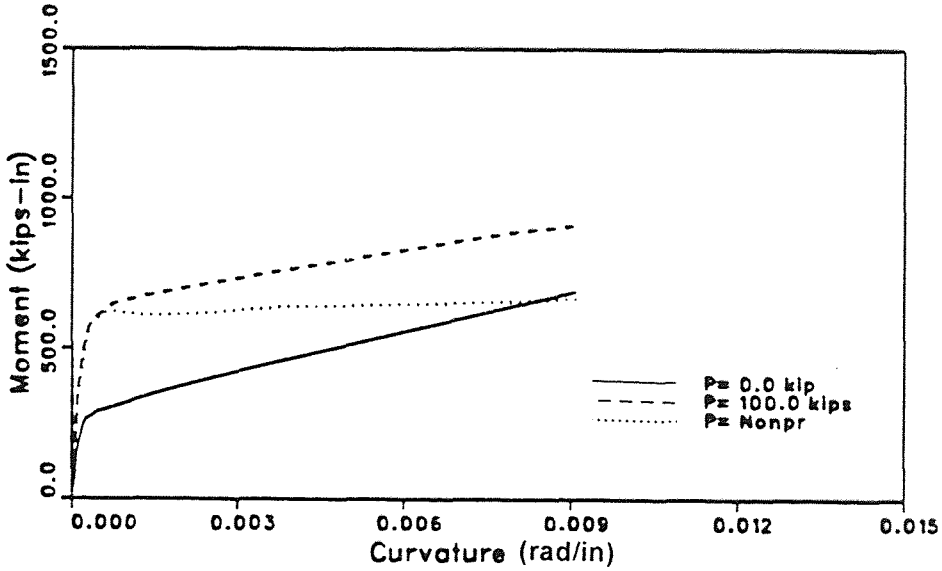

Figure 3.2 Moment-Curvature Relationships for Proportional and Nonproportional Loadings (P= 100 kips ($P<P_b$), Confined Concrete)

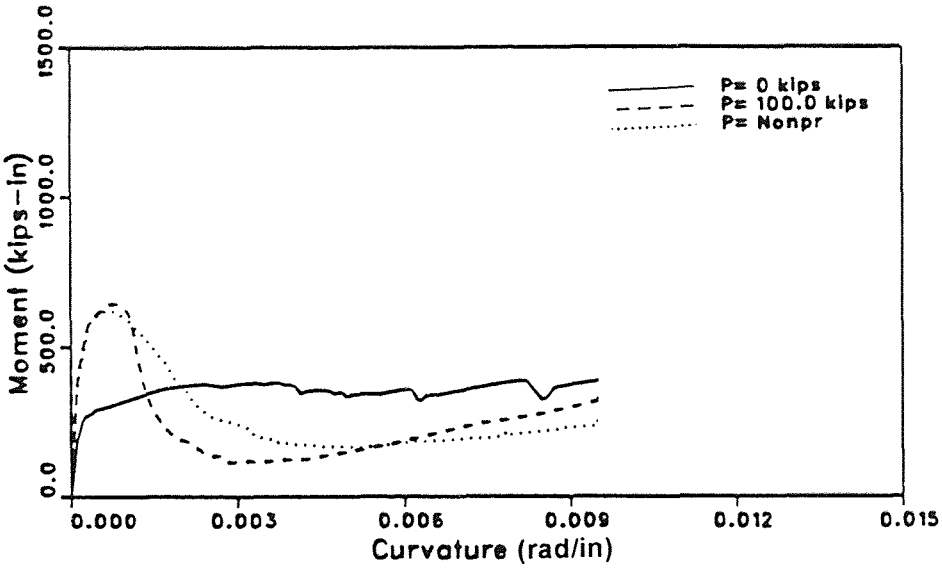

Figure 3.3 Moment-Curvature Relationships for Proportional and Nonproportional Loadings (P= 100 kips ($P<P_b$), Unconfined Concrete)

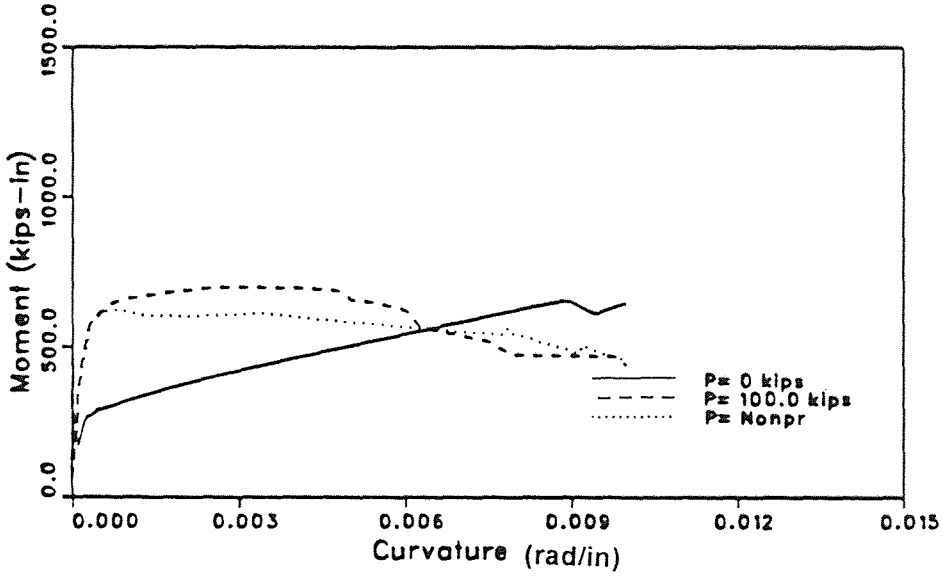

Figure 3.4 Moment-Curvature Relationships for Proportional and Nonproportional Loadings (P= 100 kips ($P<P_b$), 1% confinement)

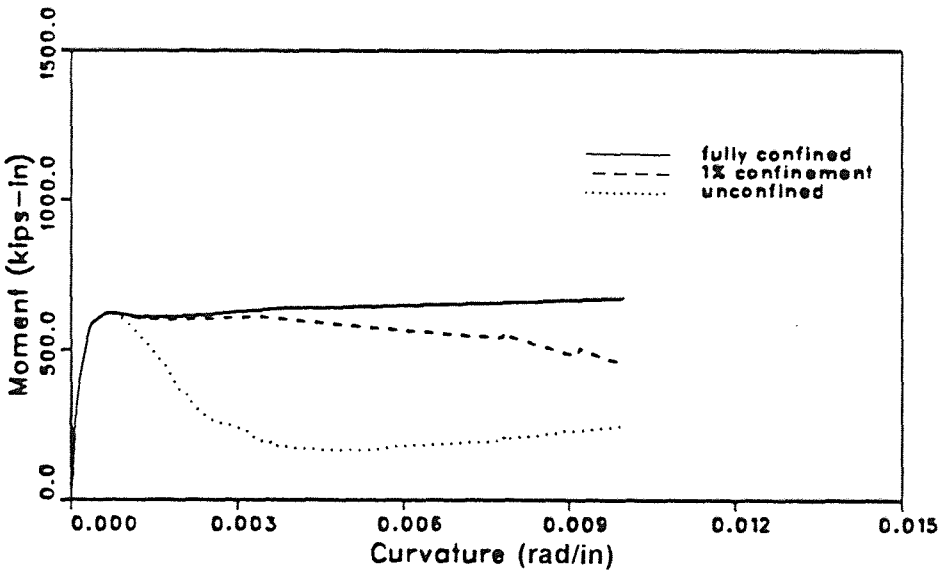

Figure 3.5 Moment-Curvature Relationships for Non-Proportional Loadings at Different Degrees of Confinement (P= 100 kips)

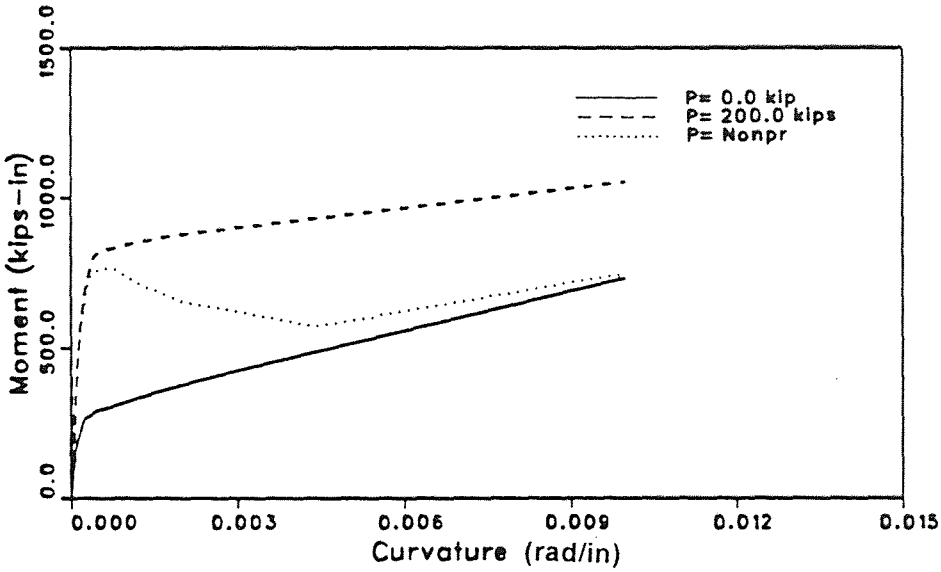

Figure 3.6 Moment-Curvature Relationships for Proportional and Nonproportional Loadings (P= 200 kips ($P \approx P_b$), Confined Concrete)

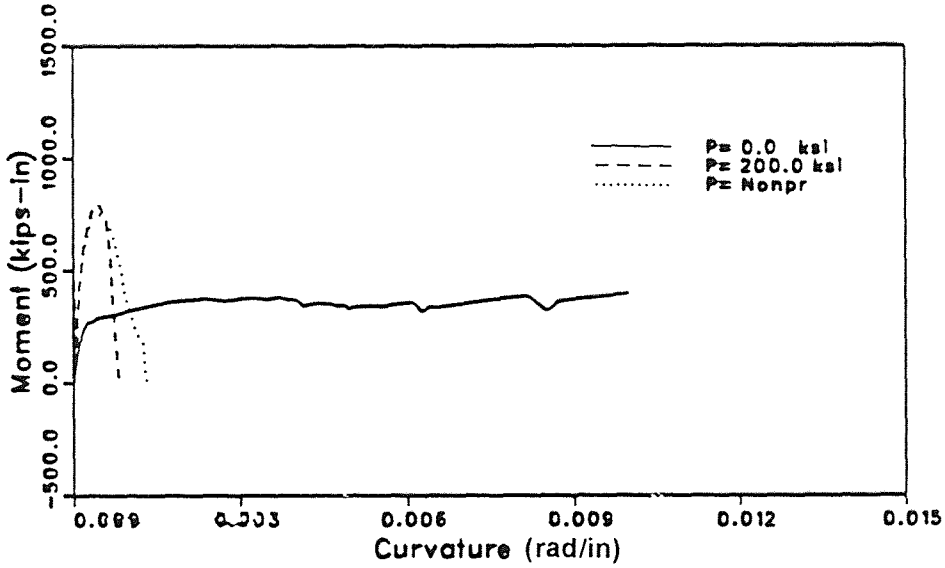

Figure 3.7 Moment-Curvature Relationships for Proportional and Nonproportional Loadings (P= 200 kips ($P \approx P_b$), Unconfined)

moment capacity drops right after the ultimate capacity and decreased to zero with a small increase in curvature.

The axial load beyond the balanced load is used in this analysis as P=300 kips. For confined concrete, the moment capacity for non-proportional loading for P=300 kips is significantly less than the capacity for P=300 kips as proportional loading throughout the curvature distribution having the same slope (Figure 3.10). For unconfined concrete, the moment capacity for proportional and nonproportional loadings decreases abruptly right after the yield moment and both of them reduce to zero at the same curvature ϕ=0.00065 rad/in. Actually they follow the same slope and are decreasing with the increase of curvature (Figure 3.11), whereas for 1% confined concrete, moment capacity is slightly higher in case of nonproportional loading after ϕ=0.0017 rad/in and reduces to zero at ϕ=0.004 rad/in (Figure 3.12).

The moment-curvature relationships at different degrees of confinement for the nonproportional axial load are plotted in Figure 3.13. It is to be noted that moment capacity attains higher value with higher degree of confinement. For confined concrete, the moment capacity increases with curvature but for partially confined and unconfined concrete, the moment capacity start decreasing after the ultimate moment and reduces to zero after ϕ=0.003 rad/in.

Then the analyses are made for nonproportional tensile axial loading. Different kind of behavior is observed during tensile loading. For non-proportional loading P=-20 kips, the moment capacity is higher than the moment capacity at P=0 and proportional P=-20 kips (Figure B-1) . It is to be noted that three curves for moment-curvature relationship followed the same slope with different capacity as curvature increases. But for unconfined concrete, the moment capacity for nonproportional loadings stays almost the same as that for proportional loadings

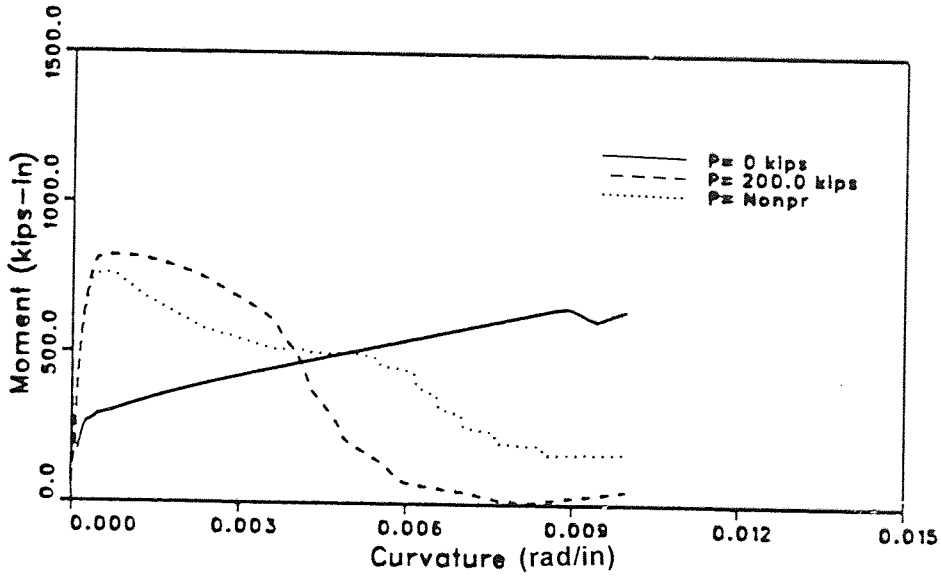

Figure 3.8 Moment-Curvature Relationships for Proportional and Nonproportional Loadings(P=200 kips ($P \approx P_b$), 1% Confinement)

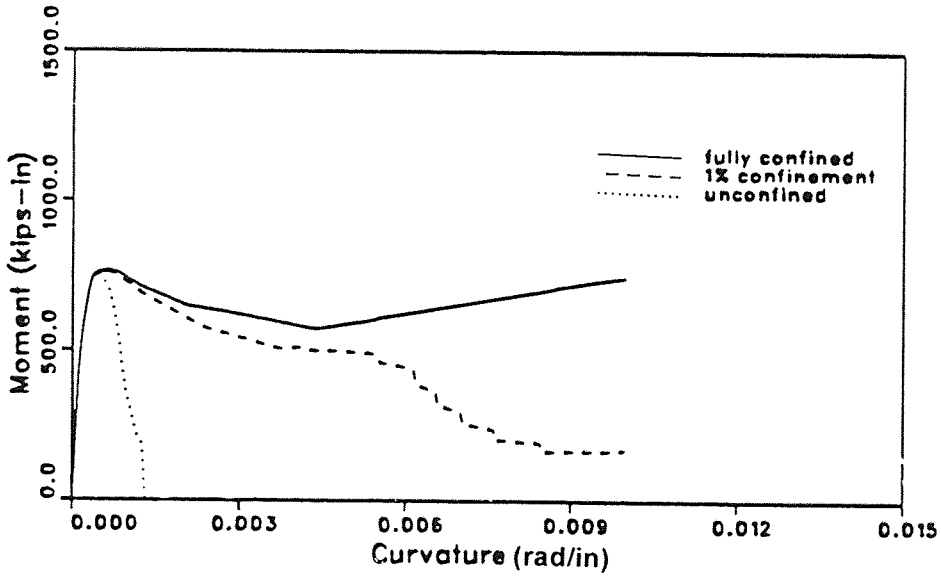

Figure 3.9 Moment-Curvature Relationships for Non-Proportional Loadings at Different Degrees of Confinement ($P \approx$ 200 kips)

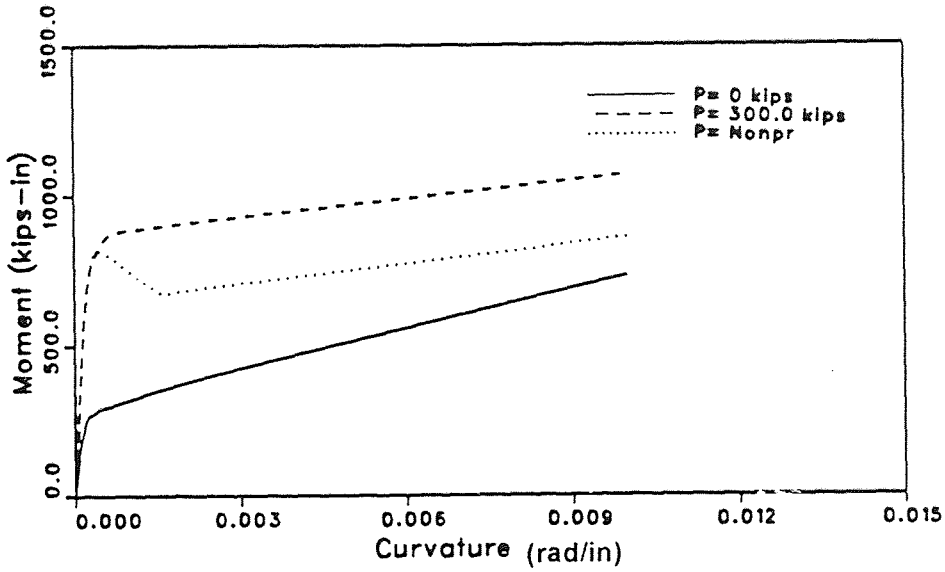

Figure 3.10 Moment-Curvature Relationships for Proportional and Nonproportional Loadings (P= 300 kips ($P>P_b$), Confined)

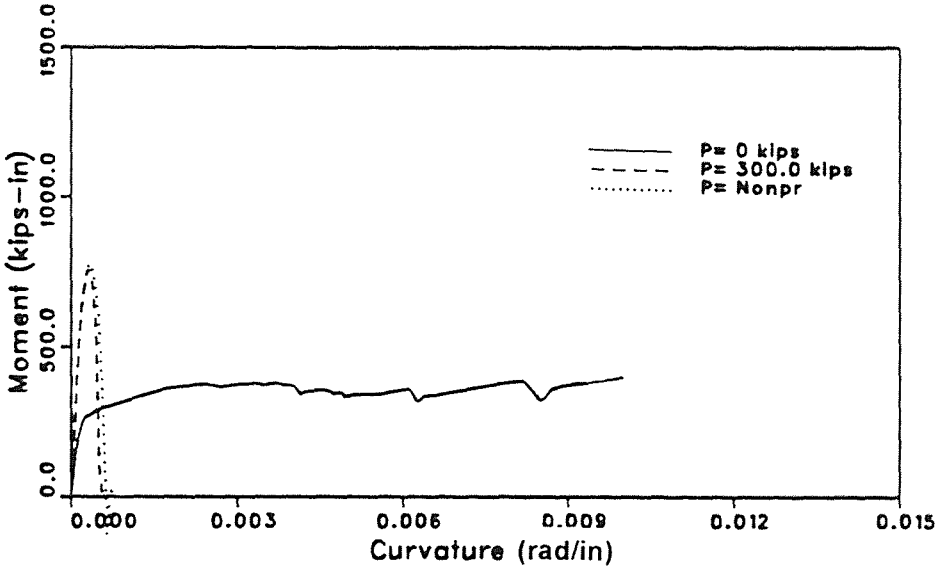

Figure 3.11 Moment-Curvature Relationships for Proportional and Nonproportional Loadings (P= 300 kips ($P>P_b$), Unconfined)

with some nonlinearity in curves with the increase of curvature (Figure B-2). For 1% confined concrete, the capacity for nonproportional loadings has little increase with the increase of curvature following the same slope as for the moment-curvature relationships for P=0 and P=-20 kips (proportional) till ϕ=0.009 rad/in (Figure B-3). After curvature ϕ=0.009 rad/in, the three curves converge and follow the same curve with the increase of curvature. The moment-curvature relationship for different degree of confinement under nonproportional loading of are plotted in Figure B-4, it seems that curves for fully confined and 1% confined concrete follow the same slope with almost same moment capacity till ϕ=0.007 rad/in. After this curvature, the moment capacity for 1% confined concrete drops with nonlinearity in curvature. The moment capacity for unconfined concrete is the least among them for different degree of confinement. The moment capacity stays almost same with some nonlinearities in curve with the increase of curvature.

When the tensile axial load increased to P=-40 kips the moment-curvature relationship appears to be different than that at P=-20 kips as nonproportional loadings. Here for confined concrete, the moment curvature curve for nonproportional loading P=-40 kips stays in the middle, lower than that for P=0 and higher than the capacity P=-40 kips as proportional loading (Figure B-5). These three curves follow the same slope with curvature distribution. For unconfined concrete, it is seen in Figure B-6 that the moment capacity for P=0, P=-40 kips (proportional) and P=-40 kips (nonproportional) increase with the increase of curvature till ϕ=0.0055 rad/in as the curve for nonproportional one stays in the middle.Then the capacity for nonproportional loadings virtually has the capacity for P=0 with the increase of curvature. For 1% confined concrete the moment curvature relationship for the axial load P=0, P=-40 kips (as proportional loading) and P=-40 kips (nonproportional) follow the same slope but moment capacity for nonproportional loading is less than the capacity for P= 0 and greater than that for

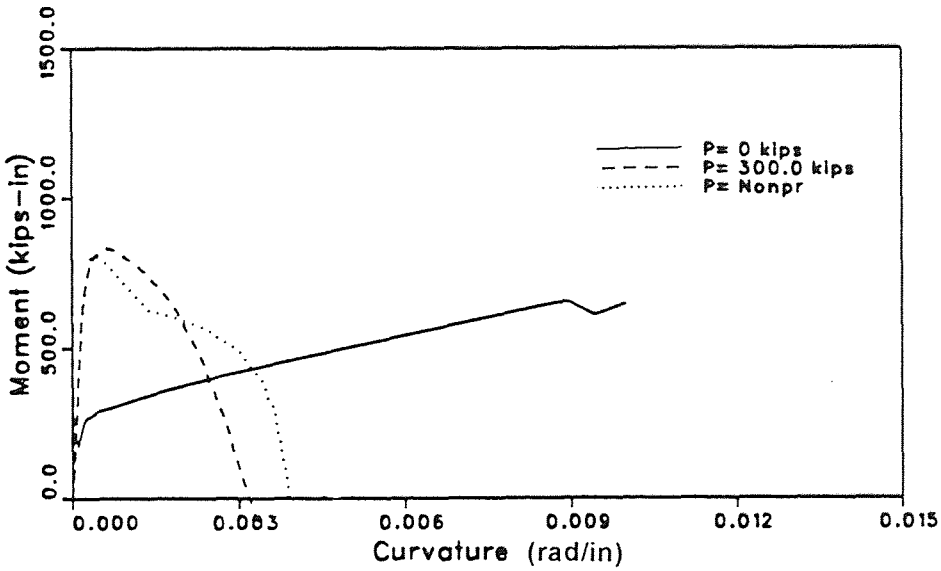

Figure 3.12 Moment-Curvature Relationships for Proportional and Nonproportional Loadings (P= 300 kips ($P>P_b$), 1% Confinement)

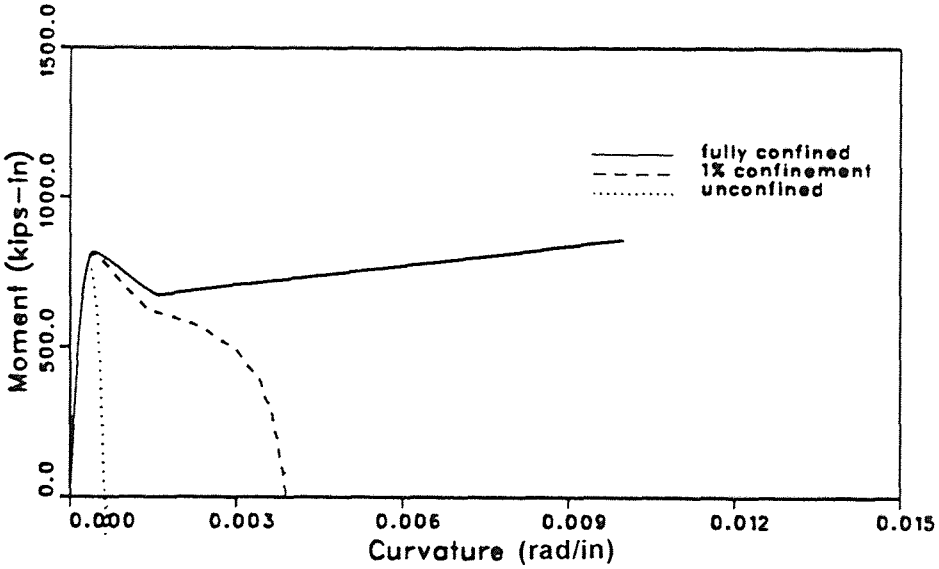

Figure 3.13 Moment-Curvature Relationships for Nonproportional loadings at Different Degrees of Confinement (P=300 kips)

P=-40 kips (proportional loading) as shown in Figure B-7. But after ϕ=0.0095 rad/in, the moment capacity for proportional and nonproportional loadings P=-40 kips converge and follow the same curve. The moment-curvature relationships for different degrees of confinement as discussed above are plotted for nonproportional loadings of P=-40 kips as shown in Figure B-8. It is seen that the moment capacity for confined and for 1% confinement have almost similar slope increasing with curvature till ϕ=0.006 rad/in after which the capacity for 1% confined concrete has a negative slope with the increase of curvature. The capacity for the unconfined concrete has the least capacity among them.

Under the action of biaxial motions of earthquake in the horizontal plane, the exterior columns of the frame structure may experience these kinds of nonproportional loadings. It is seen that the capacity of a R/C section under nonproportional loadings is different than that for monotonic loadings neglecting previous history of loading practiced for design purposes. This can be explained if the first analysis in Figure 3.2 is considered. It is seen that for P=0 kip and ϕ=0.006 rad/in, the moment capacity is equal to 830 kips-in. If the column is assumed to be the exterior one and under the biaxial motion of earthquake and assuming that the column is under zero load due to the nature of seismic loading in the X-direction and has a curvature of ϕ=0.006 rad/in which corresponds to moment capacity 525 kips-in.

Then it is assumed that the seismic loads in the Y-direction generate a compressive axial load in this column which is equal to P=100 kips. If the curvature in X-direction is assumed to stay constant and the current design method is considered, the moment capacity should be 830 kips-in. But this is not the actual capacity of the column at this stage of loading, if the history of loading at P=0 in X-direction is considered while calculating the moment capacity due to loading in Y-direction. If previous history of loading in X-direction is considered for

P=0, the moment capacity in Y-direction for P=100 kips comes as 675 kips-in. So it is seen that moment capacity under compressive nonproportional loading reduces significantly than that for proportional loading. The degree of confinement of concrete also effects the capacity of columns at different levels of nonproportional loading as depicted in Figures 3.3 and 3.4. At higher load levels, the stiffness of reinforced concrete column is very sensitive to the amount of concrete in the section under compression. For less confinement of concrete, loading beyond the ultimate strength, the stiffness and strength of concrete decreases rapidly which results in loss of overall stiffness of the section.

3.2 Influence of Nonproportinal Loadings on P-M Interaction Diagrams

The axial load influences the stiffness, flexural strength and ductility of a column. To design a column, the engineer should provide required amount of reinforcement to resist the axial loads and the bending moments due to lateral forces, one need to know what is governing the failure pattern whether compression or tension controls. The balanced load P_b (this is the axial load at which the tension steel just reaches the yield strength and extreme fiber concrete compressive strain ε_c reaches 0.003 at the same time) for a section is the controlling load which determines the failure pattern. The P-M interaction diagram shows the importance of axial load on the ultimate capacity of a section. It indicates that upto certain point (i.e., the balance point where P_b and $M_b$are located), the flexural capacity increases as the axial load increases and vice versa.

For P-M interaction diagram, a combination of axial load and bending moment are plotted. Here some analyses are done to see the effect of nonproportional loading on the P-M interaction diagram and compared with the P-M interaction diagram for proportional loading. P-M interaction diagram for proportional loading, it is assumed that loading starts from a phase where axial load and bending

moment are zero i.e., stress and strain of each fiber of the section are considered to be zero. For proportional loadings,the strain at the top fiber of the section (Figure 3.14a (i)) is ε_c=0.003 (Figure 3.14a (ii)) and bending moments are calculated for diffrent values of axial load. To generate P-M diagram for nonproportional loading, it is considered that initially the section is under loading where the top fiber strain ε_C=0.001 (Figure 3.14 (iii)) i.e, there exists some strains in the fibers of the section prior to the loading starts. The bending moments are found out for P=0, taking the stress-strain history of the fibers for top fiber strain ε_C=0.001 as initial loading condition. These stress-strain relationship is considered while computing the present stresses in the fibers of the section for the axial loadings for which the corresponding bending moments are determined considering top fiber strain ε_C=0.003 (Figure 3.14 (iv)).

3.2.1 Effect of Proportional and Nonproportional Loadings on P-M Diagrams

For the first analysis, the initial strain at top fiber is considered as ε_c=0.001 and final strain as ε_c=0.003, it is seen for proportional case, while the initial stress-strain history is not considered (i.e, stresses and strains are zero in all fibers of the section), the balanced load and moment P_b and M_b are 250 kips and 875 kips-in respectively and for nonproportional case where the previous history of stress-strain for ε_c=0.001 are considered for final top strain ε_c=0.003 (Figure 3.15). In this case the balanced load and moment are 175 kips and 900 kips-in respectively.

For ε_c=0.0015 to 0.003, as in Figure 3.16, P_b and M_b for nonproportional case are lower than nonproportional case in example 1 and the values are 95 kips and 775 kips-in respectively. In third example, the initial strain is considered as ε_C=0.002 and final as ε_c=0.003, as in Figure 3.17, it is to be noted that P-M interaction diagram is significantly irregular around P_b-M_b zone. There is a sharp

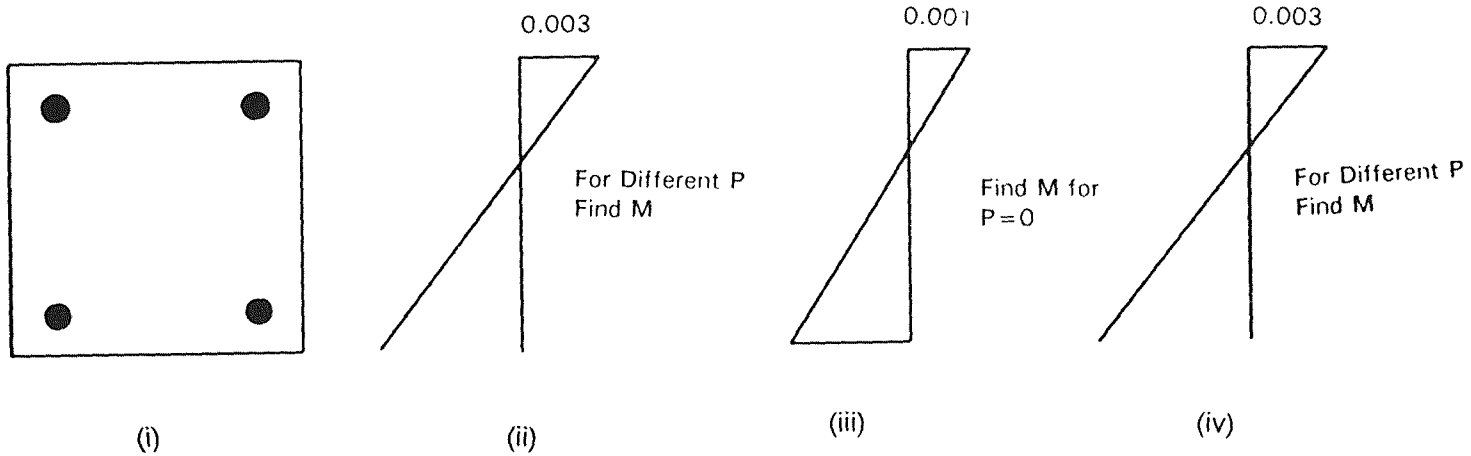

Figure 3.14 Strain Distributions For Proportional and Nonproportional Loadings

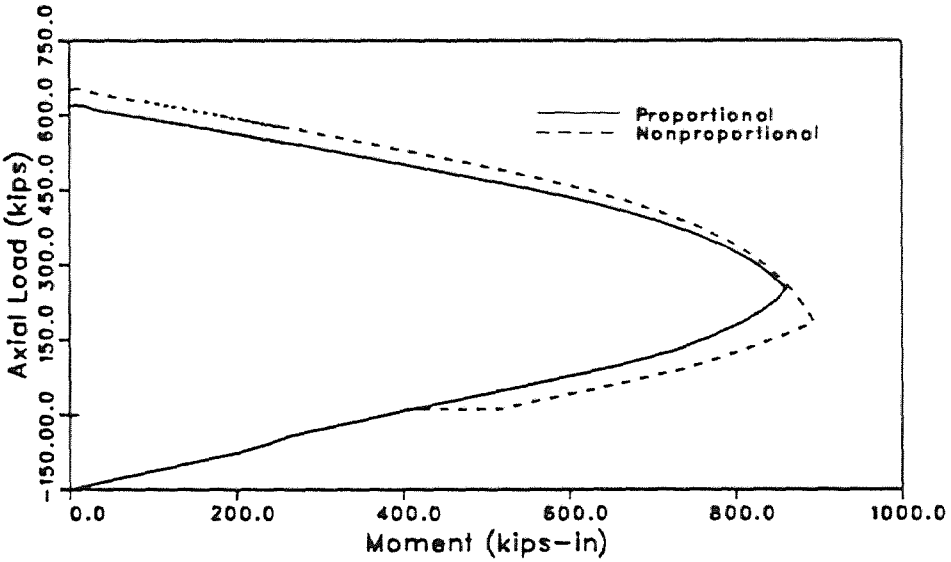

Figure 3.15 P-M Interaction Diagrams ($\varepsilon_{c\ initial}$ = 0.001 at P= 0, $\varepsilon_{c\ final}$ = 0.003)

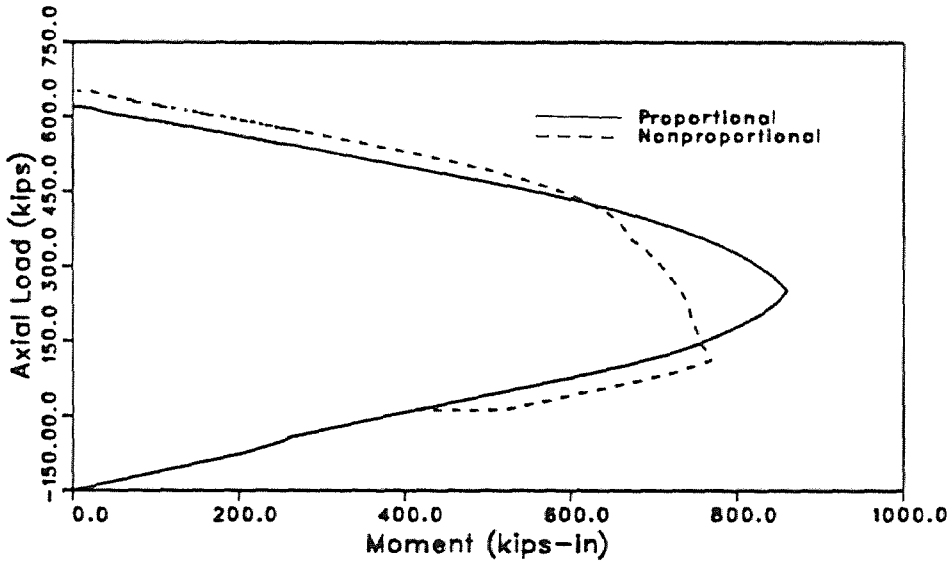

Figure 3.16 P-M Interaction Diagrams ($\varepsilon_{c\ initial}$ = 0.0015 at P= 0, $\varepsilon_{c\ final}$ = 0.003)

drop in moment capacity around the location of P_b and M_b and then the moment gradually increases with axial load. After the balanced load for proportional loading, the curve for nonproportional loading follows the normal curve as the proportional one but slightly upper than the previous one. In this case the P_b and M_b are 375 kips and 700 kips-in respectively. The P_b is higher than that of proportional one but the M_b is relatively low at the same time (Figure 3.17).

For fourth example as shown in Figure 3.18, the initial and final strains in the top fiber are ε_c=0.0025 and ε_c=0.003 respectively. It has the same pattern of P-M diagram and same P_b and M_b as the third example but with relatively higher P_b=375 kips and lower M_b=700 kips-in. But in this case the increase in P and M starts from relatively higher values after the drop relative to what happened in example 3.

The nonlinearity in P-M interaction diagram occurs because of nonlinearity of the strain diagram occurs for considering initial strain history of the fibers of the section. This kind of behavior is due to the inelastic material properties of the section. It causes great change in the strain-stress relationship of the fibers while the initial strain increases from lower value to higher value and history of previous loading is accounted for. In Figure 3.19, to analyze the effect of nonproportional loading on P-M relationship, all four P-M interaction diagrams are plotted for nonproportional loading. It is to be noted that lower the values of initial strains, the less is nonlinearity observed in the P-M diagram with higher P_b and M_b. As the initial top strains in the fibers increases untill ε_c=0.0015, the P_b and M_b decreases but from initial top strain ε_c=0.002, the nonlinearity in P-M diagram is pronounced and P-M relationship around the balanced point also significantly varies. For initial top strain ε_c=0.002 P-M relationship starts deviating from the expected P-M curve at P=21 kips and M=560 kips-in as decreasing moment with increase of axial load untill P=180 kips and M=450 kips-in. Then axial load and moment both start

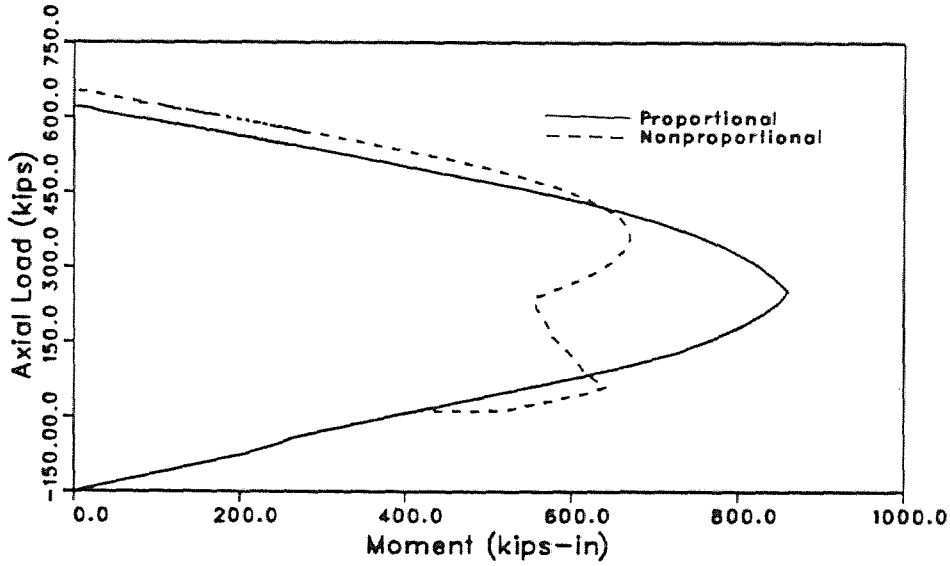

Figure 3.17 P-M Interaction Diagrams ($\varepsilon_{c\ initial}$ = 0.002 at P= 0, $\varepsilon_{c\ final}$= 0.003)

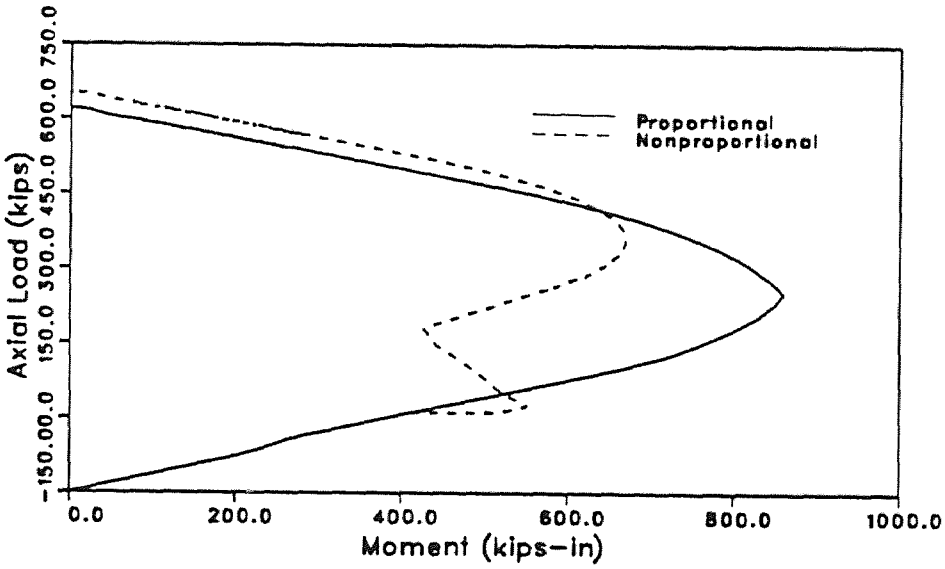

Figure 3.18 P-M Interaction Diagrams ($\varepsilon_{c\ initial}$ = 0.0025 at P= 0, $\varepsilon_{c\ final}$ = 0.003)

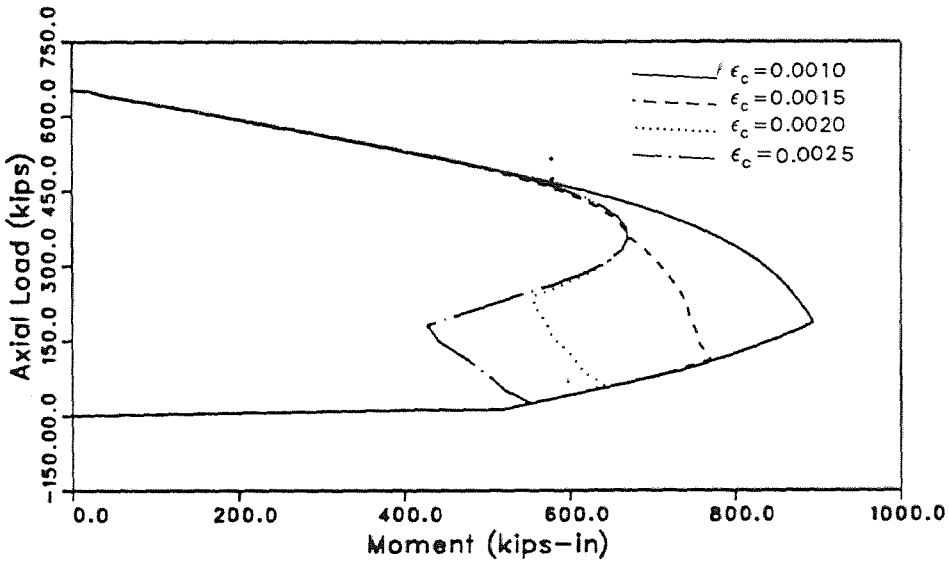

Figure 3.19 P-M Interaction Diagrams for Nonproportional Loadings

increasing following the trend of a typical P-M interaction diagram. For top initial strain ε_c=0.0025, it follows the same relationship as the previous example but the curve becomes irregular earlier in the vicinity of balanced point . The moment starts decreasing with increasing axial load at relatively higher axial load and moment (i.e.,at P=60 kips and M=650 kips-in) and eventually the moment increases again from P=220 kips and M=570 kips-in along with the increase in axial load.

3.2.2 Effect of Reinforcement Ratios for Various Shapes of R/C Sections

Some analyses are done using different shapes of R/C sections with varying reinforcement ratios. The maximum compressive Strains ,ε_{cm}, allowed in the fibers of the section are .003 and .01. To study the effect of nonproportional loadings on P-M interaction diagram, for final strain in top fiber ε_{cm}=0.003, the initial top fiber strain is varied as 0.001 and 0.002. For ε_{cm}=0.01, the initial top fiber strain varied as 0.002 and 0.006 and the reinforcement ratio is varied in the range 1-3 percent which is assumed for all shapes and strain conditions. The concrete is assumed to be perfectly confined.

First analysis is made with the square section shown in Figure 3.20 (a). For ε_{cm}=0.003, the initial top fiber strain is varied from 0.001 and 0.002 to final strain 0.003 respectively. For ε_c=0.001 (Figure 3.21), it is seen that P-M interaction diagrams with different reinforcement ratios follow the typical P-M curve with less Pb and higher Mb. For ε_c=0.002, the lower the percentage of steel, the nonlinearity in the curve is prominent as shown in Figure 3.22. For ρ=1%, Pb is slightly lower than that for ρ=2% but Mb is almost the same for these two cases. For ρ=3%, Pb is significantly less that for ρ=1% and ρ=2% but Mb is 1.25 times greater than that for ρ=2% but the curve is of typical shape for proportional loadings.

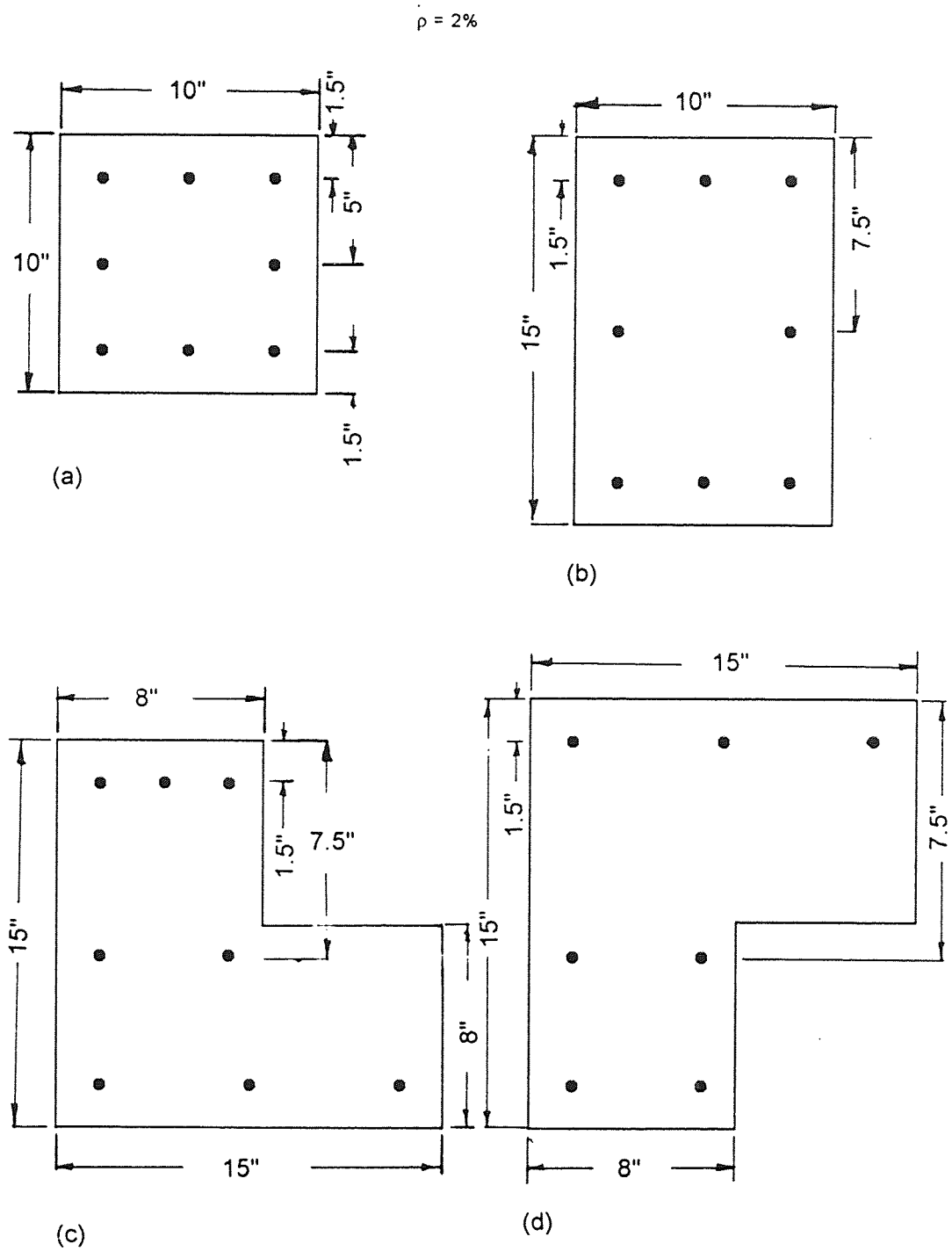

Figure 3.20 Sectional Properties for Different Types of R/C Sections

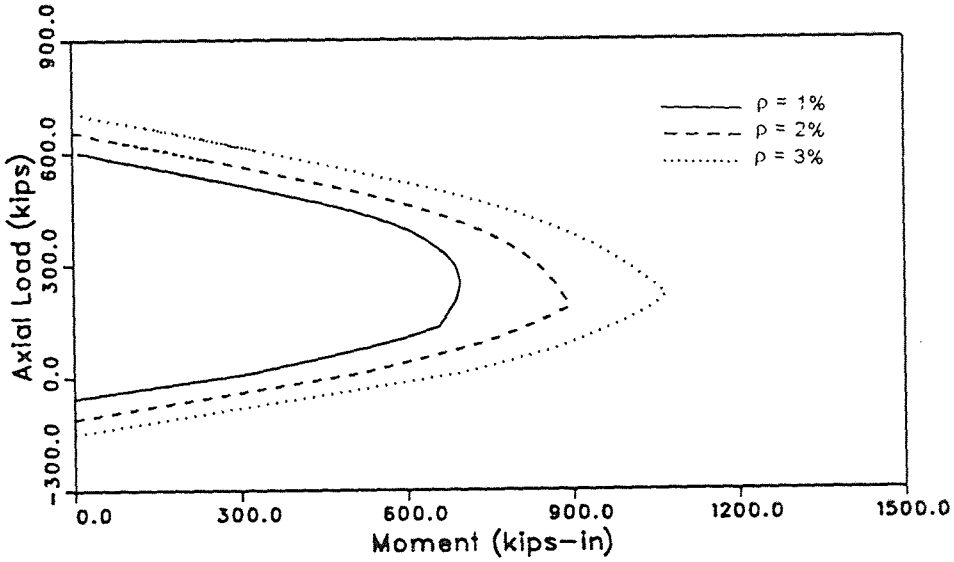

Figure 3.21 P-M Interaction Diagrams for Different Reinforcement Ratios for the Square R/C section ($\varepsilon_{c\ initial}$=0.001 at P=0, ε_{final}=0.003)

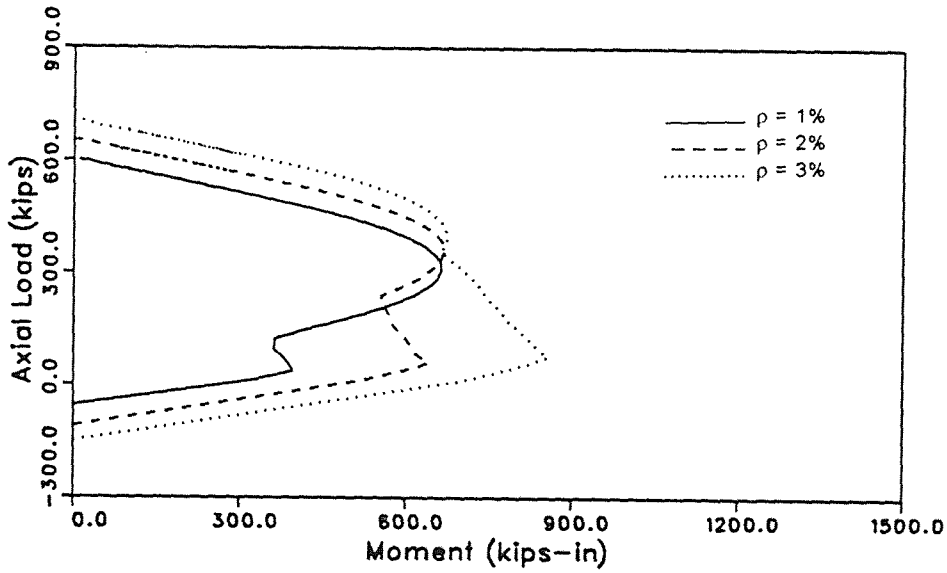

Figure 3.22 P-M Interaction Diagrams for Different Reinforcement Ratios for the Square R/C section ($\varepsilon_{c\ initial}$=0.002 at P=0, ε_{final}=0.003)

Next, the maximum allowable strain is assumed ε_{cm} =0.01 instead of 0.003 and initial strain in the top fiber is varied from 0.002 to 0.01 and 0.006 to 0.01 respectively. For nonproportional loadings, the initial strain in the top fiber is assumed as ε_c=0.002. For ρ=1%, the nonlinearity is prominent (Figure 3.23). Those with higher ρ , the balanced load and moment increase with reinforcement ratio following the typical P-M interaction curve. For initial strain, ε_c=0.006 to final strain, ε_c=0.01, for different reinforcement ratios, all three curves (Figure 3.24) started following the typical P-M curve but after certain interval, the moment starts to decrease with the increase of P upto certain interval. Then the moment starts to increase and ultimately follows the typical P-M curve for proportional loading. While the moment is increasing after this transition point, all the three curves follow the same path until the moment starts to decrease with increasing P. While the moment is decreasing, moment is the least for the lowest value of ρ for any value of P. For the nonlinear part of P-M diagram, the difference among the moments for same value of P are significantly different whereas at the second phase, the curve is similar to that for proportional loadings, moment for P is proportionally higher with the high ratio of reinforcement.

Next, the similar analyses as described above are done with a rectangular section to examine the nature of P-M diagram and the capacity of the section under nonproportional loadings (Figure 3.20 (b)). For initial strain, ε_c=0.001 to final strain, ε_c=0.003, the P-M diagrams for the three different reinforcement ratios follow the typical pattern for the proportional loadings (Figure 3.25). From these analyses it is seen that with increase in reinforcement increase in balanced moment is significant but the balanced axial load remains almost the same for all cases. For initial strain, ε_c=0.002 to final strain, 0.003, it is seen in Figure 3.26 that for low reinforcement ratio such as ρ=1%, the P-M interaction diagram becomes irregular with Pb and Mb 40 kips and 730 kips-in. For ρ=2%, the P-M interaction

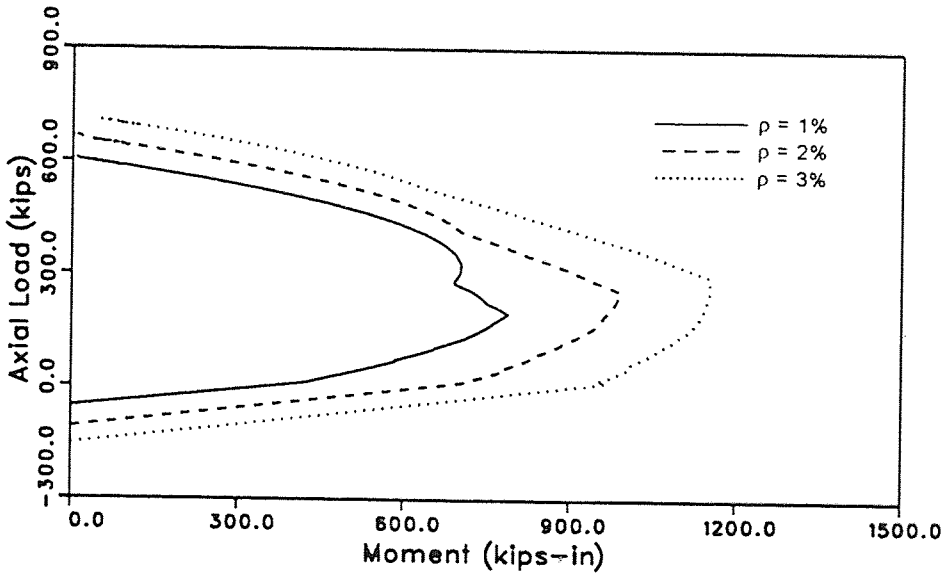

Figure 3.23 P-M Interaction Diagrams for Different Reinforcement Ratios for the Square R/C section ($\varepsilon_{c\ initial}$=0.002 at P=0, ε_{final}=0.01)

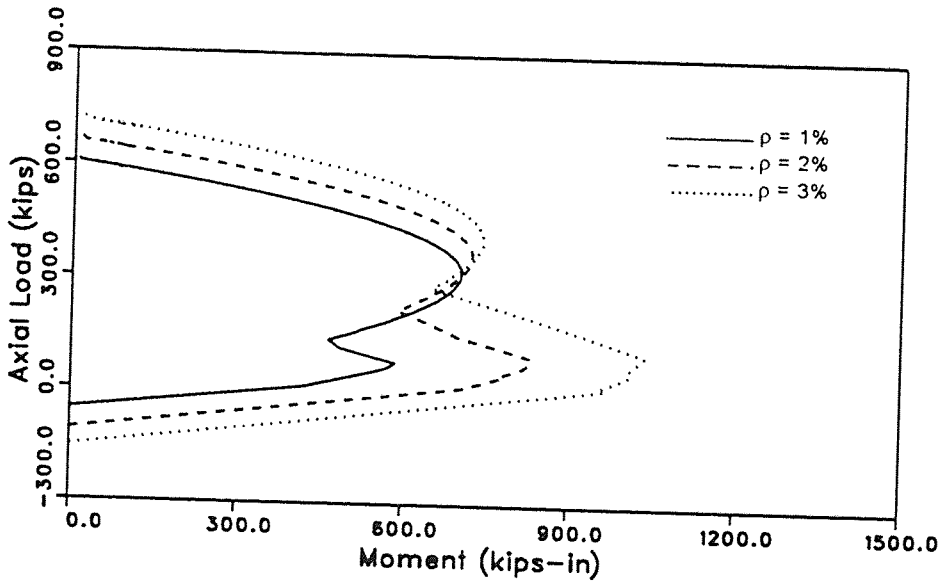

Figure 3.24 P-M Interaction Diagrams for Different Reinforcement Ratios for the Square R/C section ($\varepsilon_{c\ initial}$=0.006 at P=0, ε_{final}=0.01)

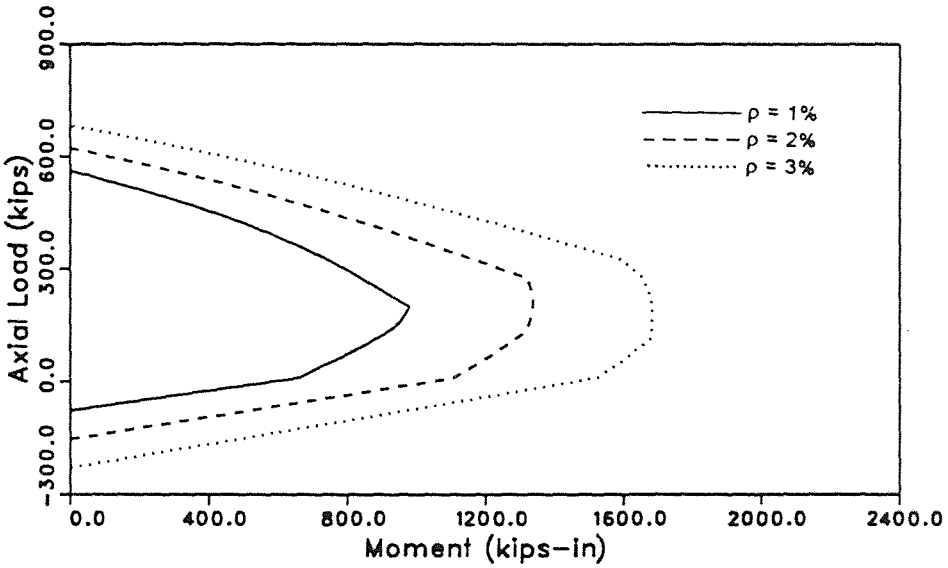

Figure 3.25 P-M Interaction Diagrams for Different Reinforcement Ratios for the Rectangular R/C section ($\varepsilon_{c\ initial}$=0.001 at P=0, ε_{final}=0.003)

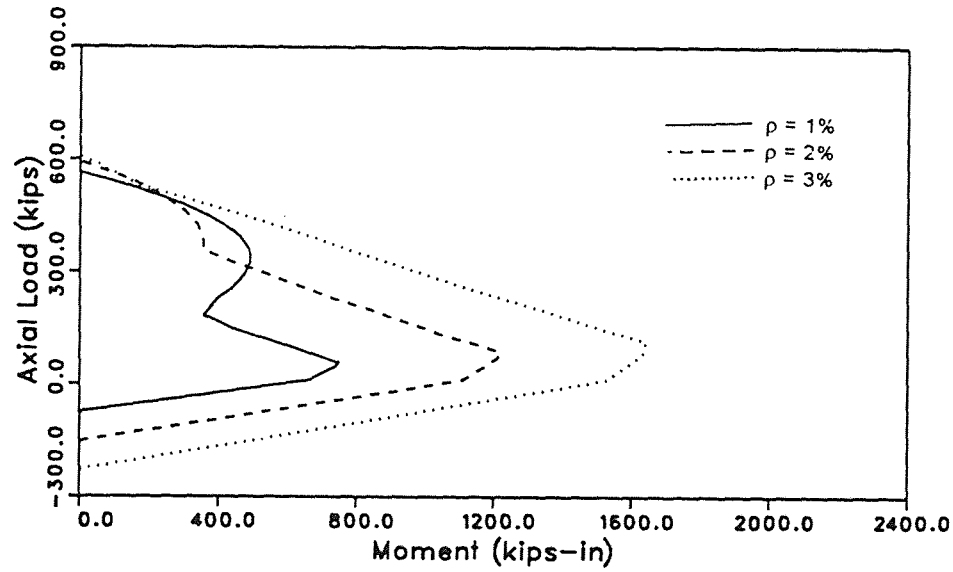

Figure 3.26 P-M Interaction Diagrams for Different Reinforcement Ratios for the Rectangular R/C section ($\varepsilon_{c\ initial}$=0.002 at P=0, ε_{final}=0.003)

diagram becomes slightly irregular after the balance point. In this case Pb and Mb are 75 kips and 1180 kips-in. For ρ=3%, the P-M diagram follows the normal pattern for proportional loadings having Pb and Mb are 112 kips and 1600 kips-in. Next the maximum allowable strain is assumed 0.01 and similar analyses are done as above. For initial strain, ε_c=0.002 to final strain, ε_c 0.01, the interaction diagrams are typical as for proportional loadings (Figure 3.27). For ρ=1%, Pb and Mb are 240 kips and 1100 kips-in, ρ=2%, Pb and Mb are 200 kips and 1600 kips-in and for ρ=3%, these values are 120 kips and 2100 kips-in i.e, the balanced axial load decreases and balanced moment increases with the increase of reinforcement ratios. For initial strain, ε_c=0.006 to final strain, ε_c=0.01, the P-M curve for ρ=1% is nonlinear with Pb and Mb 300 kips and 575 kips-in. For ρ=2% and ρ=3%, the P-M diagram is irregular after the balanced capacity. The balanced load and balanced moment of 75 kips and 1600 kips-in for ρ=2% and 50 kips and 1080 kips-in for ρ=3% as shown in Figure 3.28. If the analyses for initial top strains ε_c= 0.002 and ε_c=0.006 are compared, it is seen that the area bounded by P-M curve for ε_c=0.006 to 0.01 is less than that for the previous one.

This analysis is done with L-shaped R/C section which sometimes is used as a section for exterior corner column as shown in Figure 3.20(c). For ε_c=0.001 to ε_c=0.003, the P-M interaction diagrams follow the typical pattern of P-M diagram for proportional loadings (Figure 3.29). For initial strain, ε_c=0.002 to final strain, ε_c=0.003, the P-M diagrams follow the similar path for proportional loading except for ρ=1%, which is slightly irregular after the balance point as seen in the Figure 3.30. Balanced moment increases significantly and balanced axial load decreases with increase of reinforcement ratios.

Then, the analyses are done with maximum allowable strain, ε_{cm}= 0.01. For initial strain ε_c=0.002 to final strain, ε_c=0.01, it is seen that the nature of the curves are similar to that for proportional loading with lower Pb and higher with increase

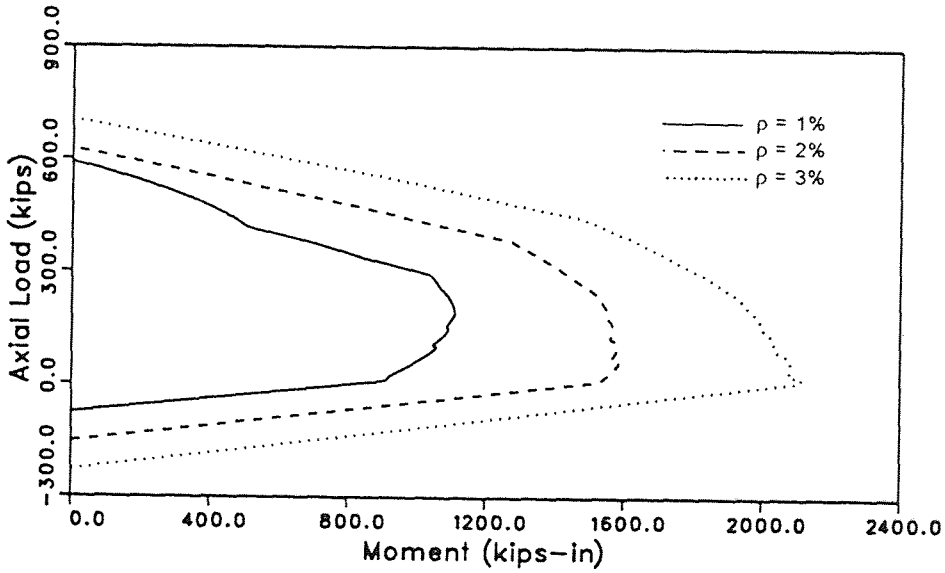

Figure 3.27 P-M Interaction Diagrams for Different Reinforcement Ratios for the Rectangular R/C section ($\varepsilon_{c\ initial}$=0.002 at P=0, ε_{final}=0.01)

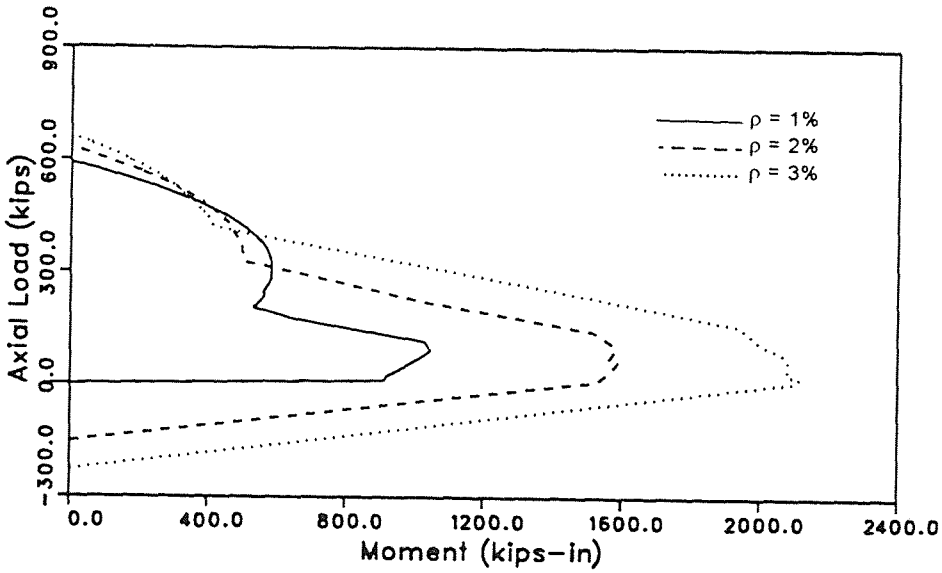

Figure 3.28 P-M Interaction Diagrams for Different Reinforcement Ratios for the Rectangular R/C section ($\varepsilon_{c\ initial}$=0.006 at P=0, ε_{final}=0.01)

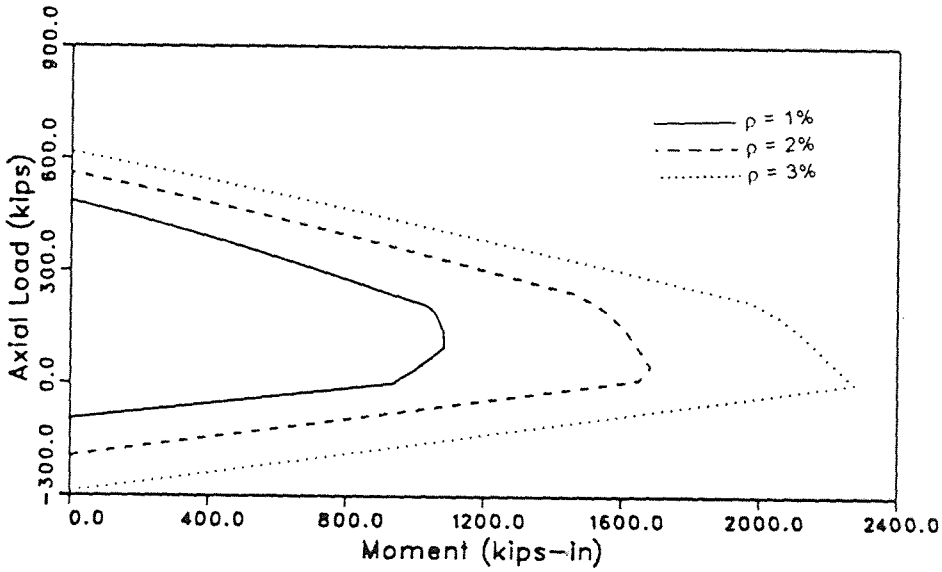

Figure 3.29 P-M Interaction Diagrams for Different Reinforcement Ratios for the L-Shaped R/C section ($\varepsilon_{c\ initial}$=0.001 at P=0, ε_{final}=0.003)

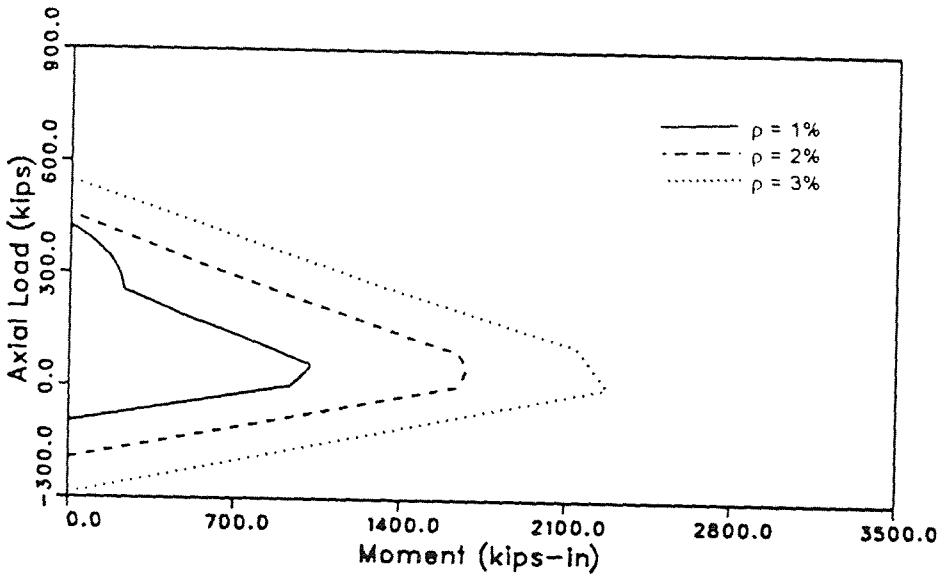

Figure 3.30 P-M Interaction Diagrams for Different Reinforcement Ratios for the L-Shaped R/C section ($\varepsilon_{c\ initial}$=0.002 at P=0, ε_{final}=0.003)

of reinforcement ratios (Figure 3.31). For initial strain, ε_c=0.006 to final strain, ε_c=0.01, the balanced moment increases significantly shown in Figure 3.32. It is seen from Figure 3.31 and 3.32 that for lower values of initial strain the balanced load and moment does not vary significant for a constant reinforcement ratio whereas extent of area covered by P-M diagrams are different .

Next, the analyses are done with another L-shaped section as shown in Figure 3.20 (d). For ε_c=0.001 to ε_c=0.003 (Figure B-9), the P-M interaction diagrams are different from the previous analyses with L-shape section. For ρ=1%, Pb and Mb are 187 kips and 1160 kips-in, for ρ=2%, Pb and Mb are 300 kips and 1800 kips-in and for ρ=3%, the P-M interaction diagram is irregular with high Pb and low Mb (i.e, 450 kips and 900 kips-in respectively). For ε_c=0.002 to ε_c=0.003, the P-M interaction diagrams are nonlinear as shown in Figure B-10. For ε_c=0.002 to ε_c=0.01, the P-M diagrams follow the pattern of P-M diagram for proportional loading with some irregularity around the balance point as shown in Figure B-11. For ρ=1%, Pb and Mb are 330 kips and 1450 kips-in, for ρ=2%, Pb and Mb are 330 kips and 1980 kips-in and for ρ=3%, Pb and Mb are 330 kips and 2540 kips-in respectively. For ε_c=0.006 to ε_c=0.01, the P-M interaction diagrams are highly nonlinear. For ρ=1%, Pb and Mb are 120 kips and 1330 kips-in, for ρ=2%, Pb and Mb are 120 kips and 2080 kips-in and for ρ=3%, Pb and Mb are 120 kips and 2740 kips-in (B-12).

3.2.3 Effect of Nonproportional Loadings on Different Shapes of R/C Sections

Here some analyses are made under nonproportional loadings with different shapes of R/C sections varying the maximum allowable strain ,ε_{cm}, in the fiber as 0.003 and 0.01. For ε_{cm}=0.003, initial top fiber strain is varied from .001 to 0.003 at the interval of 0.0005 and for ε_{cm}=0.01, initial top fiber is varied from 0.002 to 0.01 at the interval of 0.002 for each P-M interaction diagram.

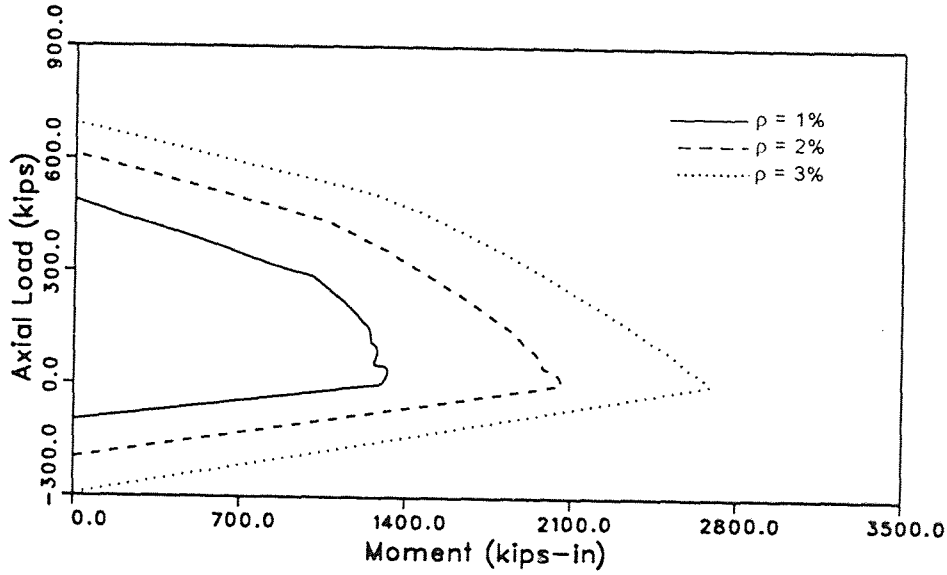

Figure 3.31 P-M Interaction Diagrams for Different Reinforcement Ratios for the L-Shaped R/C section ($\varepsilon_{c\ initial}$=0.002 at P=0, ε_{final}=0.01)

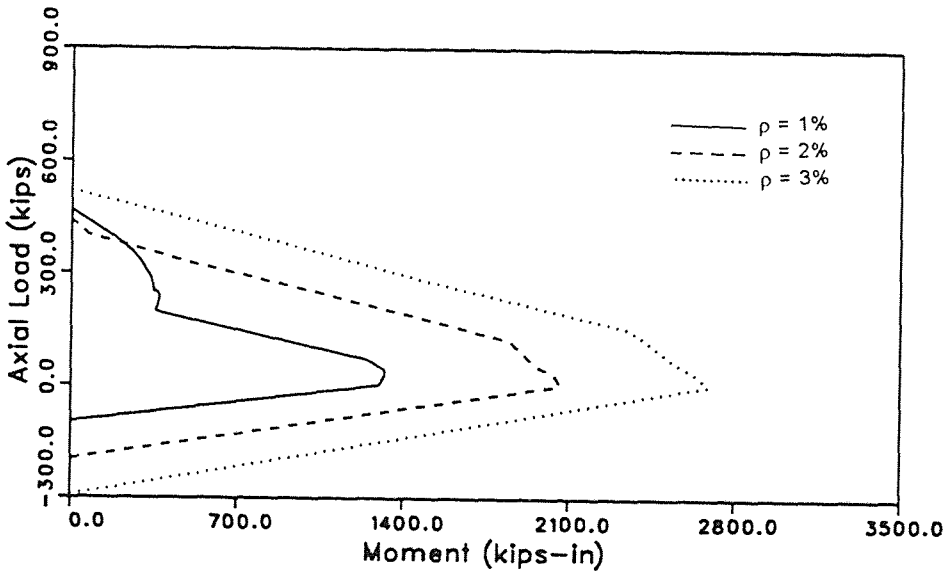

Figure 3.32 P-M Interaction Diagrams for Different Reinforcement Ratios for the L-Shaped R/C section ($\varepsilon_{c\ initial}$=0.006 at P=0, ε_{final}=0.01)

For section (a) of Figure 3.20, the interaction diagrams for ε_{cm}=0.003 are plotted in Figure 3.33. It is seen that for proportional loadings, Pb and Mb are higher than all the values for nonproportional loadings except the one where initial strain, ε_c=0.001 for nonproportional loadings. It is seen that for lower values of initial strain, the P-M interaction diagrams are similar to that for proportional loading but with higher value of initial strain,i.e, from 0.002, the P-M diagram becomes irregular in nature. For ε_{cm}=0.01, the balanced load and moment for proportional loadings are greater than that for nonproportional loadings except for ε_c=0.002 to ε_c=0.01 which also follow the same pattern of P-M diagram for proportional loadings (Figure 3.34). The other three P-M diagram where the initial strain varies from 0.004, 0.006 and 0.008 to final strain 0.01, are nonproportional in nature.

Next the same analyses are done with a rectangular section as shown in Figure 3.20 (b). For ε_{cm}=0.003, the balanced load and moment for nonproportional loadings are greater than that for proportional loadings in all cases (Figure 3.35). The last two interaction diagrams for initial strains of 0.002 and 0.0025 to final strain 0.003 are nonlinear in nature as shown in Figure. For ε_c=0.01, it is seen from Figure 3.36, that the balanced load and moment for proportional loadings is the least among them.

Then, the analyses are done with a L-shaped section as shown in Figure 3.20(c). For ε_{cm}=0.003, the balanced load and moment for proportional loadings is the least among them (Figure B-13). For higher the initial strains, lower the areas enclosed by the P-M curves. For ε_{cm}=0.01, similar nature of P-M diagrams as in previous example are obtained (Figure B-14).

Lastly, the analyses are made with L-shaped section as shown in Figure 3.27(d). For ε_{cm}=0.003, the balanced load and moment for nonproportional loadings for initial strain ε_c=0.001 to final strain ε_c=0.003 has the highest value and follows the nature of proportional loadings (Figure B-15). For initial strain

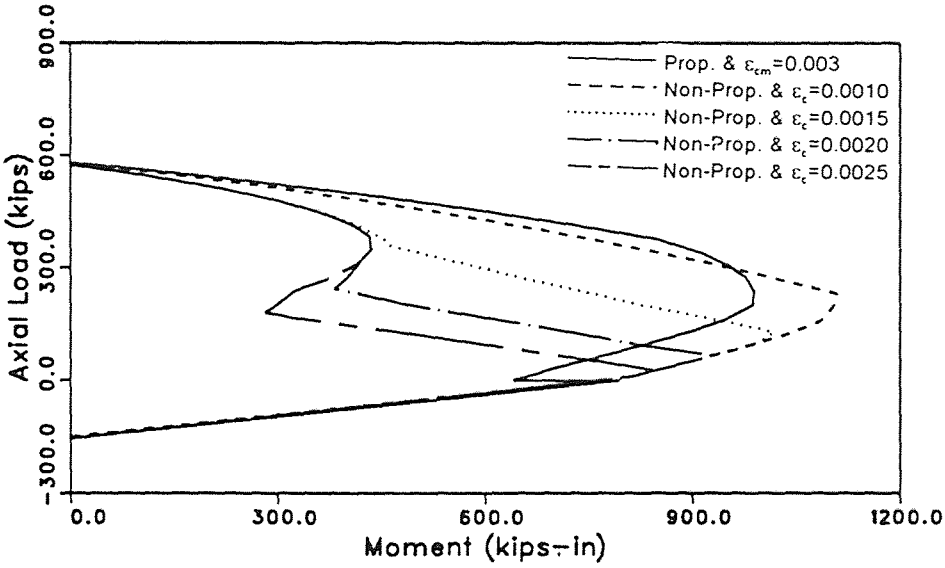

Figure 3.33 P-M Interaction Diagram for Different initial strains in the Square R/C Section (ε_{final}=0.003)

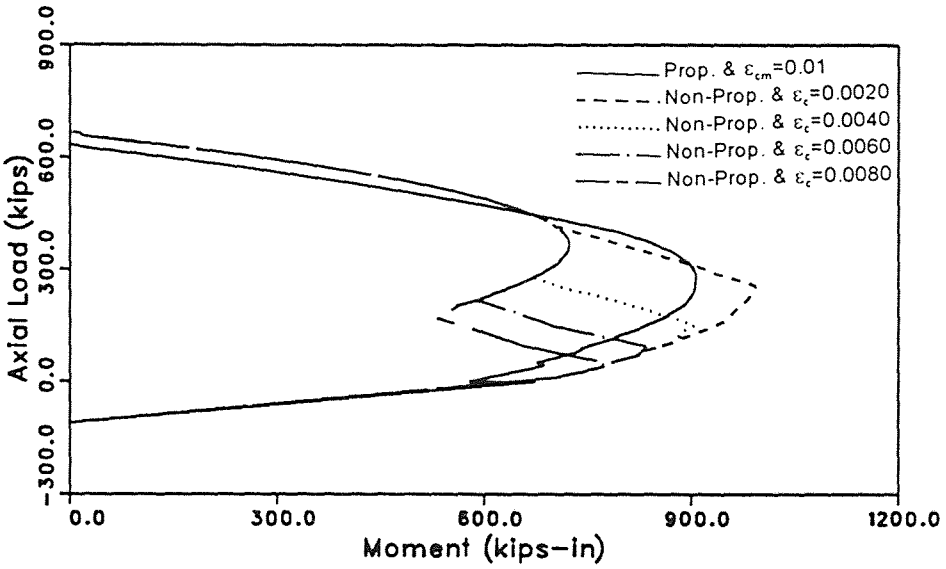

Figure 3.34 P-M Interaction Diagram for Different initial strains in the Square R/C Section (ε_{final}=0.01)

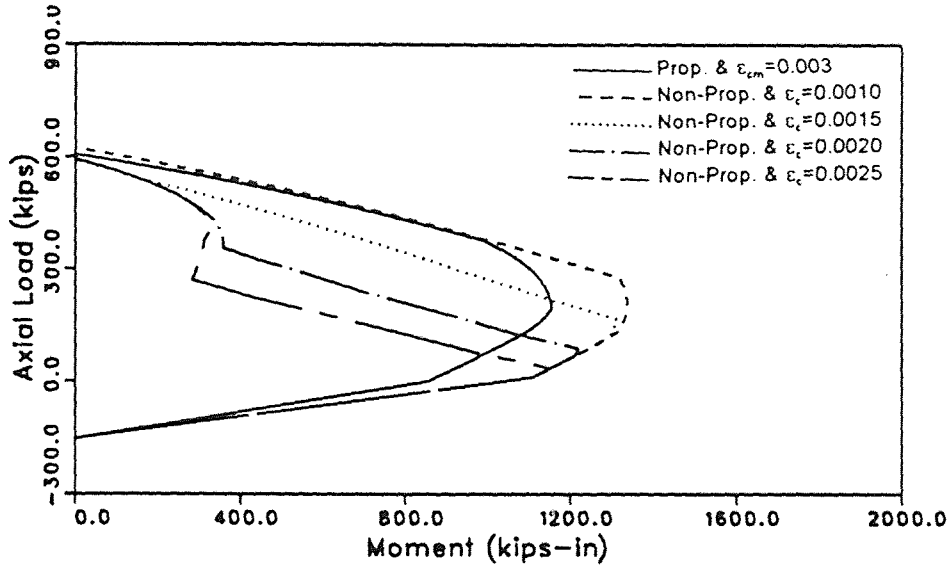

Figure 3.35 P-M Interaction Diagram for Different initial strains in the Rectangular R/C Section (ε_{final}=0.003)

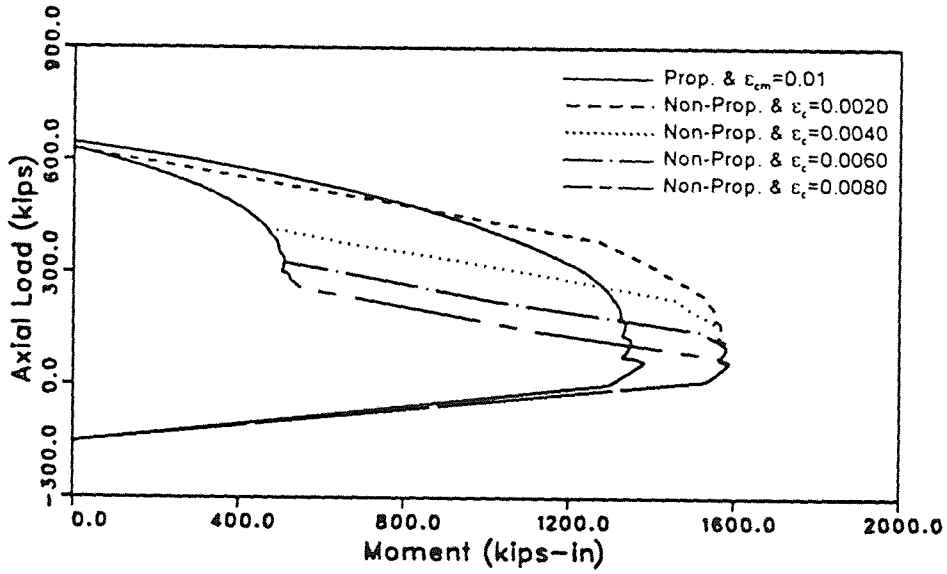

Figure 3.36 P-M Interaction Diagram for Different initial strains in the Rectangular R/C Section (ε_{final}=0.01)

ε_c=0.0015, 0.002 and 0.0025 to final strain 0.003, the curves are irregular and the areas enclosed by the curves decrease with higher value of initial strain in the section. For maximum allowable strain, ε_{cm}=0.01, the P-M diagrams are also irregular in nature (Figure B-16).

From the above analyses, it can be concluded that what is assumed in current design practice that as long as the values of axial load and bending moment are within the P-M interaction diagram are safe. But this is not true if the history of loading is considered. So for design practice it is necessary to consider the extreme cases of these type of loading if the structure is to be safe under general loadings.

3.3 Effect of Nonproportional Loadings on a Hysteresis loop during Loading and Unloading Processes

Large uncoupled axial and lateral forces can be developed in the columns of reinforced concrete structures during the biaxial or triaxial motions of earthquake. Hysteresis loops may not be masing type for some patterns of nonproportional variation of axial and lateral loads. The nature of hysteresis loop is quite different under uncoupled fluctuations in axial and lateral loads than that for proportional loadings. Here some analyses are done at different levels of axial loads to see the effect of nonproportional variations of loadings on moment-curvature relationship of the section along with different degree of confinement of concrete. It is to be noted that the axial loads used here are less (i.e, P=100 kips),axial load around (i.e, P=200 kips) and greater (i.e, P=300 kips) than the balanced load for the section for both confined and 1% confined concrete. The tests are done at two curvature levels such as ϕ=0.005 rad/in and ϕ=0.01 rad/in respectively.

The analysis is done in the following way, first the curvature is increased from zero to 0.005 rad/in or 0.01 rad/in with constant axial load P=0. Whatever level is

chosen for the analysis ϕ=0.005 rad/in or ϕ=0.01 rad/in, keeping the curvature constant the axial load is increased to P=100 kips or P=200 kips or P=300 kips and then the curvature is decreased for unloading or increased for loading with the constant axial loading of P=100 kips or P=200 kips or P=300 kips. The increment or decrement used for loading/unloading are 1%, 2%, 3%, 4% and 5% of the curvature (ϕ = 0.005 rad/in or ϕ=0.01 rad/in), at which point the changes in loading are made. Observations are made to see how the moment-curvature relationship is affected by the level of axial forces and curvatures while the unloading and reloading take place.

For the first example, it is assumed that concrete is confined (i.e, ε_u=0.1 in/in and σ_u= 5500 psi) and the axial loads are chosen as P=100 kips ($P<P_b$), P=200 kips ($P= P_b$) and P=300 kips ($P>P_b$). This analysis is made at ϕ=0.005 rad/in and ϕ=0.01 rad/in to analyze the effect of unloading on the moment-curvature relationship. For ϕ=0.005 rad/in (Figure 3.37) when the axial load is increased from P=0 to P=100 kips, P=200 kips and P=300 kips separately, the moment capacity is greater with higher axial loads for the same curvature distribution due to increase in stiffness of the section for high compressive axial loads. For P=100 kips ($P<P_b$), on loading from P=0 to P=100 kips at constant curvature ϕ=0.005 rad/in, the moment increases from 623 kips-in to 643 kips-in. Then unloading starts, the system of M-ϕ loop is generating small amount of energy rather than dissipating it. As the unloading is going on, the bending moment drops sharply from 643 kips-in to 175 kips-in within .0005 rad/in curvature difference. From that point on, the bending moment decreases slowly as the curvature decreases with constant P=100 kips during this unloading. For P=200 kips ($P \sim P_b$), at ϕ=0.005 rad/in, the moment capacity decreases from 623 kips-in to 589 kips-in while the axial load increases from P=0 to P=200 kips. Unloading takes place with severe

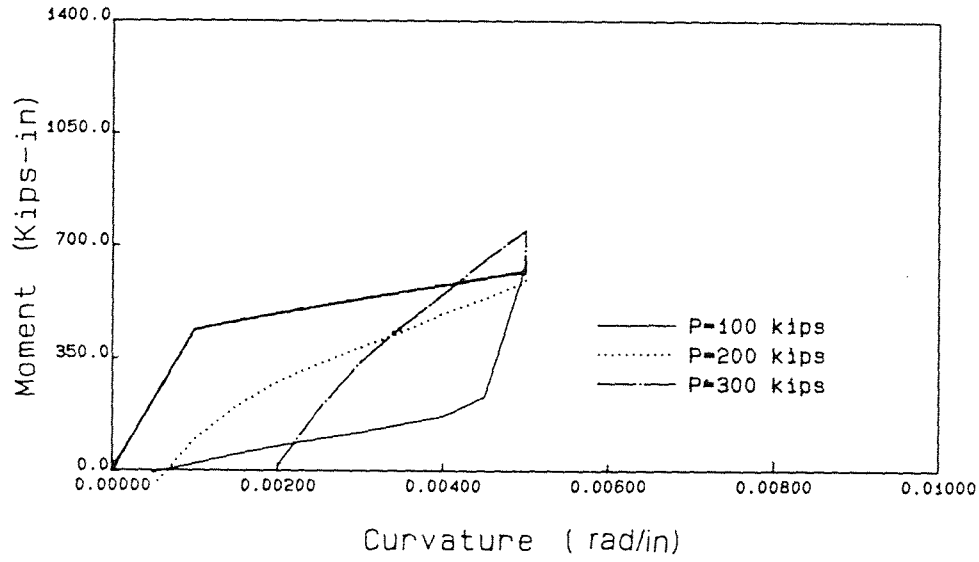

Figure 3.37 Moment-Curvature Relationships for Nonproportionl Unloading (at ϕ= 0.005 rad/in, Confined Concrete)

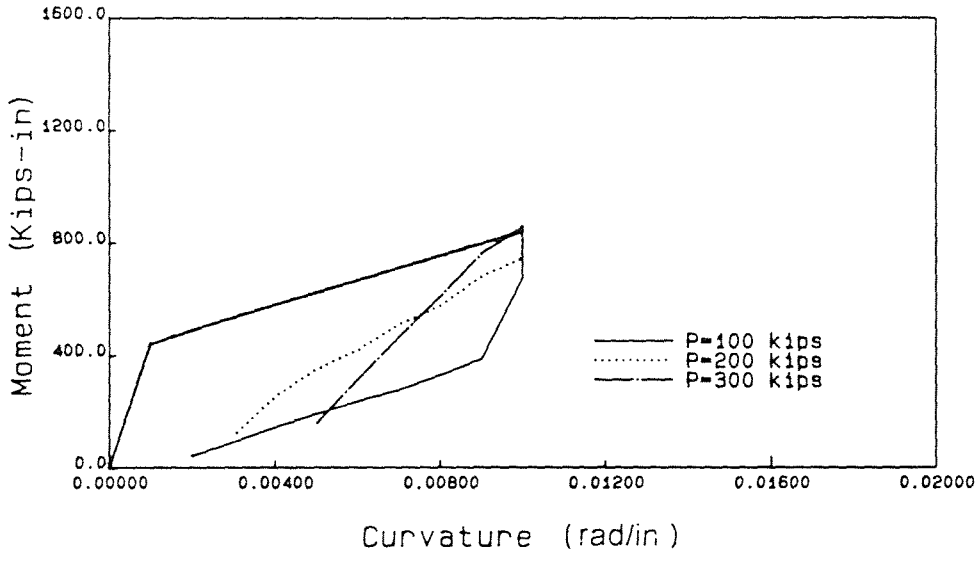

Figure 3.38 Moment-Curvature Relationships for Nonproportional Unloading (at ϕ= 0.01 rad/in, Confined Concrete)

pinching in such a way that the enclosed area between loading and unloading curves is very small (Figure 3.37). For P=300 kips ($P > P_b$), at ϕ=0.005 rad/in, axial load increases from P=0 to P=300 kips, the moment capacity increases from 623 kips-in to 750 kips-in. Upon unloading, it seems to generate energy rather than dissipating energy. After crossing the loading branch, unloading takes place with a pinch (Figure 3.37).

Same analyses are done as discussed above at the curvature ϕ=0.01 rad/in (Figure 3.38). When the axial load (P) is increased from P=0 to P=100 kips and to P=200 kips respectively, the moment capacity decreases from 842 kips-in to 673 kips-in and 745 kips-in respectively and for P=0 to P=300 kips, the moment capacity increased to 860 kips-in while the curvature is hold constant at ϕ=0.01 rad/in. The nature of the unloading curves are similar as those at ϕ=0.005 rad/in except for P=300 kips. There is no significant negative energy dissipation loop as observed in the case with curvature ϕ=0.005 rad/in.

To analyze the effect of nonproportional axial loading right after the axial load is increased from P=0 to P=100 kips, 200 kips and 300 kips etc while holding the curvature constant and then the same axial loading is continued proportionally throughout the curvature distribution. The analyses are done at ϕ=0.005 rad/in and ϕ=0.01 rad/in. For ϕ=0.005 rad/in, the moment capacity in all levels of axial loads, increases with curvature except for P=200 kips, it decreases by 10% while the curvature is held constant at ϕ=0.005 rad/in, then the moment capacity increases increase of curvature. Higher the axial load, higher is the capacity (Figure 3.39). Similar analysis is done with ϕ=0.01 rad/in, same type of moment-curvature relationship as in ϕ=0.005 rad/in for P=100 kips and P=200 kips i.e the moment capacity decreases while the curvature is kept constant as the axial load increases from P=0 to P=100 kips or P=200 kips. With the increase in curvature, the moment capacity increases with the constant axial loading of P=100 kips and P=200 kips.

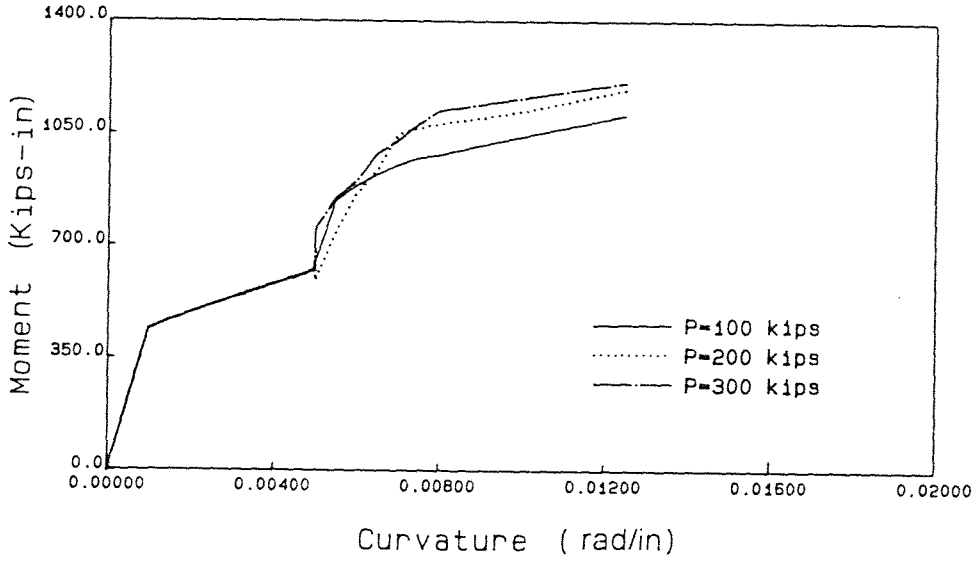

Figure 3.39 Moment-Curvature Relationships for Nonproportional Loadings (at ϕ= 0.005 rad/in, Confined Concrete)

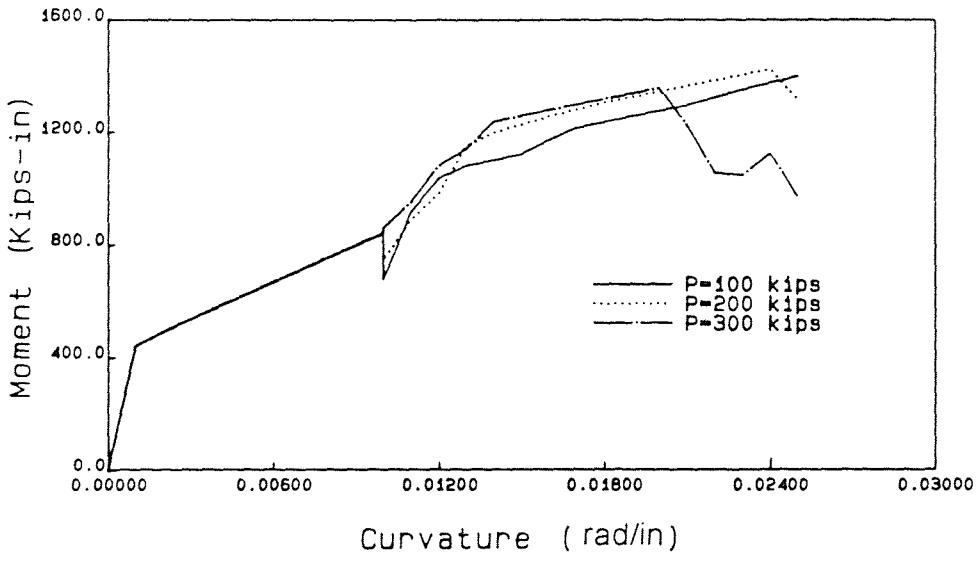

Figure 3.40 Moment-Curvature Relationships for Nonproportional Loadings (at ϕ= 0.01 rad/in, Confined Concrete)

For P=300 kips, the moment capacity decreases shortly after ϕ=0.015 rad/in (Figure 3.40). Similar analyses are made with 1% confined concrete (ε_u=0.025 and σ_u= 0.0) to see influence of nonproportional loading on moment-curvature relationship for partially confined concrete section. From Figure B-17 and Figure B-18, it is evident for unloading, the hysteresis loops are different from that of confined concrete as discussed above. At ϕ=0.005 rad/in, axial load is increased nonproportionally from P=0 to P=100 kips, P=200 kips and P=300 kips, the moment capacity is decreased from 620 kips-in to 612 kips-in, 475 kips-in and 120 kips-in respectively. Upon unloading the capacity decreases almost linearly with curvature for P=100 kips and P=300 kips. For P=200 kips, the unloading proceeds with a pinching in the loop with the decrease of curvature (Figure B-17). Same analysis is done at ϕ=0.01 rad/in, for increase of P=0 to P=100 kips, P=200 kips and P=300 kips, the moment capacity drops abruptly to 420 kips-in and 133 kips-in and 180 kips-in from 740 kips-in for axial load, P=0. On unloading, they follow a linear slope with the decrease of curvature (Figure B-18). Next the analysis is done for loading after the nonproportional axial load acted on the section which is 1% confined and is done at ϕ=0.005 rad/in and ϕ=0.01 rad/in. For ϕ=0.005 rad/in (Figure B-19), while loading from P=0 to P=100 kips, P=200 kips and P=300 kips, the moment capacity suddenly drops from 620 kips-in to 612 kips-in, 475 kips-in and 120 kips-in respectively due to decrease in strength and ductility. On loading beyond ϕ=0.005 rad/in, the curve for P=100 kips shows some nonlinearities with a drop in moment capacity after ϕ=0.006 rad/in (Figure B-19). For P=200 kips, the moment capacity is decreased sharply at ϕ=0.005 rad/in and it starts increasing after ϕ=0.005 rad/in with increase in curvature. For P=300 kips, the curve is different from other two. Moment capacity decreases while the axial load increases from P=0 to P=300 kips holding the curvature constant at ϕ=0.005 rad/in and the moment capacity starts increasing with increase in

curvature with the constant axial loading. For ϕ=0.01 rad/in same analysis is done (Figure B-20). Here the moment capacity for P=100 kips, P=200 kips and P=300 kips directly drops from 740 kips-in at P=0 to 420 kips-in, 133 kips-in and 180 kips-in respectively. While loading from this point, moment capacity increases with the increase of curvature. The curve for P=100 kips meets the curve for P=300 kips at ϕ=0.016 rad/in and follow the same curve with some nonlinearity till ϕ=0.018 rad/in and then the curves for the two loading diverge. For P=100 kips, the moment capacity is less than that for P=300 kips. The curve for P=200 kips leads to the least moment capacity for the section among them.

From these analyses done, it is seen that there are significant differences in the path they follow in the same level of loading for different curvatures and different confinement of concrete. As it is observed from these examples, varying axial and lateral forces have great influence on strength, stiffness, energy dissipation capacity of a reinforced concrete section. It is to be noted from the study for 1% confined concrete that moment capacity of a reinforced concrete section significantly changed when the concrete is not fully confined and is much more path dependent.

CHAPTER 4

EFFECTS OF NONPROPORTIONAL AXIAL LOADS ON R/C COLUMNS

4.0 Introduction

For a reinforced concrete column, the nature of hysteresis loop under uncoupled fluctuation in axial load is significantly different from what happens under proportionally varying axial load (i.e. masing type behavior). Such behavioral characteristics are due to changes in strength, stiffness and ductility of the column as a result of variations in axial load. One of the most important effects of varying axial load on the hystersis loop is that it causes a decrease in lateral displacement while the lateral load increases. This is due to the increase in stiffness of the column as a result of variation in the axial load. Therefore a model is developed on the basis of fiber representation of a section to make possible the analysis of reinforced concrete column indepently under nonproportional variations of axial and lateral loadings.

The member is divided into slices and each slice is further discretized into concrete/steel fibers. The state of fibers are monitored and stresses are found out from the material properties of concrete and steel considering plane sections remain plane. Moment-curvature relationship is found out for each slice for the corresponding axial and lateral forces acting on the column. The deflection for the whole column is found out by integration over the length of the column assuming linear flexibily between slices. By monitoring the various fibers and slices, it is possible to obtain the local response at critical sections including moment-curvature and shear histories. The model is capable to analyze:

a) the effect of energy dissipation capacity of R/C members when the axial load varies non-proportionally.

b) the effect of the parameters such as degree of concrete confinement on the

response of R/C members subjected to large uncoupled variations in the axial load and lateral load.

4.1 Example Column

The column shown in Figure 3.1 was used by Saadeghvaziri (1990) to analyze the effect of uncoupled variations in lateral and axial loads on R/C columns. Assuming the point of inflection to be at midheight, in the study half of the column is modelled as a cateliver column. The material properties were assumed to be: ρ=2%, σ_t=0.45 ksi, σ_c=5.5 ksi, ε_c=0.0025, σ_u=5.0 ksi, ε_u=0.006, f_y=60 ksi and E=29 ksi with 3% strain hardening.

4.2 Analytical Investigations

Three analysis are being done with this fiber model described above with the reinforced concrete column illustrated in section 4.1. The objective is to investigate the effect of nonproportionally varying axial load on the distribution of curvature along the length of column. Also, the effect of the degree of concrete confinement on the response of R/C column subjected to large uncoupled variations in axial and lateral loads are also investigated.

In the first example, the column is analyzed under two different loading histories. Firstly, the column is subjected to lateral load in terms of shear force as 20 kips and axial load of -50 kips. (tensile) respectively. Then in the second case, first a shear of 20 kips and an axial load of 250 kips are applied proportionally and then the shear is held constant but the axial force is decreased to -50 kips. Thus the final state of applied forces is same for both cases. The shear vs displacement curves are shown in Figure 4.1. It is seen from the curve that the nature of the

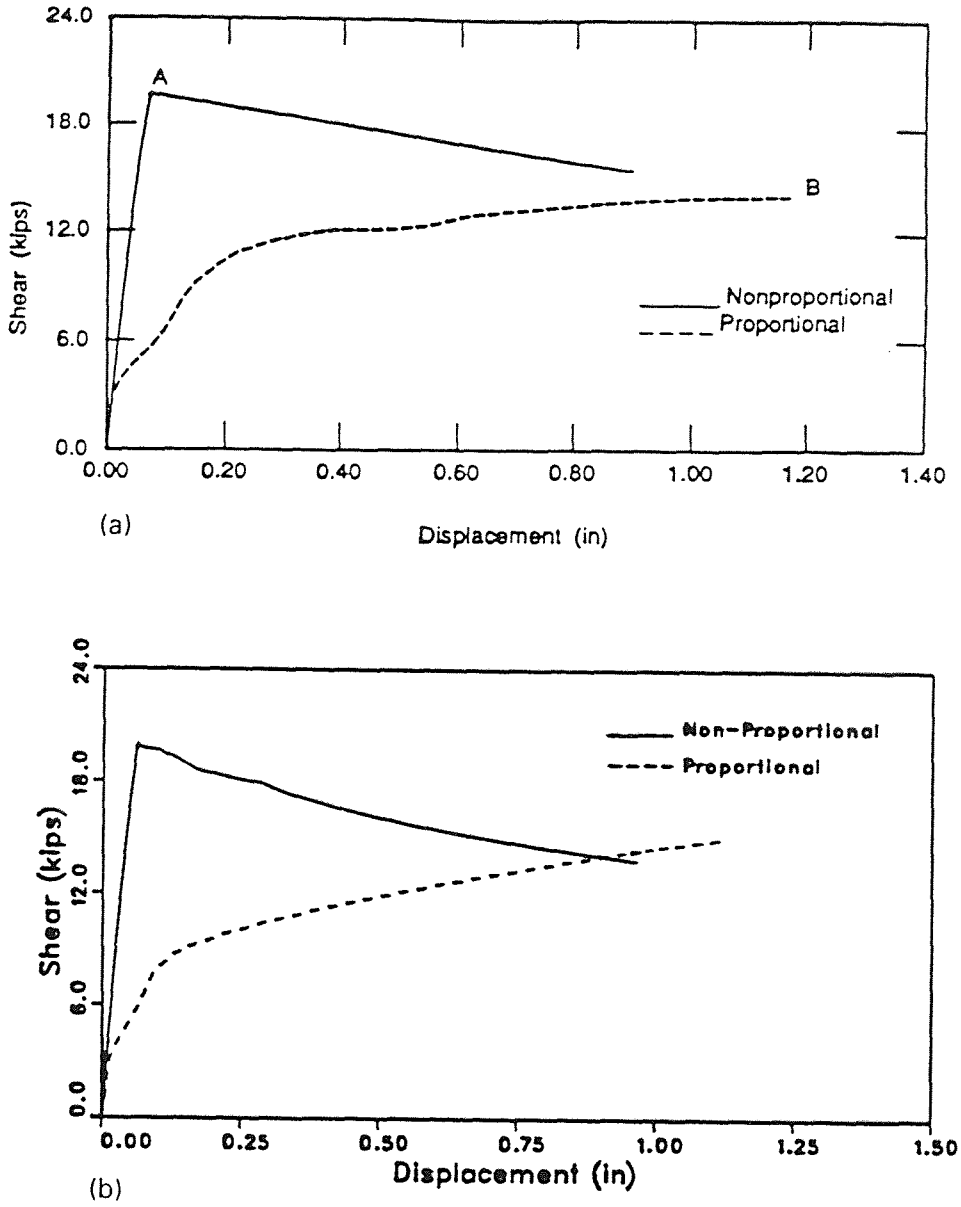

Figure 4.1 Load-Deflection Relationships for Example 1
(a) Saadeghvaziri (1990), (b) Present Study

displacement curve are sigficantly different and the response for the second case shows a softening portion due to the reduction in the stiffness of the column as a result of the decrease in the compressive axial load. The analysis is compared with Saadeghvaziri (1990), as shown in Figure 4.1, the load displacement curve is similar. The curvature distribution shown in Figure 4.2 for the first case is typical of a R/C member i.e, a significant plastic deformation happened over a distance which is about the same length of the depth of the cross-section. The curvature also decreases from the fixed end of high moment region to the free end of low moment region. The overall pattern of curvature distribution is in good shape and in good agreement with Saadeghvaziri (1990). But for the second case, curvature distribution is significantly different from that of Saadeghvaziri (1990).

According to the results for analysis of the curvature distribution obtained by him, the plastic zone is not limited to a region equal to the depth of the cross section and in some region along the height of the column, the curvature is increasing while the moment is decreasing. But the analysis with the fiber model shows that for the uncoupled variations of the axial and lateral forces, the curvature distribution follows the overall pattern of typical R/C column i.e, plastic deformation occurs over a length equal to depth of cross-section and decreases towards the free end (Figure 4.2). In the second analysis, a R/C column is analyzed with adequate confinement. Two types of analyses are being done. For the first case, a shear force of 11 kips and an axial force of 230 kips are applied proportionally. In the second case, a shear force of 11 kips and an axial force of -50 kips are applied and then holding the shear constant, the axial force is increased to 230 kips. Thus the final state of applied forces are same for both cases. While the load-deformation curves (Figure 4.3) for both cases are analyzed, it is seen for second case, the lateral deformation decreases while applied shear is kept constant, The deflection for proportional loading is 0.031 in and for

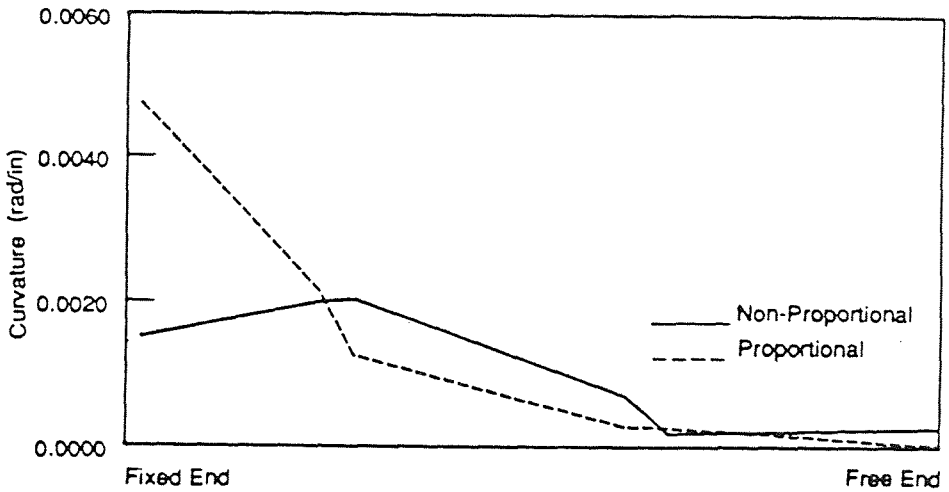

(a)

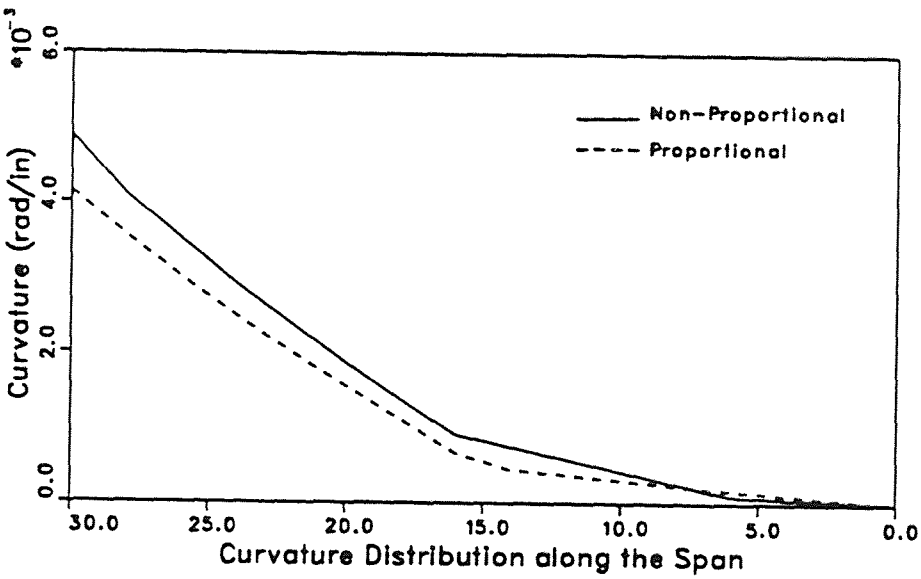

(b)

Figure 4.2 Curvature Distributions along the Span for Example 1 (a) Saadeghvaziri (1990), (b) Present Study

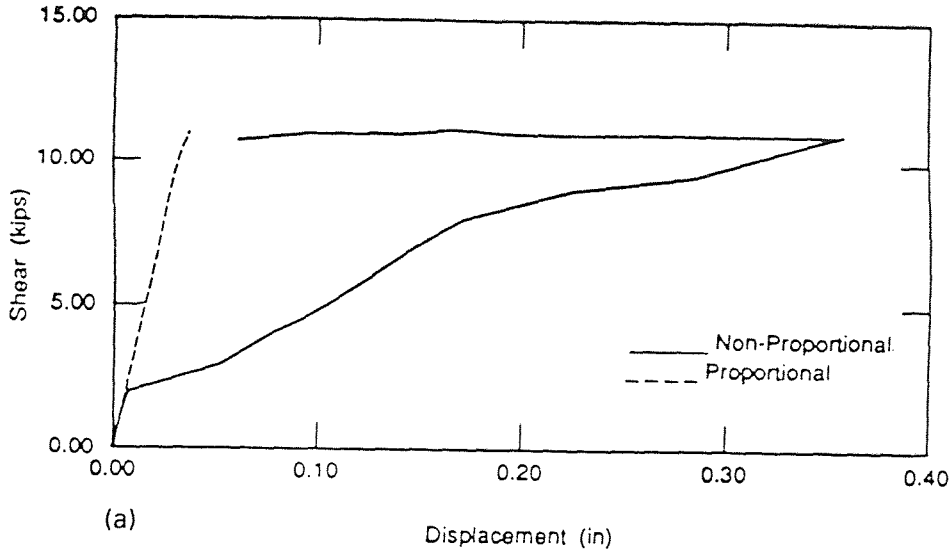

(a)

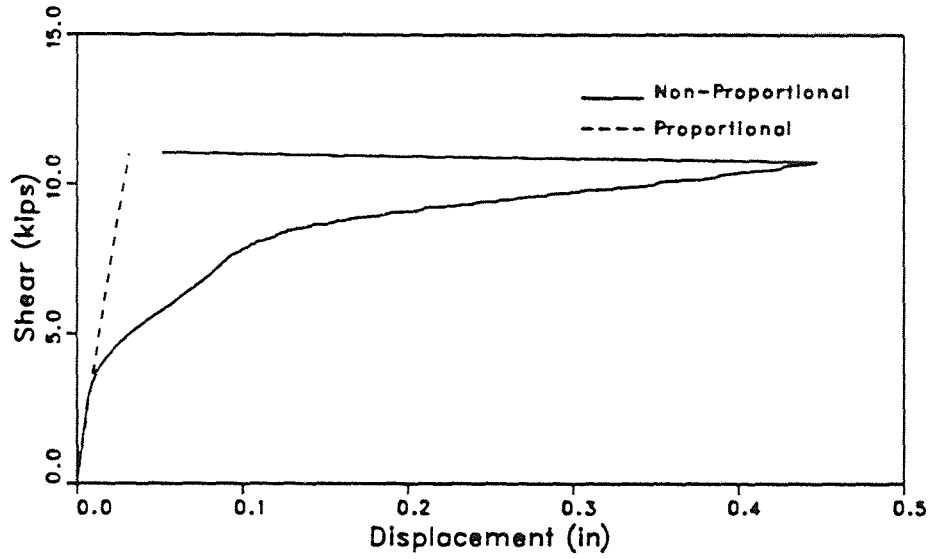

(b)

Figure 4.3 Load-Deflection Relationships for Example 2 (Confined Column) (a) Saadeghvaziri (1990), (b) Present Study

nonproportional loading, it is 0.052 in which is more or less consistent with Saadeghvaziri (1990) which are 0.037 in for proportional case and 0.061 in for non-proportional case. Whatever inconsistencies in the value of displacement came out may be removed by adjusting the convergence limit, discretizing the elements to smaller values and assuming smaller load steps. Furthermore, there is also insignificant variation in curvature distributions. The ratio between the curvature at the fixed end for non-proportional loading and proportional loading is 2.3 in present study by fiber model compared to 2.5 by Saadeghvaziri (1990) as shown in Figure 4.4.

In the third example, the analysis is done to see the effect of nonproportional fluctuation in the axial load on the response of unconfined R/C columns. The same problem as the second one is solved using the concrete as unconfined (i.e; the ultimate strain (ε_u) of concrete is taken as 0.0028 in/in instead of 0.006 in/in which is for confined concrete). The load-deformation curves for both cases are shown in Figure 4.5. Under proportional variation, the column can carry 11 kips shear and 230 kips of axial load and it appears that even it can carry more load. But under non-proportional variations of axial and lateral loads, the column can sustain only 140 kips of axial load which is much smaller than intended maximum load of 230 kips. That is under uncoupled variations in lateral and axial loads, the capacity of the member can be significantly smaller than the case in which the axial load is constant or for proportional variations. So for nonproportional axial and lateral loadings, the structure may fail below the design capacity which is estimated considering proportional loading. It is seen from Figure 4.6 that the curvature distribution is also different from example 2 in Figure 4.4 and the maximum curvature for the unconfined column is greater than that of example 2 for the confined column in both proportional and nonproportional case regardless of the nature of variations in axial and lateral forces. This is due to the failure of concrete

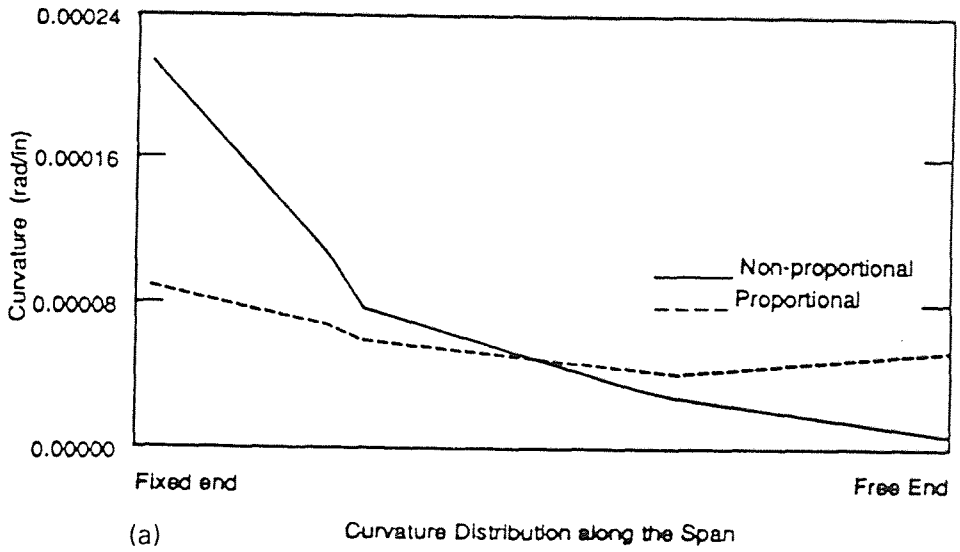

(a)

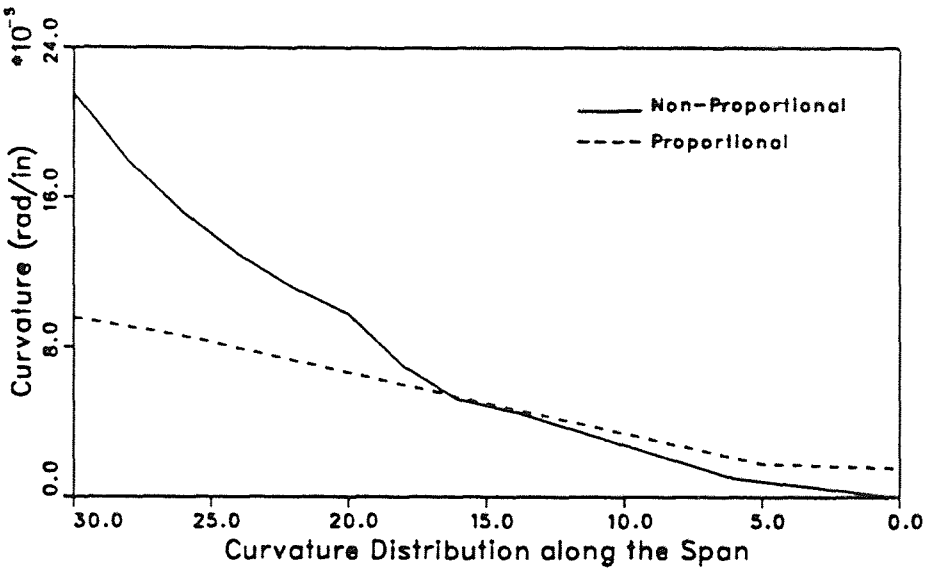

(b)

Figure 4.4 Curvature Distributions along the Span for Example 2 (a) Saadeghvaziri (1990), (b) Present Study

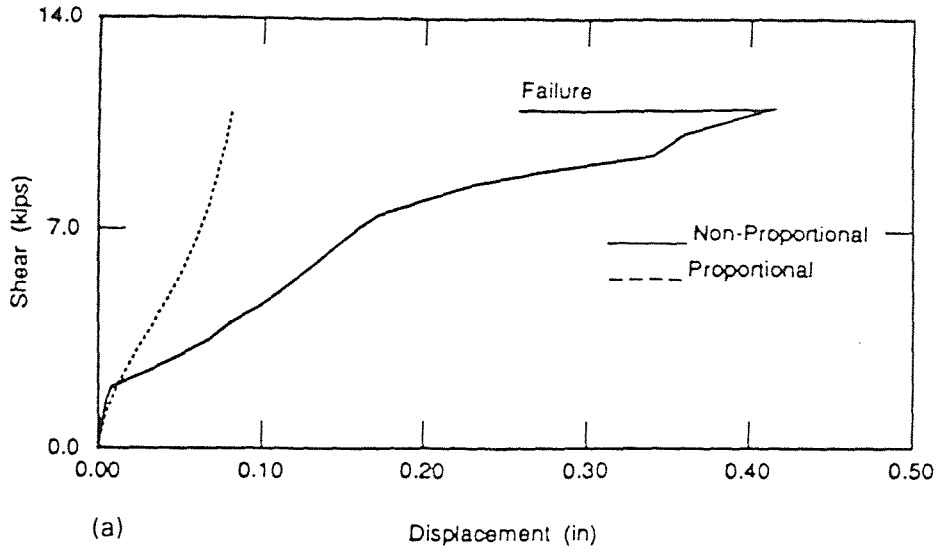

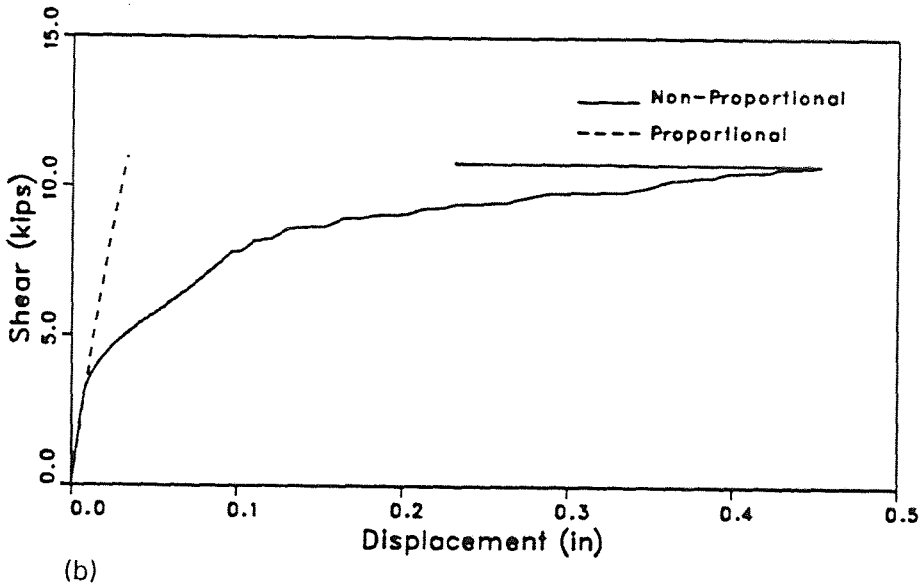

Figure 4.5 Load-Deflection Relationships for Example 3 (Unconfined Column) (a) Saadeghvaziri (1990), (b) Present Study

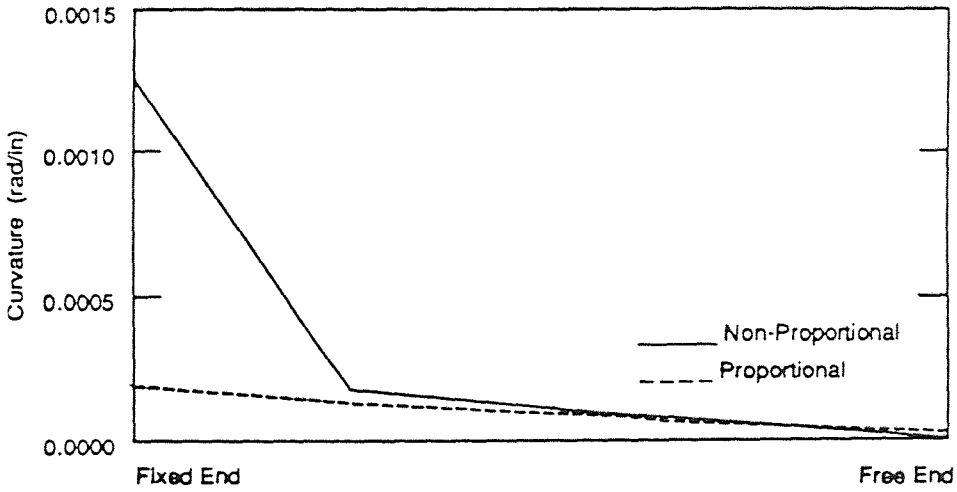

(a)

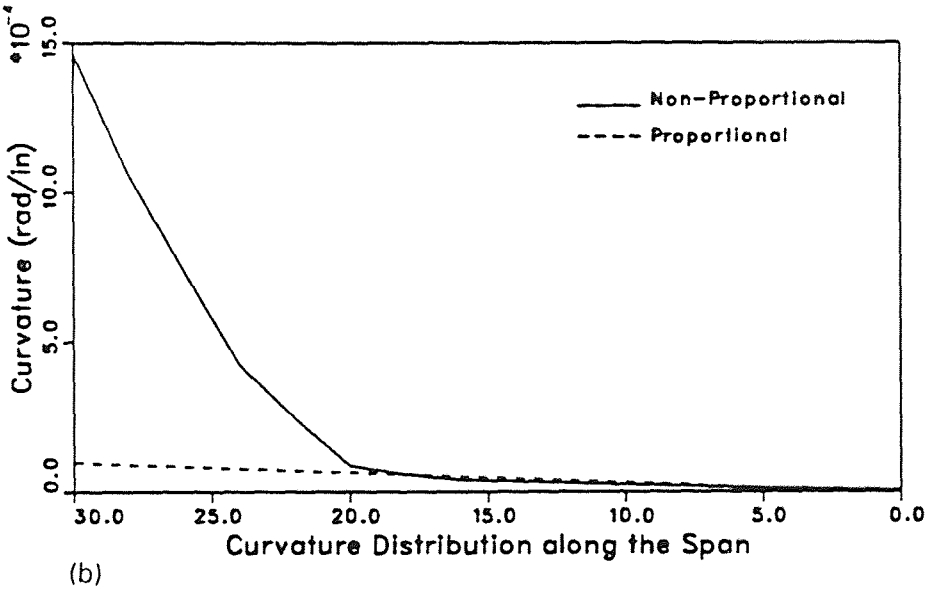

(b)

Figure 4.6 Curvature Distributions along the Span for Example 3 (a) Saadeghvaziri (1990), (b) Present Study

material and its subsequent effect on the reduction in the effective depth of the cross-section.

The results of the study in this chapter indicates that the load-deflection relationship of concrete column under proportional and nonproportional loadings are different. The phase-diffrence between the axial and lateral load makes the relationship more complicated. For example 1, the response under nonproportional loadings produced a softening portion which is due to the reduction in stiffness of the column as result of decrease in compressive loads. Although the input energy for proportional and nonproportional loadings are not equal but the area under the load deformation hysteresis loops are almost equal. This indicates that the energy dissipation capacity of the column under nonproportional loadings is not only proportional to the area bounded by lateral load-deformation hysteresis loops but also the other sources like axial hysteresis energy and axial load-deformation must be considered (Saadeghvaziri and Foutch (1988)). It is shown in example two and example three that for unconfined concrete, the capacity is significantly smaller than that for confined concrete under nonproportional loadings.

CHAPTER 5

CONCLUSIONS

The fiber model is developed for the investigation of the effects of nonproportional axial loads on nonlinear response of reinforced concrete members. When the structure is subjected to earthquake motions, large uncoupled axial and lateral forces can be developed in the exterior columns of a frame structure. This model is capable of simulating the complex behavior of reinforced concrete columns when the loading pattern is not proportional. The versatility is due to the fact that no predefined rules are involved in dictating the overall hysteretic behavior of any cross-section. It is shown through different analyses in chapter three and chapter four that nonproportional fluctuations in the axial force have a significant effect on post-elastic response of reinforced concrete columns.

The analytical fiber model developed in chapter two which demonstrates good ability in predicting ultimate strength and capacity of a R/C column and reasonably reproduced the hysteresis loops of the experimental study by Kent (1969). All characterstics of the inelastic response of R/C columns are incorporated through the material properties of concrete and steel. The material model of concrete includes the degree of concrete confinement, cracking and crushing and a set of hysteretic rules to simulate the cyclic behavior. For reinforcement, a bilinear elastic-plastic material model with kinematic hardening is incorporated in the model.

The inelastic response of R/C section under nonproportionally varying axial loads are investigated in chapter three. Analyses are done to examine the effects of nonproportional loadings on stiffness, strength, ductility and energy dissipation capacity of a section along with the influence of different degree of concrete confinement. It is shown in the analyses that the capacity of the section under

nonproportional loading varies greatly depending on initial loading conditions, It is assumed in the design practice that if the axial load and moment are within P-M interaction loop, the design is safe. But while the section is under nonproportional loadings, the P-M diagram as well as the balanced load and balanced moment vary depending on the initial loading conditions. It is seen that for higher values of initial strain causes nonlinearity in P-M diagram which effects the capacity of a section. Some analyses are done to examine the nature of hysteresis loop under nonproportional loadings. It is shown that the hysteresis loop and energy dissipation capacity depends on the level of loadings, curvature and degree of confinement of concrete.

The results of the study in chapter four indicates that large uncoupled variations in axial and lateral loads results in nonlinear type load-deflection relationships for reinforced concrete columns. Under nonproportional loadings, the changes in the behavior is attributed to the changes in the strength, ductility and stiffness of the column due to the uncoupled variations in axial and lateral loads. The Proportional case represents the behavior of a typically reinforced concrete member. But for nonproportional case, the response of the column is totally different from that for proportional loadings. The load-deformation relationship for uncoupled variations in axial and lateral loading, the capacity of the member is significantly different than a case when the axial load is constant or proportional. This an important factor that should be considered in seismic performances of the structure especially, the exterior columns of a frame system which may experience this kind of loading. During previous earthquakes, many columns are believed to have failed failed before they reached their design capacity.

APPENDIX A

SUBROUTINE P-M

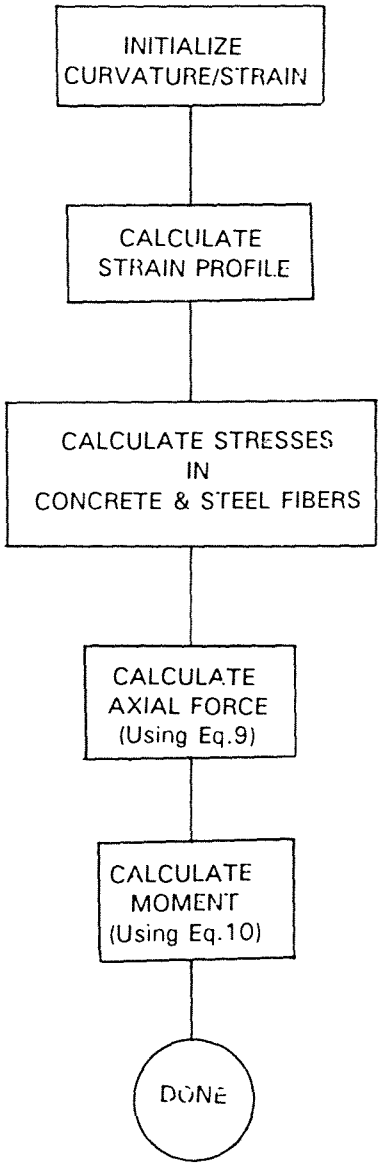

Figure A-1 Flow Chart for Subroutine P-M

SUBROUTINE AXIAL_LOAD

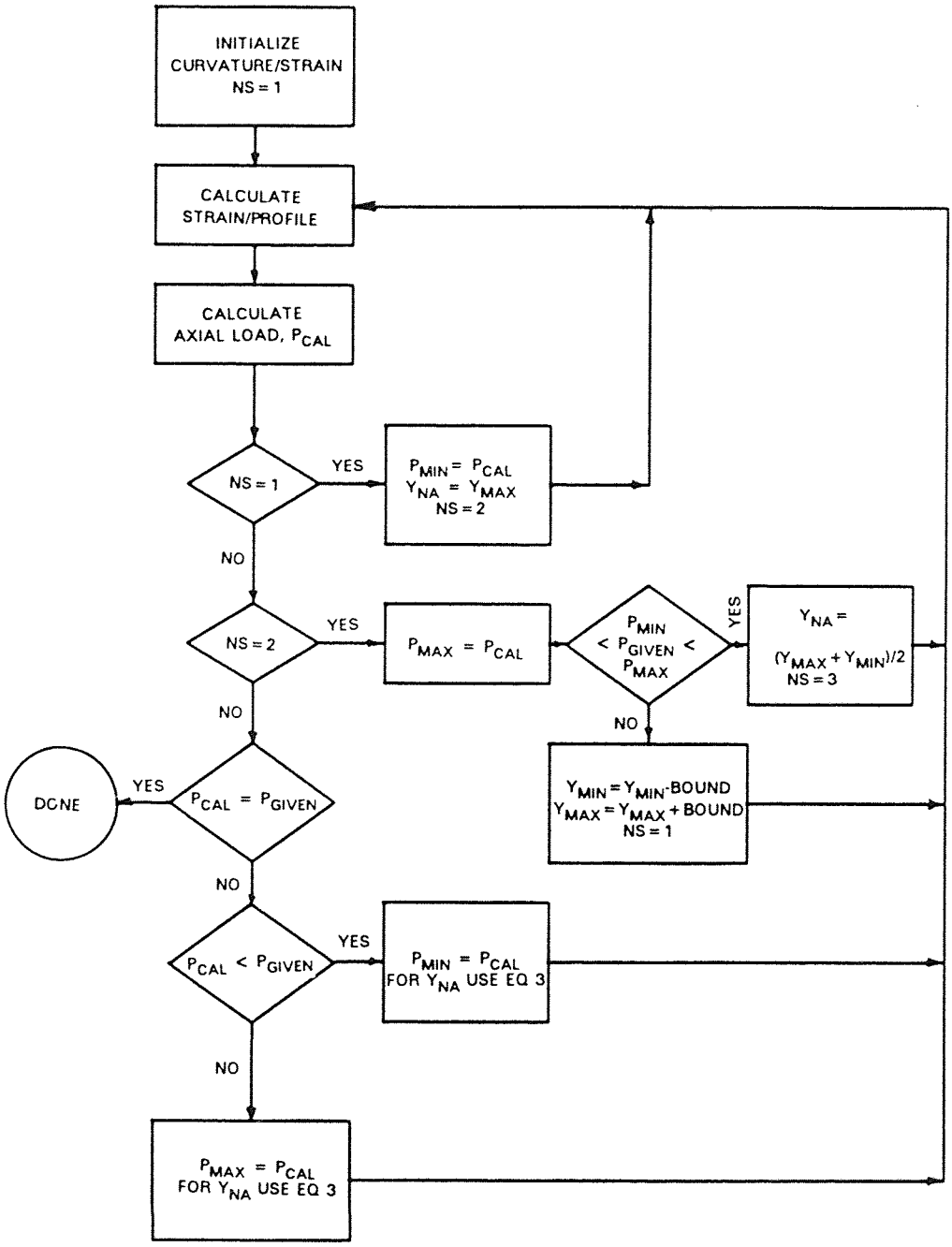

Figure A-2 Flow Chart for Subroutine AXIAL_LOAD

SUBROUTINE PHY

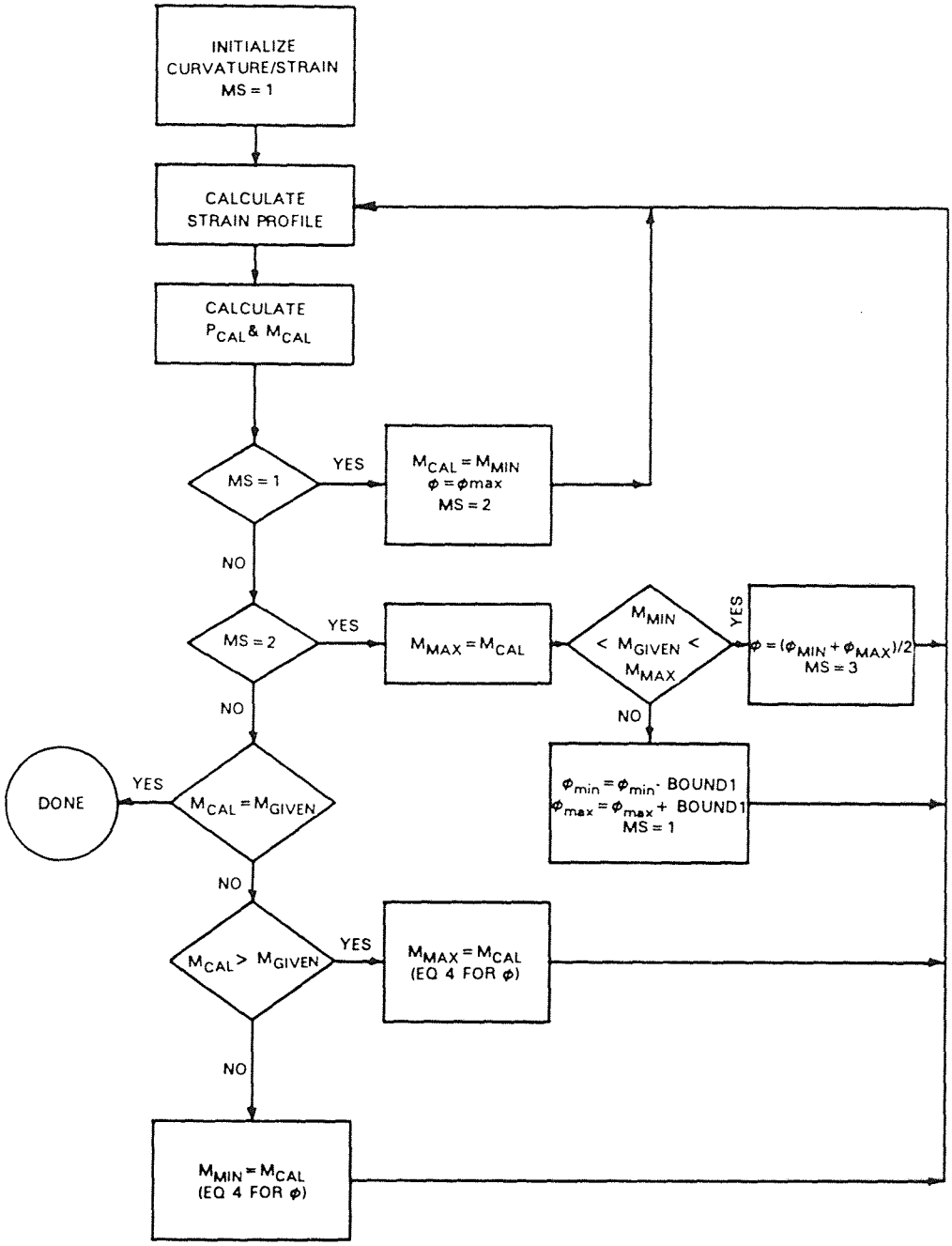

Figure A-3 Flow Chart for Subroutine PHY

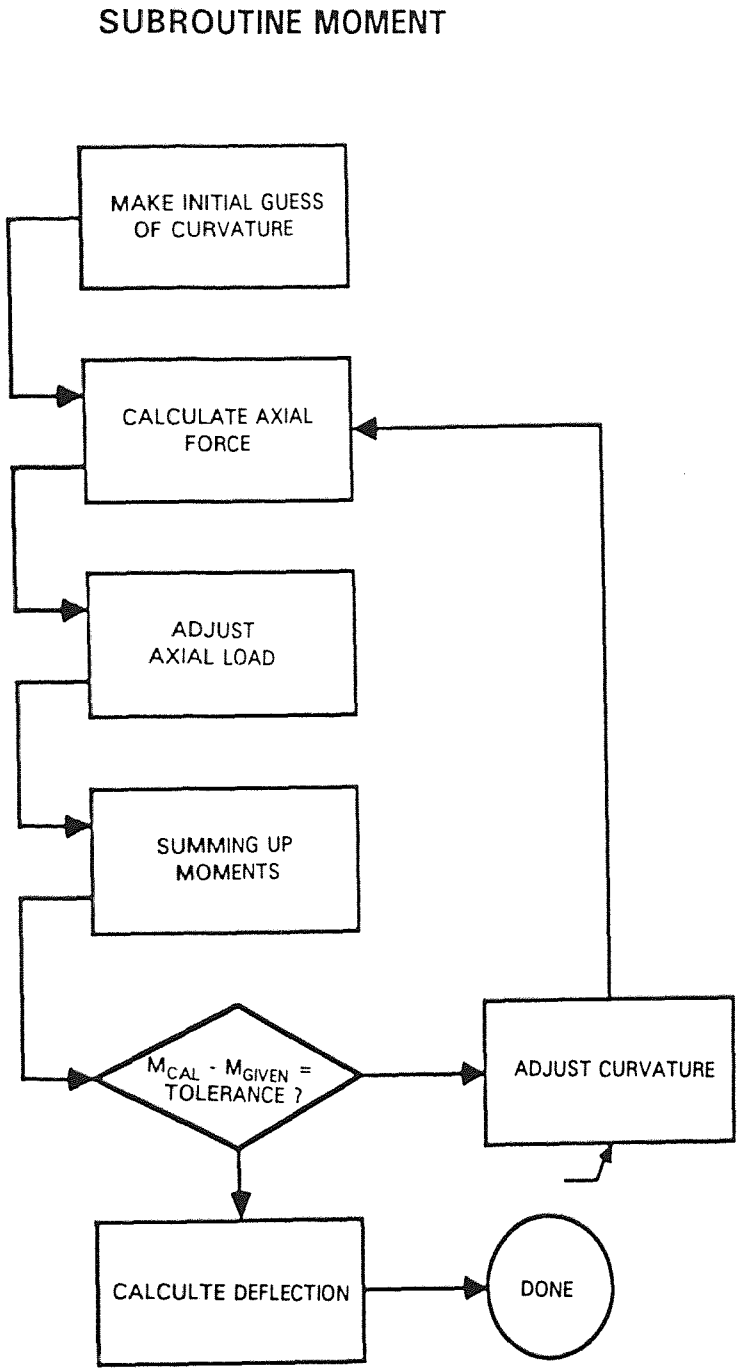

Figure A-4 Flow Chart for Subroutine Moment

SUBROUTINE DEFLECTION

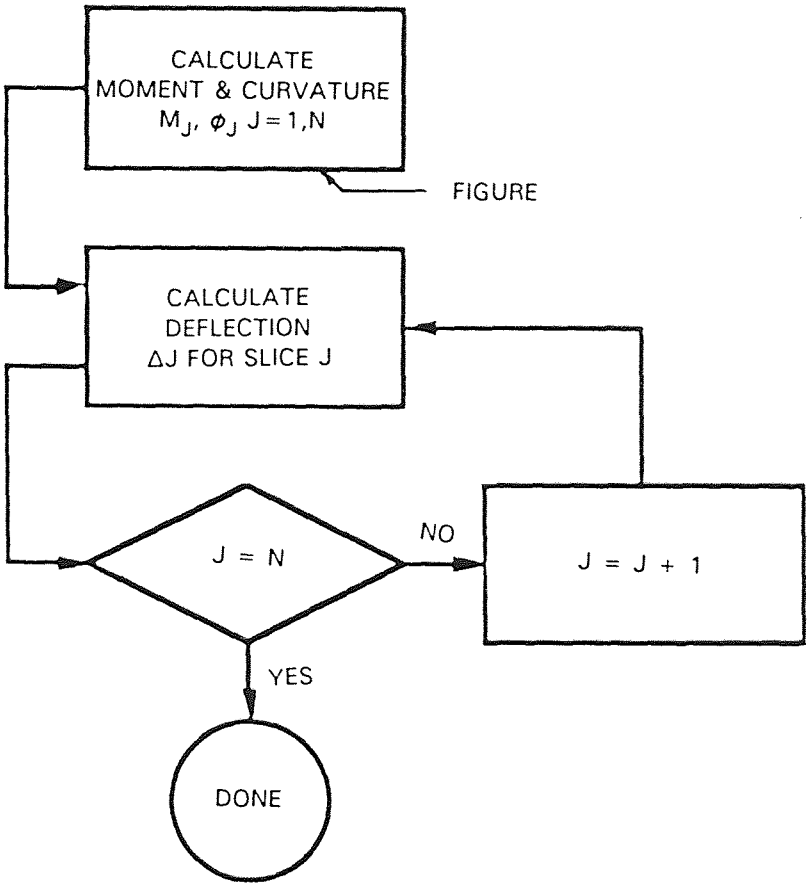

Figure A-5 Flow Chart for Subroutine Deflection

APPENDIX B

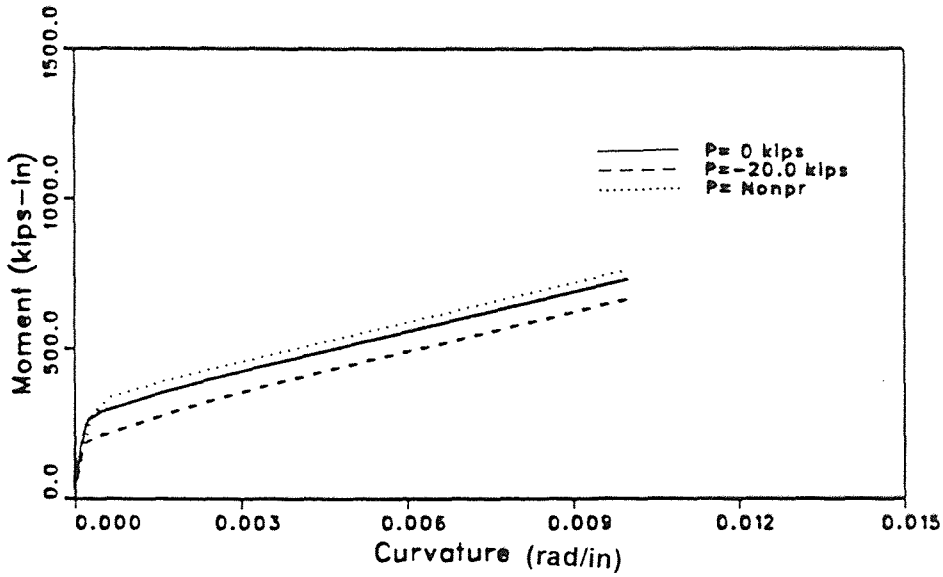

Figure B-1 Moment-Curvature Relationships for Proportional and Nonproportional Loadings (P= 20 kips, Confined)

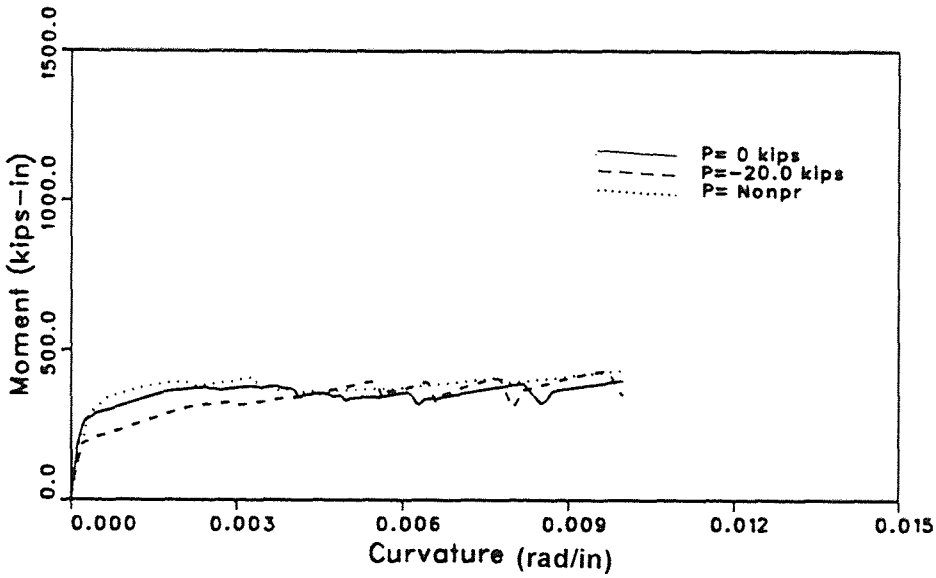

Figure B-2 Moment-Curvature Relationships for Proportional and Nonproportional Loadings (P=-20 kips, Unconfined)

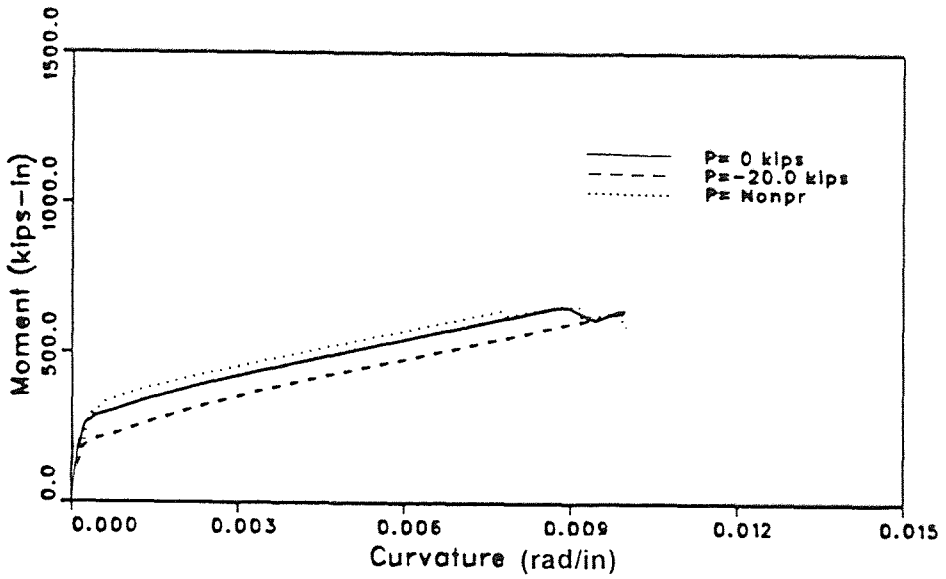

Figure B-3 Moment-Curvature Relationships for Proportional and Nonproportional Loadings (P=-20 kips, 1% Confinement)

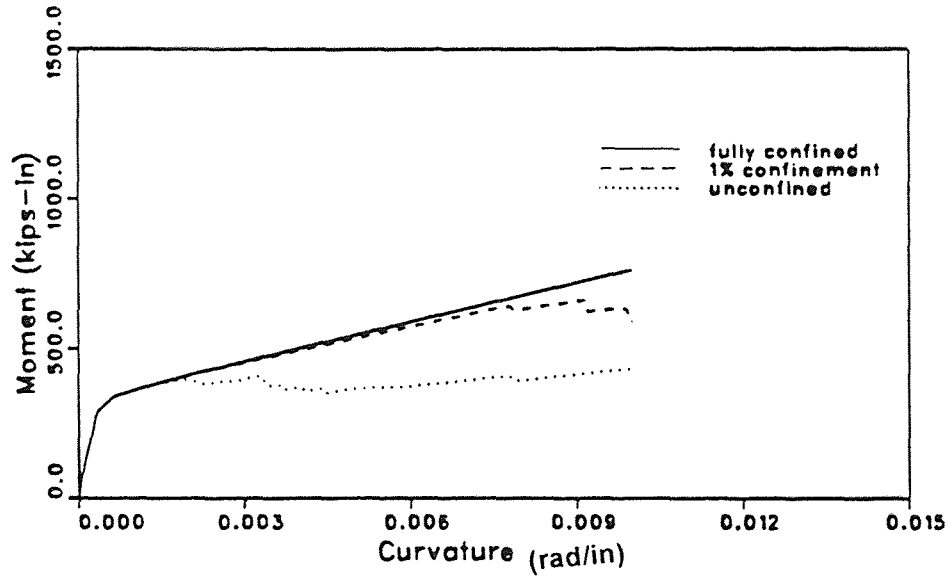

Figure B-4 Moment-Curvature Relationships for Nonproportional Loadings at Different Degrees of Confinement (P=-20 kips)

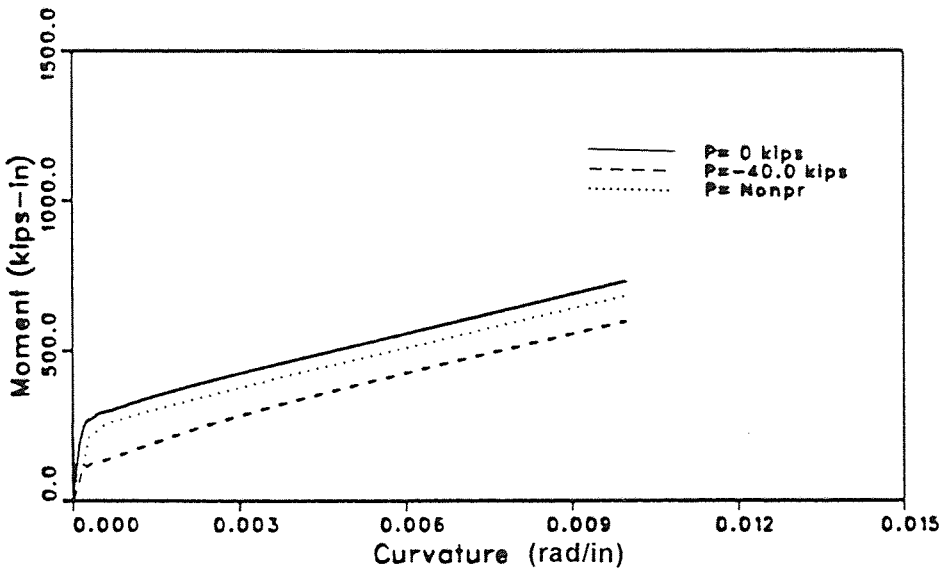

Figure B-5 Moment-Curvature Relationships for Proportional and Nonproportional Loadings (P=-40 kips, Confined)

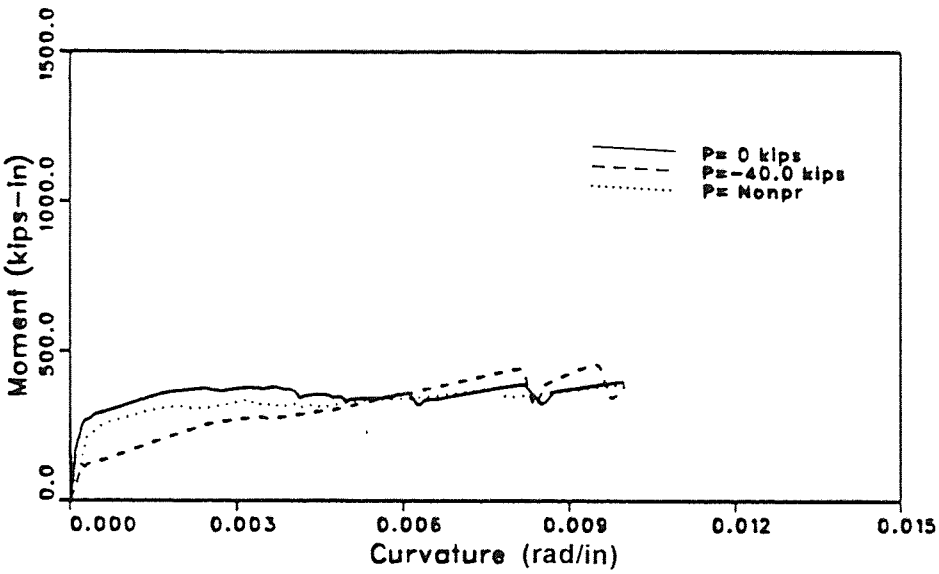

Figure B-6 Moment-Curvature Relationships for Proportional and Nonproportional Loadings (P=-40 kips, Unconfined)

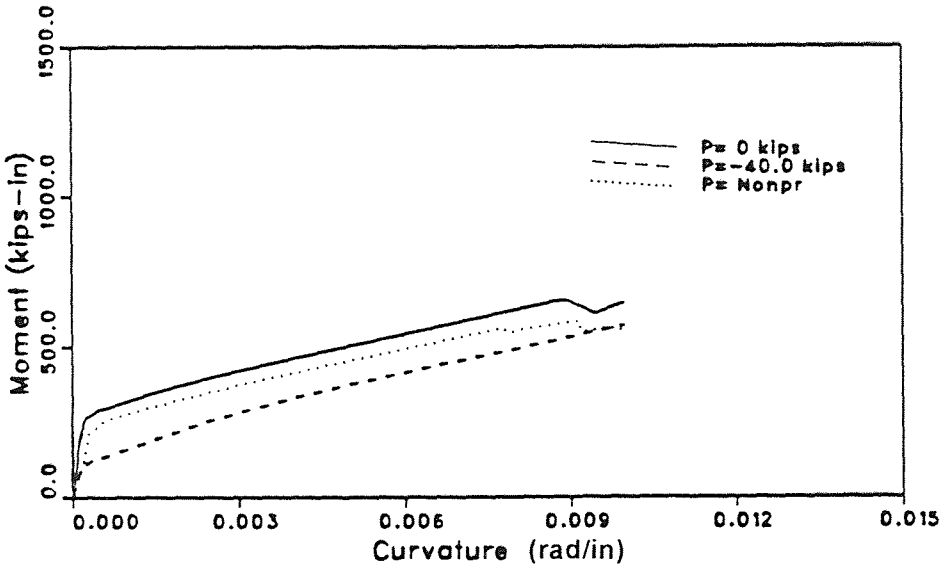

Figure B-7 Moment-Curvature Relationships for Proportional and Nonproportional Loadings (P=-40 kips, 1% Confinement)

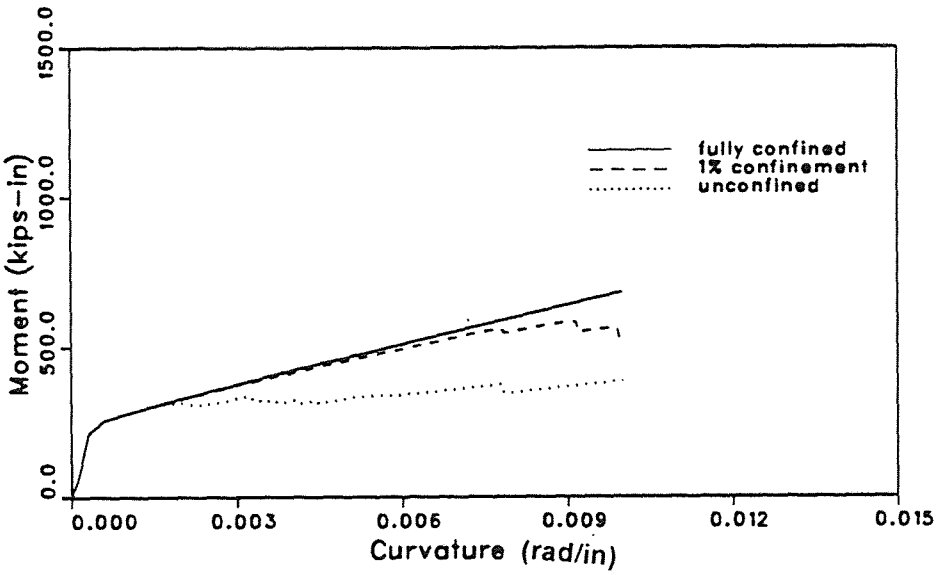

Figure B-8 Moment-Curvature Relationships for Nonproportional Loadings at Different Degrees of Confinement (P=-40 kips)

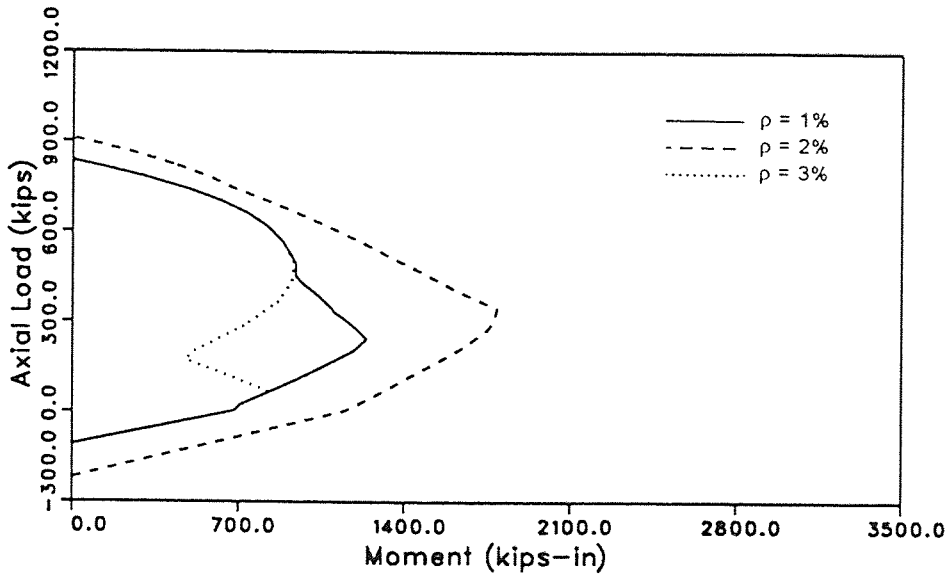

Figure B-9 P-M Interaction Diagrams for Different Reinforcement Ratios for the L-Shaped R/C section ($\varepsilon_{c\ initial}$=0.001 at P=0, ε_{final}=0.003)

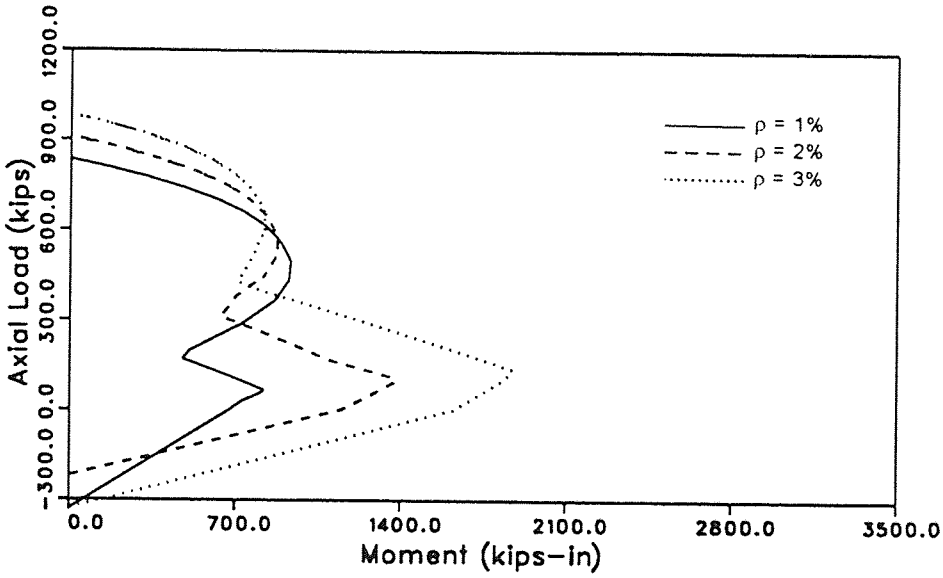

Figure B-10 P-M Interaction Diagrams for Different Reinforcement Ratios for the L-Shaped R/C section ($\varepsilon_{c\ initial}$=0.002 at P=0, ε_{final}=0.003)

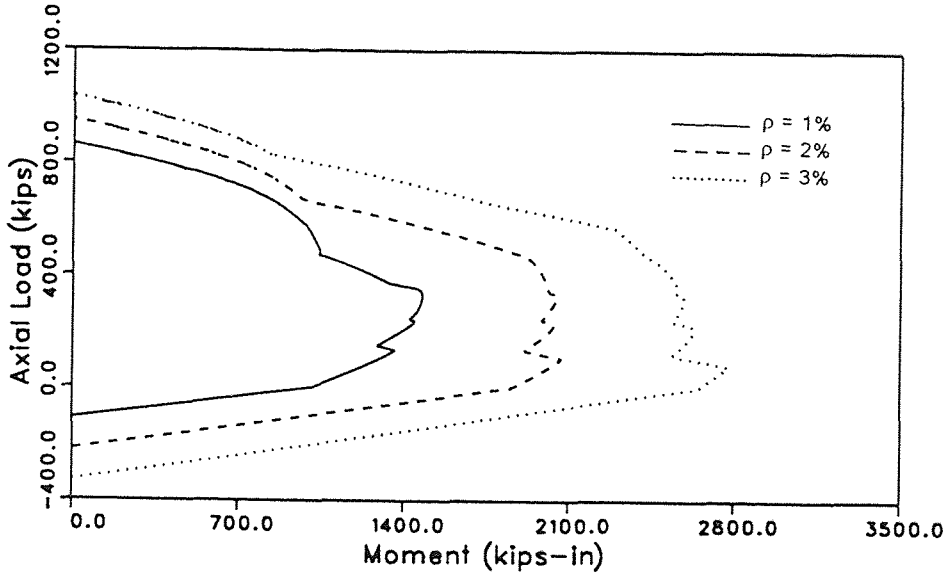

Figure B-11 P-M Interaction Diagrams for Different Reinforcement Ratios for the L-Shaped R/C section ($\varepsilon_{c\ initial}$=0.002 at P=0, ε_{final}=0.01)

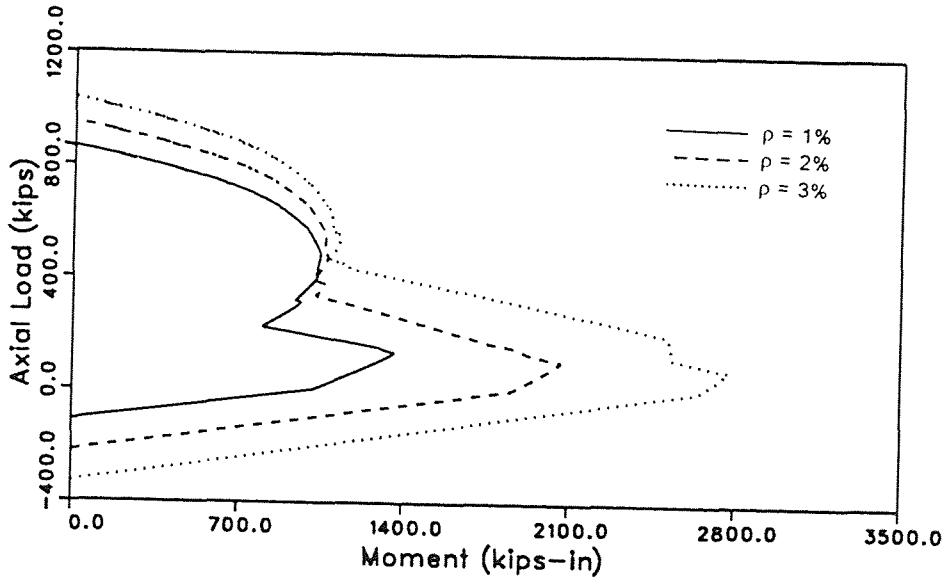

Figure B-12 P-M Interaction Diagrams for Different Reinforcement Ratios for the L-Shaped R/C section ($\varepsilon_{c\ initial}$=0.006 at P=0, ε_{final}=0.01)

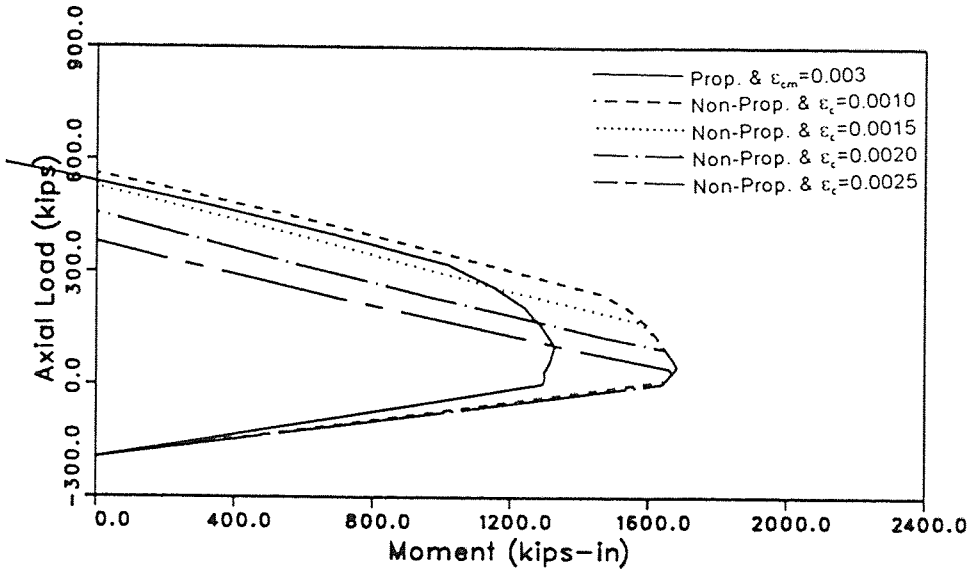

Figure B-13 P-M Interaction Diagram for Different initial strains in the L-Shaped R/C Section (ε_{final}=0.003)

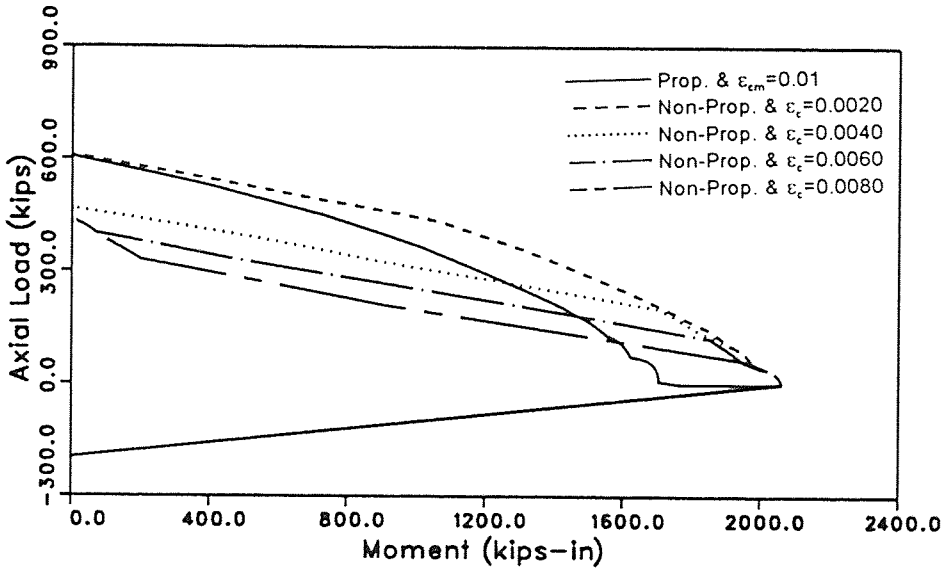

Figure B-14 P-M Interaction Diagram for Different initial strains in the L-Shaped R/C Section (ε_{final}=0.01)

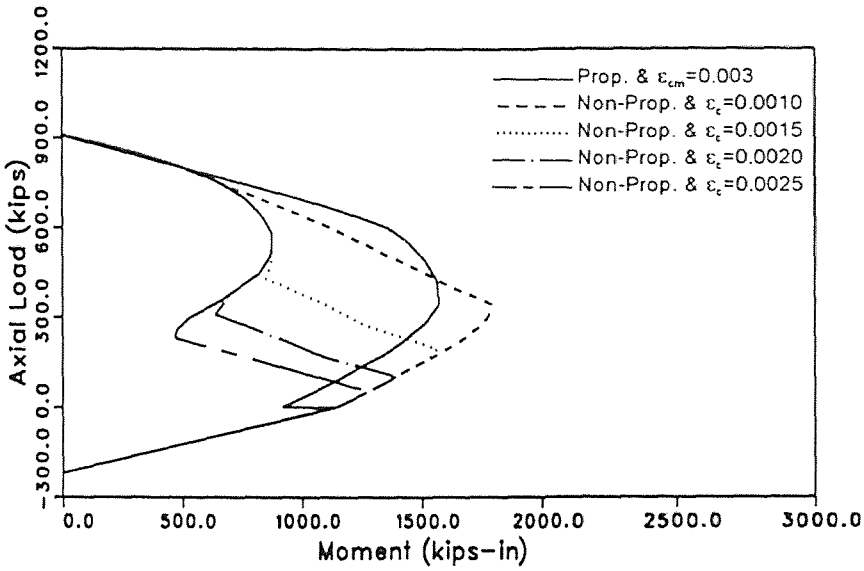

Figure B-15 P-M Interaction Diagram for Different initial strains in the L-Shaped R/C Section (ε_{final}=0.003)

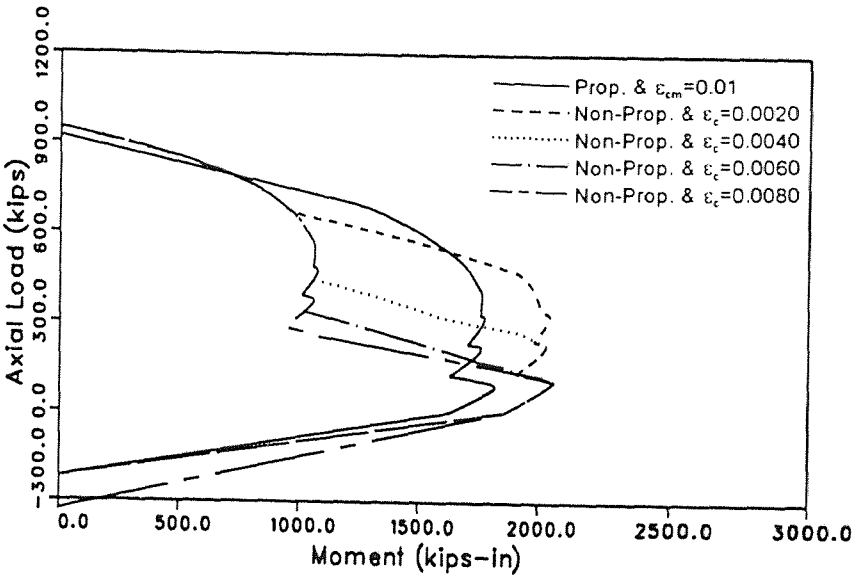

Figure B-16 P-M Interaction Diagram for Different initial strains in the L-Shaped R/C Section (ε_{final}=0.01)

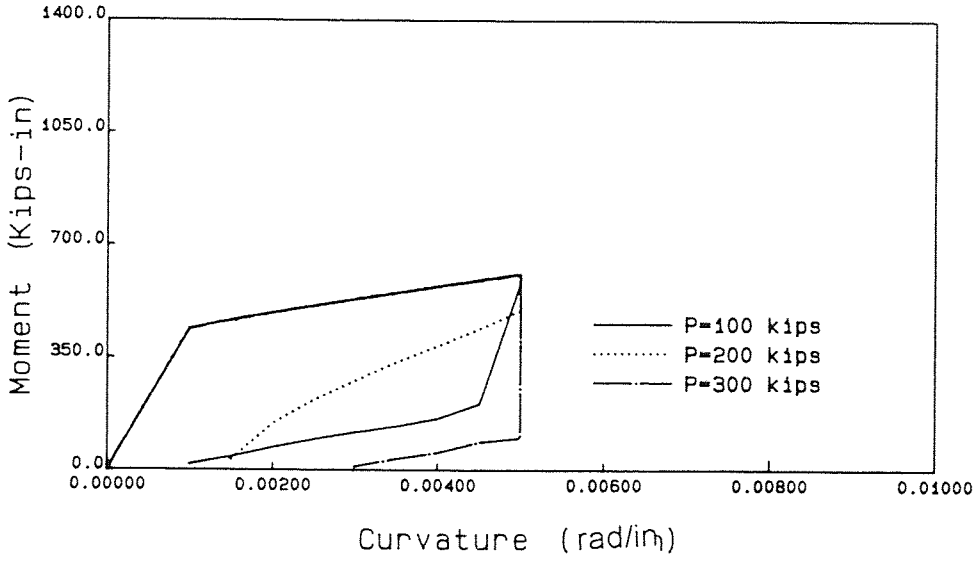

Figure B-17 Moment-Curvature Relationships for Nonproportional Unloading (at ϕ= 0.005 rad/in, 1% confinement)

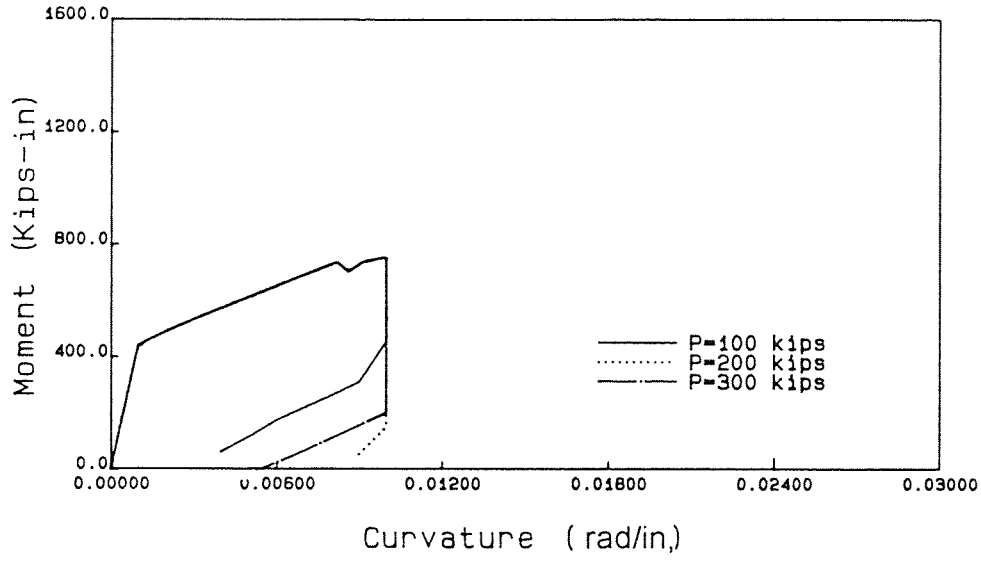

Figure B-18 Moment-Curvature Relationships for Nonproportional Unloading (at ϕ= 0.01 rad/in, 1% confinement)

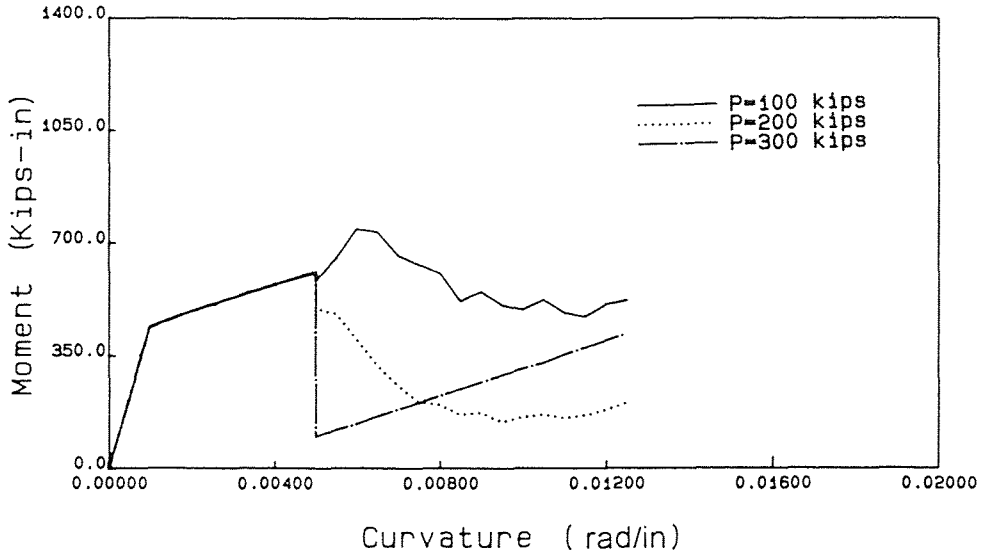

Figure B-19 Moment-Curvature Relationships for Nonproportional Loadings (at ϕ= 0.005 rad/in, 1% confinement)

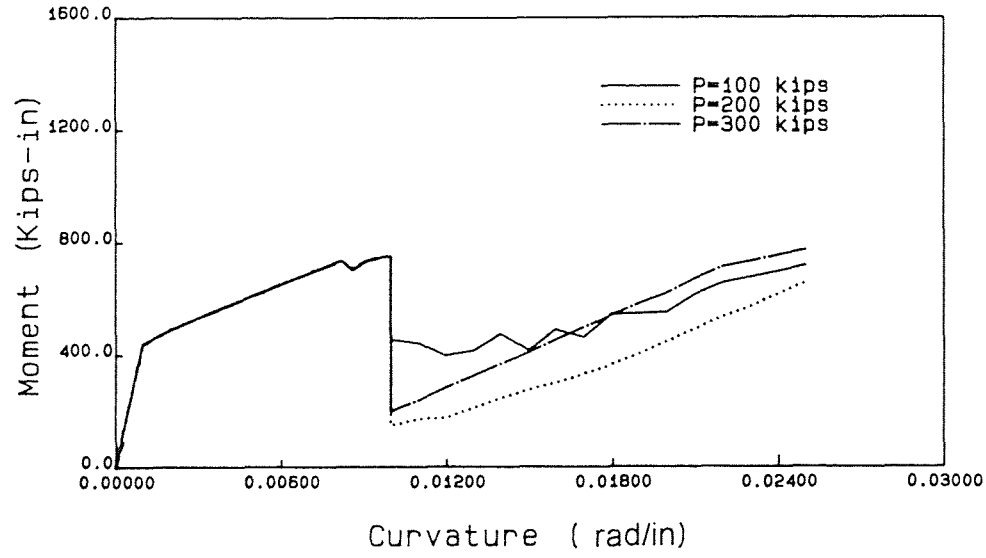

Figure B-20 Moment-Curvature Relationships for Nonproportional Loadings (at ϕ= 0.01 rad/in, 1% confinement)

REFERENCES

Abrams, D.P. "Influence of Axial Force Variation on Flexural Behavior of Reinforced Concrete Columns", ACI Structural Journal, May-June, 1987, pp. 246-254.

Agrawal, A.B., L.G. Jaeger, and A.A. Mufti. "Crack Propagation and Plasticity of Reinforced Concrete Shear Walls under Monotonic and Cyclic Loading", Conference on Finite Element Methods in Engineering, Adelaide, Australia, December 1976

Arzoumanidis, S.G., and C. Meyer. "Modelling Reinforced Concrete Beams Subjected to Cyclic Loads", Dept. of Civil Engineering and Engineering Mechanics, Columbia University, New York, Report No. NSF-PFR-79-24695-CU-1, 1981.

Bazant, Z.P., and P. D. Bhat. "Prediction of Hysteresis of Reinforced Concrete Members", Journal of the Structural Division, ASCE, Vol. 103, No. ST1, January 1977, pp 153-167.

Bedell, R.H., and D.P. Abrams. "Scale Relations for Concrete Columns", Structural Research Series No 8302, Civil Engineering Department, University of Colorado, Boulder.

Clough, R.W., K.L. Benuska, and E.L. Wilson. "Inelastic Earthquake Response of Tall Buildings", Proceedings of the Third World Conference on Earthquake Engineering, Auckland and Wellington, New Zealand, January 1965, Vol. II, pp.68-84.

Clough, R.W., and K.L. Benuska. "Nonlinear Earthquake Behavior of Tall Buildings", Journal of Engineering Mechanics Division, A.S.C.A., Vol.93,No 93, No. EM3,June 1967,pp 129-146.

Cervenka, V. "Inelastic Finite Element Analyses of Reinforced Concrete Panels Under In-Plane Loads", PhD Dissertation, Dept. of Civil Engineering, University of Colorado, Boulder, 1970.

Chen, P.F., and G.H. Powell. "Generalized Plastic Hinge Concepts for 3D Beam-Column Elements", EERC Report No. 82/20, University of California, Berkeley, November 1982.

Emori, K., and W.C. Schnobrich. "Analysis of Reinforced Concrete Frame-Wall Structures for Strong Motion Earthquakes", Civil Engineering Studies, SRS No. 457, University of Illinois at Urbana-Champaign, Urbana, Illinois, December, 1978.

EPP, W.H. "The Effect of Loading Path on the Hysteretic Response of Concrete Column", Masters Thesis, Department of Civil Engineering, University of Colorado, Boulder, 1984.

Fowler, T.J. "Reinforced Concrete columns Governed by Concrete Compressions", PhD Dissertation, The University of Texas at Austin, January, 1966

Gilbertsen, M.F. "The Response of Nonlinear Multistory Structures to Earthquake Excitation", Earthquake Research Laboratory, California Institute of Technology, Pasadena, May 1967.

Gilbertsen, N.D., and J.P. Moehle. "Experimental Study of Small-Scale R/C Columns Subjected to Axial and Shear Force Reversals", Civil Engineering Studies, SRS No.481, University of Illinois at Urbana-Champaign, Urbana, Illinois, July, 1980.

Hognestad, E. "A Study of Combined Bending and Axial Load in Reinforced Concrete", University of Illinois Experiment Station ,Bulletin Series No.339, November 1951.

Hsu, L.W. "Behavior of Multi-Story Reinforced Concrete Walls During Earthquakes", Ph.D. Thesis, Dept. of Civil Eng, University of Illinois, Urbana, 1974.

Jiang, Y., and M. Saiidi. "Four-Spring Element for Cyclic Response of R/C Columns", Journal of Structural Engineering, ASCE, Vol. 116, No, April, 1990.

Kaba, S.A., and S.A. Mahin. "Interactive Computer Analysis Methods for Predicting the Inelastic Cyclic Behavior of Structural Sections", EERC Report No. 83/18, University of California, Berkeley, August, 1983.

Kaba, S.A., and S.A. Mahin. "Refined Modelling of Reinforced Concrete Columns for Seismic Analysis", EERC Report No. UCB/Eerc-84/3, University of California, Berkeley, California, April, 1984.

Kent, D.C. "Inelastic Behavior of Reinforced Concrete Members with Cylic Loadings", Ph.D Thesis, University of Canterbury, Christchurch, New Zealand,1969.

Kent, D.C., and R. Park. "Flexural Members with Confined Concrete" Journal of the Structural Division, ASCE, Vol. 97, ST7,July 1971, pp 1961-1990.

Keshavarizan, M., and W.C. Schnobrich. "Computed Non-linear Seismic Response of R/C Wall-Frame Structures", Civil Engineering Studies, SRS No. 515. University of Illinois at Urbana-Champaign, Urbana, Illinois, May, 1984.

Kreger, M.E., and L. Linbeck. "Behavior of Reinforced Concrete Columns Subjected to Lateral and Axial Load Reversals", Proceedings, Third U.S. National Conference on Earthquake Engineering, Charleston, South Carolina, August 24-28, 1986.

Lai, S., Will, G. and S. Otani. "Model for inelastic Bi-axial Bending of Concrete Members'", Journal of Structural Division, ASCE, Vol 110, No 11, November 1984.

Ma, S.M., V.V. Bertero, and E.P. Popov. "Experimental and Analytical Studies of the Hysteretic Behavior of R/C Rectangular and T-Beams", EERC Report No.76-2, Berkeley,May, 1976

Mahin, S.A. "An Evaluation of the Seismic Response of Reinforced Concrete Building", Phd Dissertation, Dept. of Civil Engineering, University of California, Berkeley, October 1974.

Mahin, S.A., and V.V. Bertero. "A Computer Program for R/C Column Analysis Users Manual And Documentation", Department of Civil Engineering,University of California,Berkeley,

Mark, K.M.S., and J.M. Roesset. "Nonlinear Dynamic Response of Reinforced Concrete Frames", Publication R76-38, Department of Civil Engineering, M.I.T., August 1976.

Meyer, C., S.G. Arzoumanidis, and M. Shinozuka. "Earthquake Reliability of Reinforced Concrete Buildings", Proceedings of the Symposiums on Probabilistic Methods in Structural Engineering, ASCE, New York 1981, pp 378-398.

Otani, S., and M.A. Sozen. "Behavior of Multistory Reinforced Concrete Frames During Earthquakes", Civil Engineering Studies, Structural Research Series No. 392, University of Illinois, Urbana, November 1972.

Park, R., C.D. Kent, and A.R. Sampson. "Reinforced Concrete Member with Cyclic Loading." Journal of the Structural Division, Proceeding of the American Society of Civil Engineers, Vol. No. 98, No ST7 July. 1972.

Park, R., and T. Paulay. "Reinforced Concrete Structures." John Wiley and Sons, New York , 1975

Powell, G.H., and D.G. Row. "Influence of Analysis and Design Assumptions on Computed Inelastic Response of Moderately Tall Frames", EERC Report No 76/11, University of California, Berkeley, April 1976.

Rabbat, B.G., J.I. Daniel, T.L. Weinmann, and N.W. Hanson. "Seismic Behavior of Lightweight and Normal Weight Concrete Columns", Journal of the American Concrete Institute, Proc. Vol. 110, No. 1, January-February, 1986, pp 69-79.

Ramirez, H., and J.O. Jirsa. "Effect of Axial Load on Shear Behavior of Short R/C Columns under Cyclic Lateral Deformations", PMFSEL Report, No 80-1, The University of Texas at Austin, June 1980.

Saadeghvaziri, M.A., and D.A. Foutch. "Inelastic Behavior of R/C Highway Bridges under Horizontal and Vertical Earthquake Motions" , Civil engineering Studies, SRS No. 540, University of Illinois at Urbana-Champaign, Urbana, Illinois, June, 1988.

Saadeghvaziri, M.A. "Behavior of R/C Columns Under Uncoupled Variations in Lateral and Axial Loads", Proceedings of Fourth U.S National Conference on Earthquake Engineering, Palm Springs, California (Vol 2), May 20-24, 1990

Saiidi, M., and M.A. Sozen. "Simple and Complex Models for Nonlinear Seismic Response of Reinforced Concrete Structures", Report to the National Science Foundation, Dept. of Civil Engineering, University of Illinois, Urbana, August 1979.

Schnobrcih, W.C. "Behavior of Reinforced Concrete Structures Predicted by the Finite Element Method", An International Journal, Computer and Structure, Vol.7, No.3, June 1977, pp.365-376.

Sheikh, S.A., and S.M. Uzumeri. "Strength and Ductility of Tied Columns", Journal of Structural Divisions, ASCE, Vol. 106, ST5, May 1980, pp 1079-1102.

Sheikh, S.A., and S.M. Uzumeri. "Analytical Model for Concrete Confinement in Tied Columns", Journal of the Structural Division, ASCE, vol.108 . No.ST12, December 1982.

Suharwardy, M. I. H. "Inelastic Response of Reinforced Concrete Columns Subjected to Two Dimensional Earthquake Motions, " PhD Thesis, University of Illinois at Urbana-Champaign, Urbana, Illinois, December, 1976

Takeda, T., M.A. Sozen, and N.N. Nielsen. "Reinforced Concrete Response to Simulated Earthquake", Journal of the Structural Division, ASCE, Vol. 96, ST12, December 1970, pp 2557-2573.

Takayanagi, T., and W.C. Schnobrich. "Computed Behavior of Reinforced Concrete Coupled Shear Walls", Civil Engineering Studies, Structural Research Series No.434, University of Illinois, Urbana, December 1976.

Takizawa, H. "Notes on Some basic Problems in Inelastic Analysis of Planer R/C Structures (Parts 1 and 2)", Transactions of the Architectural Institute of Japan, No.240, February, 1976, pp 51-62.

Umehara, H., and J.O. Jirsa. "Short Rectangular R/C columns under Bi-directional Loadings", Journal of Structural Division, ASCE, Vol. 110, ST3, March, 1984, pp 605-618.

Vallenas, J., V.V. Bertero, and E.P. Popov. "Concrete Confined by Rectangular Hoops and Subjected to Axial Loads", Report No. UCB/EERC-77/13, Earthquake Engineering Research Center, University of California, Berkeley, August 1977.

Umemura, H., H. Aoyama, and H. Takizawa. "Analysis of the Behavior of Reinforced Concrete Structures During Strong Earthquakes Based on Empirical Estimation of Inelastic Restoring Force Characteristics of Members", Proceedings of the Fifth World Conference on Earthquake Engineering, Rome, Italy, June 1973, Vol. 2 pp 2201-2210.

Umemura, H., and H. Takizawa. "Strong Motion Response Analysis of R/C Frames." Transactions of Architectural Institute of Japan, 1972.

Yuzugulu, O., and W.C. Schnobrich. "A Numerical Procedure for the Determination of the Behavior of a Shear Wall Frame System", Journal of the ACI, Proc. Vol. 70, No. 7, July 1973, pp 474-479.